

**MICROBIAL ACTIVITY IN SEDIMENTS:
EFFECTS ON SOIL BEHAVIOR**

A Dissertation
Presented to
The Academic Faculty

by

Verónica Rebata-Landa

In Partial Fulfillment
of the Requirements for the Degree
Doctor of Philosophy in the
School of Civil & Environmental Engineering

Georgia Institute of Technology
December 2007

**MICROBIAL ACTIVITY IN SEDIMENTS:
EFFECTS ON SOIL BEHAVIOR**

Approved by:

Dr. J. Carlos Santamarina, Advisor
Professor, Goizueta Foundation Chair,
School of Civil & Environmental
Engineering
Georgia Institute of Technology

Dr. James K. Mitchell
Emeritus University Distinguished
Professor, Department of Civil &
Environmental Engineering
Virginia Tech

Dr. Susan Burns
Professor, School of Civil &
Environmental Engineering
Georgia Institute of Technology

Dr. Glenn Rix
Professor, School of Civil &
Environmental Engineering
Georgia Institute of Technology

Dr. David Frost
Professor, School of Civil &
Environmental Engineering
Vice Provost & Director
Georgia Institute of Technology

Dr. Patricia Sobecky
Professor, School of Biology
Georgia Institute of Technology

Date Approved: August 14th, 2007 □

To my family for all their support...

To Pierre, Vivi, Juan, Davi, Abel, Tati, Fiore, Efra,
and all the others who saved me from losing my mind...

ACKNOWLEDGEMENTS

I would like to thank my grandpa for always believing in me, my family for all their support, and my friends for staying in touch despite the distance.

I wish to thank the Particulate Media Research Laboratory members, for their help, guidance and friendship, the Geosystems Group faculty for all the precious knowledge they gave me and my friends at the Geosystems Group for all the fun we had together complaining about research.

I would also like to thank The Goizueta Foundation and The National Science Foundation for providing the resources that made this research possible.

And finally, I wish to thank Didier Contis for saving my data when my hard drive crashed few days before my thesis defense.

TABLE OF CONTENTS

	Page
ACKNOWLEDGEMENTS	iv
LIST OF TABLES	vii
LIST OF FIGURES	viii
SUMMARY	x
<u>CHAPTER</u>	
1 INTRODUCTION	1
Motivation	1
Organization	2
2 PRELIMINARY BIOLOGICAL CONCEPTS	4
Bacteria	4
Factors that affect bioavailability	7
Conclusions	10
3 MECHANICAL LIMITS TO MICROBIAL ACTIVITY IN SOILS	11
Introduction	11
Materials and methods	12
Results	20
Discussion and conclusions	27
4 MECHANICAL EFFECTS OF BIOGENIC GAS IN SOILS	29
Introduction	29
Review on biogenic gas bubbles	30
Experimental study	37
Results and observations	42

Analysis and discussion	47
Conclusions	57
5 BIOLOGICAL CLOGGING OF SOILS UNDER RADIAL FLOW	59
Introduction	59
Literature review	60
Experimental studies	65
Discussion – Coupled clogging phenomena	78
Conclusions	79
6 BIOLOGICAL DEPOSITION OF CaCO_3 IN SOILS	81
Introduction	81
Literature review	81
Experimental studies	87
Discussion and analysis	102
Conclusions	104
7 GENERAL CONCLUSIONS AND FUTURE WORK	106
General conclusions	106
Future work	108
APPENDIX A: PARTICLE LEVEL ANALYTICAL MODELS	110
APPENDIX B: P-WAVE SIGNATURES	124
APPENDIX C: COMPLEMENTARY DATA	130
REFERENCES	134
VITA	162

LIST OF TABLES

	Page
Table 3.1: Sediment preparation	15
Table 3.2: Mechanical and geometrical properties of bacteria	17
Table 3.3: Models for bacteria-sediment interaction	19
Table 3.4: Colony-forming units per mL of sediment in recovered specimens	24
Table 4.1: Previous studies on biogenic gas generation	31
Table 4.2: Common metabolisms that generate gas as a byproduct	32
Table 4.3: Measured values of supersaturation needed to cause bubble nucleation on aqueous solutions	37
Table 4.4: Tested specimens - Preparation	40
Table 4.5: Bulk stiffness, mass density and propagation velocity	49
Table 6.1: Amount of urea and CaCl_2 per liter of solution in the different nutrient combinations used	88
Table 6.2: Crystal nucleation on mineral surfaces – Main observations	90

LIST OF FIGURES

	Page
Figure 2.1: Typical growth curve for a bacterial population in a batch culture	5
Figure 2.2: Temperature-based taxonomy of microorganisms	8
Figure 2.3: Effect of pH on growth rate for a typical soil microorganism	9
Figure 3.1: Experimental device	14
Figure 3.2: Pore and pore-throat size	21
Figure 3.3: Presence of bacteria in sediments	23
Figure 3.4: Sediment-bacteria mechanical interactions: Predicted boundaries	25
Figure 3.5: Bacteria's fate in sediments	26
Figure 4.1: Nitrate and nitrite reduction – Enzymes involved	33
Figure 4.2: Critical radius for N ₂ bubble nucleation under different bubble nucleation pressures and supersaturation values	36
Figure 4.3: Experimental device and peripheral electronics	39
Figure 4.4: Evolution of P-wave signatures during biogenic gas formation	43
Figure 4.5: P-wave velocity and saturation	44
Figure 4.6: Initial (t = 0) and final (t = 30 days) steady-state P-wave velocity for all specimens, both single grained soils and mixtures, as a function of the specific surface	45
Figure 4.7: P-wave velocity recovery as a function of time after the step increase in the pore fluid pressure	46
Figure 4.8: Initial rate and maximum volume of generated gas versus specific surface	48
Figure 4.9: P-wave velocity, saturation and log-normal distribution of gas bubble size	52
Figure 4.10: Relationship between B-value and P-wave velocity	54
Figure 4.11: Initial and final (steady-state) value of Skempton's B parameter computed for all single grained soils and mixtures as a function of specific surface	55

Figure 4.12: Variation in Normalized Cyclic Stress Ratio (NCSR) with respect to P-wave velocity (left) and B-value (right)	56
Figure 5.1: Bioclogging effectiveness versus soil type	64
Figure 5.2: Viscosity measurements	66
Figure 5.3: Experimental device – Pore-scale test	67
Figure 5.4: Evolution of pressure head and mean flow velocity in the pore-scale tube test	69
Figure 5.5: Set of images at different stages of clogging	72
Figure 5.6: Bioclogging in radial flow: pressure heads	73
Figure 5.7: Bioclogging in radial flow: heads at $t = 0$ and $t = 30000$ min	75
Figure 5.8: Bioclogging in radial flow: evolution of hydraulic conductivity within each specimen as a function of the radial distance r and time	77
Figure 5.9: Bioclogging in radial flow: hydraulic conductivity in the “clogged annulus” as a function of time	78
Figure 5.10: Coupled clogging phenomena	79
Figure 6.1: Experimental setup	89
Figure 6.2: Effects of time and nutrient type on biogenic cementation as described in Study #2	94
Figure 6.3: CaCO_3 content for specimens in Study #2	94
Figure 6.4: CaCO_3 content and models as a function of grain size as described in Study #3	96
Figure 6.5: Evolution of cementation in unsaturated heterogeneous specimens (Study #5)	101
Figure 6.6: Effects of biogenic cementation on soil properties	103

SUMMARY

Microorganisms have played a critical role in geological processes and in the formation of soils throughout geological time. It is hypothesized that biological activity can also affect soil properties in short engineering time-scales. Bioactivity in sediments is determined by the classical limiting factors (i.e., nutrients, water, C for biomass, temperature and pH) as well as by pore-size geometrical limits and mechanical interactions between bacterial cells and soil particles. These constraints restrict the range of grain size and burial depth where biomediated geochemical processes can be expected in sediments, affect the interpretation of geological processes and the development of engineering solutions such as bioremediation. When biological, geometrical and mechanical limiting factors are satisfied, bioactivity can be designed to alter the mechanical properties of a soil mass, including lowering the bulk stiffness of the pore fluid through controlled gas bio-generation, increasing the shear stiffness of the soil skeleton by biomineralization, and reducing hydraulic conduction through biofilm formation and clogging. Each of these processes can be analyzed to capture the bio-chemo-hydro-mechanical coupling effects, in order to identify the governing equations that can be used for process design. Design must recognize the implications of spatial variability, reversibility and environmental impacts.

The results of this study: (a) define the main regions in a particle-size versus depth space that characterize the fate of bacteria: “active and motile,” “trapped inside pores,” and “dead or dormant”, (b) demonstrate the viability of biogenic gas generation as a tool to reduce pore pressure generation during undrained shear, (c) show that biofilm growth on pore surfaces is pore size and flow velocity limited so that a characteristic radial distance to clogging appears in radial flow, and (d) identify biomineralization

habits on sediment surfaces and their implications on the mechanical properties of the soil skeleton.

CHAPTER 1

INTRODUCTION

Motivation

The study of soil behavior has been conducted from different perspectives throughout the centuries: Coulomb (XVIII) and Rankine (XIX) advanced physical and mechanical insight, Terzaghi (>1920's) combined geological and mechanical concepts, and Lambe and Mitchell (>1950's) among other researchers incorporated colloidal chemistry and mineralogy. The biological dimension is being discovered [Mitchell and Santamarina, 2005] and it is explored herein.

Environmental conditions act as growth limiting factors for bacterial cells. Among them, moisture content, pH, temperature, nutrient availability, oxygen, and light have been extensively studied in the literature and are reviewed in most microbiology textbooks. However, mechanical and geometrical constraints have not been studied in detail and are often neglected. The motivation of the first section of this thesis is to identify geometric restrictions for bioactivity, to develop particle-level mechanical models for bacteria-sediment interaction, and to define regions for bacteria's fate in the two dimensional space of sediment grain size versus burial depth. The scope of this study is limited to microorganisms present in natural and artificially compacted, fracture-free sediments.

Microorganisms living in soils play important roles in geological processes; they influence soil and rock formation, are able to change the soil or rock properties once formed and can also affect geochemical processes taking place in the soil. Thus, biogeochemical processes can have significant geotechnical consequences over relatively

short times [Ehrlich, 1996]. Microorganisms can generate gas bubbles, biofilms, and mineral precipitates through their metabolism. The presence of small gas bubbles affects the pore fluid bulk stiffness and consequently hinders pore pressure generation during shear. The production of biofilms reduces the hydraulic conductivity of soils and fractured rocks, alters fines migration, clogs filters, enhances hydrodynamic dispersion, and increases chemical retardation. Finally, bio-mineralization leads to mineral deposition on soil grains, causes soil cementation and increase in shear stiffness. The second section of this thesis explores the effectiveness and control of these metabolisms in sediments. The general methodology used for this investigation combines the detailed evaluation of databases gathered from published sources, particle level and macroscale experiments, and complementary models and analyses.

Organization

This research centers on the fundamental understanding of the microbial influence on soil behavior and properties, from the survivability of microbial cells in sediments under diverse mechanical and geometrical conditions, to the alteration of soil properties by microbial manipulation and its possible applications in the geotechnical field.

Chapter 2 reviews basic biological concepts relevant to the coexistence of soil particles and microbial cells and their interactions in the soil matrix. The main requirements for microbial growth and bio-availability are reviewed, as well as microbial cell characteristics that may affect their interactions with soil particles.

Chapter 3 addresses the viability of microbial activity in soils. The likelihood of microbial survivability inside the soil matrix is analyzed from the mechanical and geometrical points of view.

Chapter 4 focuses on microbial gas generation. The study starts with a review of the principal bacterial metabolisms that generate gas as a by-product, as well as the

process of biogenic gas generation in soils. A set of unique experiments are designed to assess the evolution of biogenic gas in soils. Experimental data are analyzed using poroelastic models that capture the influence of gas bubbles on P-wave velocity and Skempton's B parameter.

Chapter 5 concentrates on biologically-mediated clogging of soils. The scope of this study encompasses the identification of the fundamental factors and mechanisms of microbial clogging. Then, an experimental program is implemented to study clogging in radial flow.

Chapter 6 documents the investigation of biologically-mediated cementation of soil grains, starting with a review of the conditions required to trigger biogenic CaCO_3 precipitation in the soil mass. Several experimental and conceptual studies follow to explore: the nucleation "habits" of biogenic CaCO_3 crystals over mineral surfaces, the influence of nutrient type and time, grain-size, diffusion-versus-advection process control, and the coupling between spatial variability and hydro-bio-mechanical phenomena in biogenic soil cementation.

Chapter 7 summarizes general conclusions and provides a series of recommendations for future research.

CHAPTER 2

PRELIMINARY BIOLOGICAL CONCEPTS

The behavior of viable microbial cells is influenced by their capacity to metabolize, grow and reproduce. The factors that affect microbial growth are reviewed in this Chapter.

Bacteria

Bacteria are microorganisms that undergo metabolism, reproduction and growth, differentiation, communication, movement and evolution. Bacterial activity requires a source of carbon for cell mass, a source of energy to sustain life-activity, water, other nutrients and a favorable environment (including temperature, pH, salinity, and sufficient space). Any of these can act as the "growth limiting factor".

Bacterial Growth

Bacterial growth curves depend on the type of culture system utilized. In a batch culture, an initial amount of cells is inoculated into an initial amount of substrate (nutrients) and incubated for the desired time without incorporating external sources of either cells or substrate. A typical growth curve under these conditions is shown in Figure 2.1. Four "growth phases" can be identified: (1) a "lag" period when cells are adapting to their new environment, macromolecules are being synthesized and therefore not all cells are dividing, (2) an "exponential" phase when cells utilize the substrate provided and duplicate fast, (3) a "stationary" phase when cells reach a maximum population density due to either nutrient exhaustion, waste accumulation, oxygen depletion, the development of an unfavorable pH, or a combination of these factors, and (4) the "death" phase, when

cells undergo autorespiration and eventually die without having other cells to replace them because they lack the necessary nutrients. The exact shape of the curve is species-dependent and it is also affected by the factors that contributed to cell death [Audesirk *et al.*, 2006; Moat and Foster, 1995; Sadava *et al.*, 2006].

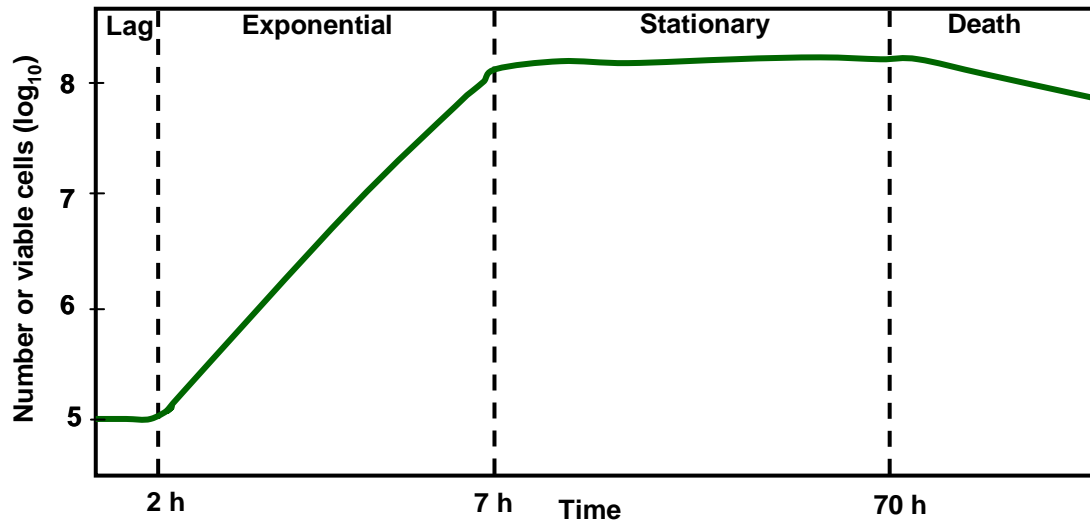


Figure 2.1 Typical growth curve for a bacterial population in a batch culture (no additional nutrients added after test initiation). Numbers shown were experimentally measured for *Pseudomonas fluorescens* in Luria-Bertani broth. Four growth phases can be identified: (1) “lag” period when cells are adapting to their new environment, (2) “exponential” phase when cells utilize the substrate provided and duplicate, (3) “stationary” phase when most of the substrate has been utilized and therefore the net growth is almost negligible, and (4) “death” phase when cells die without having other cells to replace them because they lack the necessary nutrients. From [Madigan *et al.*, 2003].

Biosynthesis: Carbon Sources

Biosynthesis is the energy-consuming formation of new cellular constituents using different carbon sources. Microorganisms can be divided into two large categories

on the bases of energy and carbon sources for nutrition. Autotrophic organisms (self-feeding) use inorganic carbon (mainly carbon dioxide) as carbon source and either inorganic redox (chemolithotrophic) or radiant energy (photolithotrophic) as energy source. Heterotrophic organisms (non-self-feeding) use organic carbon (e.g., glucose, acetate) as carbon source and either organic redox (chemoorganotrophic) or radiant energy (photoheterotrophic) as energy source [Atlas, 1995; Madigan *et al.*, 2003].

Note that autotrophic microorganisms do not require an organic substrate (provided source of carbon); however, heterotrophic organisms need organic substrates to achieve metabolism, reproduction and growth (e.g., glucose, acetate). Also, many microorganisms are capable of mixotrophy, i.e., they can switch from one type of source to another if the conditions in the surrounding environment change.

Biosynthesis: Energy Production

High-energy compounds such as Adenosine Triphosphate (ATP) are produced in biological systems through the energy released in oxidation-reduction (REDOX) reactions. Bacterial energy production and biosynthesis are complex processes that can be accomplished by many different metabolic pathways. A brief summary of the principal processes follows.

Oxidation is the removal of electrons, while reduction is the addition of electrons from a substance. REDOX reactions involve electrons being donated by an electron donor also known as “energy source” (which becomes oxidized) and being accepted by an electron acceptor (which becomes reduced). The tendency of a substance to become oxidized or reduced is expressed as the reduction potential. In biochemistry, oxidation and reduction processes usually involve the transfer of whole hydrogen atoms, not only electrons [Audesirk *et al.*, 2006; Madigan *et al.*, 2003].

Energy production follows different pathways in different types of microorganisms. In chemoorganotrophic microorganisms, energy is generated by catabolic break-down of organic compounds through fermentation, or either aerobic or anaerobic respiration. In phototrophic microorganisms (both photolithotrophic and photoheterotrophic) the energy required for biosynthesis is gathered by photosynthesis. And, in chemolithotrophic microorganisms, energy is generated mainly by either inorganic compound oxidation (aerobic) or by hydrogen oxidation in which carbon dioxide acts as the electron acceptor (anaerobic) [Atlas, 1995; Sadava *et al.*, 2006].

Factors that Affect Bioavailability

There are many factors that control the viability of microorganisms in soils in addition to the sources of carbon and energy. Other known growth limiting factors include moisture, temperature, oxygen, pH, light radiation and reduction potential [Alexander, 1961; Atlas, 1995; Hattori, 1973; Moat and Foster, 1995]. Any one of them can act as the “limiting factor” controlling the capability of the microorganism to survive, metabolize and reproduce. Space availability in sediments is a limiting factor generally neglected in the literature. Its relevance is explored in Chapter 3.

Moisture

Moisture affects microbial activity in two different ways. On the one hand, water is essential for life and it is the main constituent of the cell cytoplasm. On the other hand, the degree of water saturation in sediments controls the gaseous exchange and the availability of oxygen, i.e. the aerobic or anaerobic nature of the environment [Alexander, 1961].

Temperature

Four types of microorganisms can be identified on the bases of the optimal growth temperature (Figure 2.2): psychrophiles (optimum 5°C-to-15°C), mesophiles (optimum 20°C-to-40°C), thermophiles (optimum 45°C-to-60°C) and hyperthermophiles (>80°C) [Madigan *et al.*, 2003; Moat and Foster, 1995]. Temperature affects the rate of all processes occurring in microbes, including metabolism and reproduction, and can also alter cell properties such as size and shape [Hattori, 1973]. Most bacteria in soils are mesophiles, with optimal temperature in the vicinity of 25°C to 35°C and a capacity to grow from about 15°C to 45°C [Alexander, 1961].

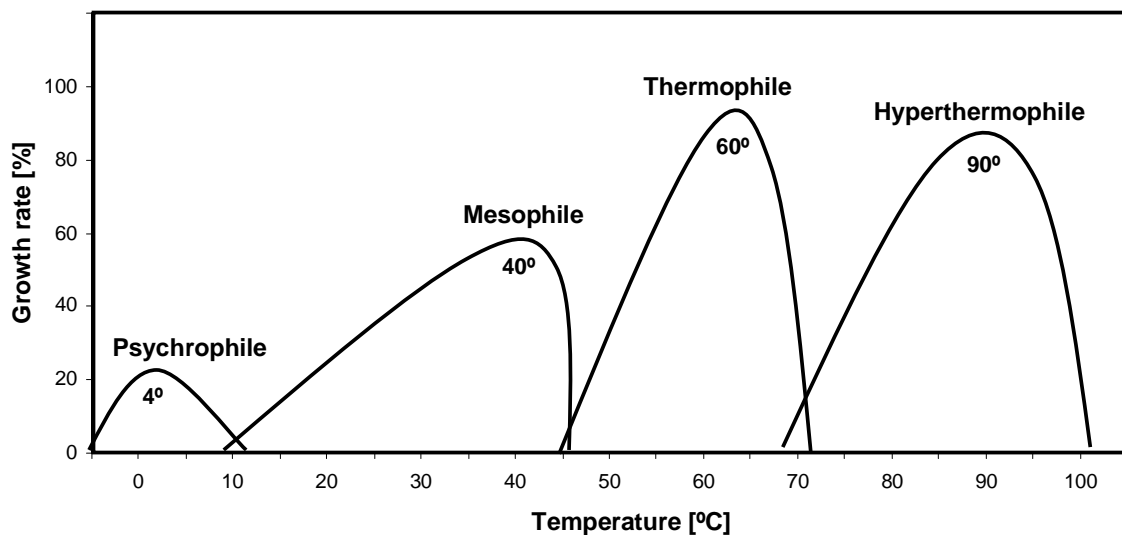


Figure 2.2 Temperature-based taxonomy of microorganisms: psychrophile, mesophile, thermophile and hyperthermophile. From [Madigan *et al.*, 2003].

Oxygen

Microorganisms that require oxygen as an electron donor (energy source) are called aerobes, while those that cannot utilize oxygen are anaerobes. Some microorganisms can switch between respiration (using oxygen) and fermentation (in the absence of oxygen), and therefore are named facultative. Also, among anaerobes, some

microorganisms are aerotolerants (i.e. cannot utilize oxygen but can live in the presence of it), but for others, oxygen is toxic [Moat and Foster, 1995].

Acidity and Alkalinity (pH)

Some cell substances such as chlorophyll, RNA, DNA, ATP, phospholipids and proteins are very sensitive to pH. Bacteria exhibit the least tolerance among microorganisms to highly acid or alkaline conditions. The optimum for most bacterial species is near neutrality [Alexander, 1961]. Changes in pH influence microbial growth and behavior, alter cell-surface charge, and affect bacteria interaction with the surroundings. Figure 2.3 shows the influence of pH on microbial growth rate [Hattori, 1973; Madigan *et al.*, 2003].

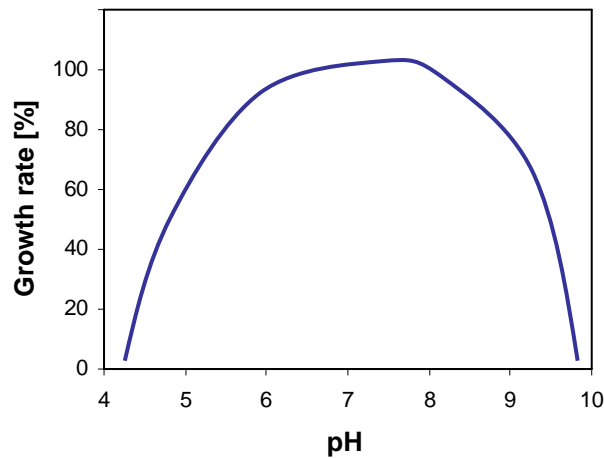


Figure 2.3 Effect of pH on growth rate for a typical soil microorganism. Organisms with pH optimum below 7 are called acidophiles and those with optimum above 7 are known as alkaliphiles. From [Hattori, 1973].

Light Radiation

Light radiation may have two types of effects on microbial activity. Exposure to visible light can cause the transformation of singlet oxygen and produce bacterial death.

On the other hand, phototrophic microorganisms use radiant energy as energy source and the rate of photosynthesis is a function of light intensity (some species can process very low intensity light) and wavelength (depending on their pigmentation) [Atlas, 1995; Audestirk *et al.*, 2006].

Reduction Potential

The reduction potential is the tendency of a molecule to become oxidized or reduced. Molecules with the higher negative reduction potential donate electrons to neighboring molecules or substances. Cells utilize the more favorable electron acceptors first (i.e. the substance with more positive reduction potential). As favorable sources get depleted, less efficient substances are used next, and therefore lower energy is gradually released [Madigan *et al.*, 2003].

Conclusions

The minimum requirements for bacterial growth include a carbon source, an energy source, sufficient water, and other trace minerals. Other known bacterial-growth limiting factors include temperature, pH, light radiation and reduction potential.

Many soil bacteria are facultative aerobes (they can live with or without oxygen), mesophiles (their optimal temperatures are around 30°C), prefer a neutral pH and are heterotrophs (require organic compounds for metabolism). Exemptions are often encountered.

CHAPTER 3

MECHANICAL LIMITS TO MICROBIAL ACTIVITY IN SOILS

Introduction

Microorganisms have played a critical role in geological processes leading to the formation of near surface and submerged sediments [Ehrlich, 1996; Hattori, 1973]. The ubiquitous presence of microorganisms in sediments is presumed and extensively reported in the literature. The observed decline in microbial abundance with increasing depth [Fierer *et al.*, 2003; Howard-Jones *et al.*, 2002; Kieft *et al.*, 1998; Parkes *et al.*, 1994; Parkes *et al.*, 2000; Phelps *et al.*, 1994; Wellsbury *et al.*, 2002; Zhang *et al.*, 1998]; has been associated to the influence of preferential paths in the transport of microbes through the sediment profile [Abu-Ashour *et al.*, 1994], limited input of fresh organic carbon at the surface and/or use of recalcitrant old buried organic matter by deep bacteria [Parkes *et al.*, 2000; Wellsbury *et al.*, 2002; Zhang *et al.*, 1998], and low hydraulic conductivity or diffusion for the transport of required chemicals [Fredrickson *et al.*, 1991; Phelps *et al.*, 1994].

However, geometrical constraints and mechanical interactions must be considered as well. For example, it has been recognized that small pores restrict bacteria movement and activity [Fredrickson *et al.*, 1997], limit nutrient transport [Boivin-Jahns *et al.*, 1996; Wellsbury *et al.*, 2002], diminish space availability [Zhang *et al.*, 1998], slow the rate of division [Boivin-Jahns *et al.*, 1996], and lead to reduced biodiversity; in fact, spatial isolation due to lack of pore connectivity implies that all cells in a pore are lineal descendants of a bacterium that became entombed at the time of geologic deposition [Boivin-Jahns *et al.*, 1996; Kieft *et al.*, 1998; Treves *et al.*, 2003; Zhou *et al.*, 2002; Zhou

et al., 2004]. Previous studies suggest that the size of pore throats must be around twice the cell diameter for bacteria transit [Updegraff, 1982]. Still, a detailed analysis is lacking.

The goals of this study are to identify geometric restrictions for bioactivity, to develop cell-level mechanical models for bacteria-sediment interaction, and to define regions for bacteria's fate in the two dimensional space of sediment grain size versus burial depth. The scope of this study is limited to microorganisms present in natural and artificially compacted, fracture-free sediments.

Materials and Methods

Three approaches are used for this study: data compilation from published studies, experimental study, and analyses based on particle-level geometrical-mechanical models.

Data Synthesis: Geometric Constraints Represented by Pore and Pore-throat Sizes

A database of published scanning electron microscopy (SEM) pictures and mercury intrusion porosimetry (MIP) data was compiled to explore the presence of habitable pore space and traversable pore throats in fine-grained sediments subjected to various stress levels. (Note: the term “sediment” is used herein to refer to either residual or transported materials made of mineral grains).

Assuming a nominal 1 μm microbial cell diameter, a sediment is considered to contain habitable pore space if more than 5% of the pores are larger than 1 μm (estimated as area ratio from SEM pictures). On the other hand, a sediment is considered to have traversable pore throats if the probability of having a pore throat larger than 1 μm is higher than 5% (taken as the area ratio under the MIP curve). The particle size and depth (surrogate for effective overburden stress level) corresponding to each data point is extracted from the information provided in the published works. The selected

representative particle size is the 10th percentile d_{10} because the finer fraction that fills the voids between large particles determines the hydraulic conductivity, porosity, pore size distribution and therefore the effective pore size in the sediment mass [Santamarina *et al.*, 2001]. In the case of laboratory studies, depth is computed from the applied effective overburden stress.

Data Synthesis: Bacteria in Sediments

The second database that is compiled consists of reported cases of “viable” bacteria in sediments. Each entry in the database includes the representative particle size d_{10} and the corresponding depth as a surrogate for effective overburden stress level. Even though each case history was carefully analyzed, there may be biases in the database related to contamination and sampling effects [Boivin-Jahns *et al.*, 1996], reactivation of dormant cells during core extraction [Zweifel and Hagstrom, 1995], cell growth during storage [Sinclair *et al.*, 1990] and our interpretation of particle size when authors provide descriptive information only.

Experimental Study

One-dimensional compression tests were used to explore the d_{10} versus depth space where biological evidence is insufficient. The following sediments, cells and devices were used.

Sediments

Five sediments were chosen for their particle size, compatible solution pH and grain strength characteristics: Crushed silica flour (Sil-co-sil, $d_{10} = 10\ \mu\text{m}$), Precipitated silica flour (Zeo; $d_{10} = 20\ \mu\text{m}$ uncrushed; $0.1\ \mu\text{m}$ after crushing), Kaolinite (RP2, $d_{10} = 0.36\ \mu\text{m}$), Illite (IMt-1, $d_{10} = 0.04\ \mu\text{m}$), and Montmorillonite (Bent, $d_{10} = 0.0034\ \mu\text{m}$).

Bacterial Species

The selected strain is *Pseudomonas fluorescens*; this is a mesophilic, non-spore-forming species naturally present in sediments.

Test Device

The system consists of a set of six stainless steel one-dimensional compression chambers (see Figure 3.1) which are loaded using pneumatic cylinders. The air pressure control permits applying preselected effective overburden stress levels between 30 kPa and 9 MPa (i.e., ~3 m to ~900 m burial depth).

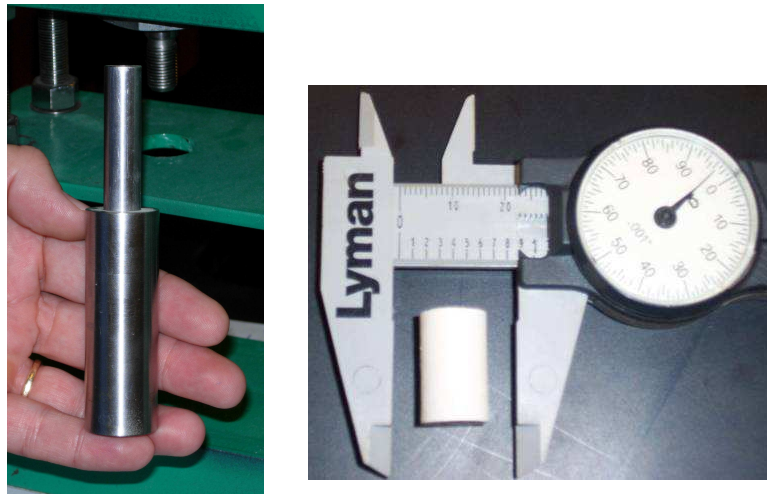


Figure 3.1 Experimental device: One dimensional compression chamber and piston (left). Soil core after extraction (right).

Other Materials

The nutrients are Difco Nutrient Broth for pore fluid, and Difco Nutrient Agar for Petri plates (Fisher Scientific). Sterile hydrophilic microfilter discs (13 mm diameter, 0.2 μ m filtration – Fisher Scientific) were used at both ends of the specimen to facilitate drainage during consolidation and to prevent external contamination.

Test Procedures

All procedures were conducted under aseptic conditions. Sediments, broth, agar and all device parts in contact with the sediment (piston, chamber and base) were autoclaved at 124°C and 125 kPa for 35 min. Sediments and broth were stored at 3°C in sterile containers, while agar was poured into Petri plates and stored at 3°C. Frozen cells were transferred into sterile Petri plates containing agar and incubated 24 hours at the optimum growth temperature (25°C for *Pseudomonas fluorescens*). Then, a 24 hours colony was transferred into 5 mL sterile broth, shaken thoroughly and incubated for additional 24 hours at the optimum growth temperature. A total of six 5 mL vials were prepared following this procedure (one per chamber). Prior analyses demonstrated that this procedure produces $\sim 10^8$ cells/mL.

Prior to assemblage, device parts were rinsed thoroughly with alcohol. The microfilter disc was placed on the base and the testing chamber was set in place. Half of the sterile sediment was transferred aseptically inside the chamber, culture from the vials and sterile broth were added and mixed with the sediment; then, the rest of the sediment was incorporated and mixed until a uniform paste was obtained. The amounts of sediment, culture and nutrient vary with sediment type (to achieve saturation) and are shown in Table 3.1.

Table 3.1 Specimen Preparation

Soil type	Sterile soil mass (g)	Culture volume (mL)	Sterile nutrient volume (mL)
Crushed silica flour	1.0	2.0	2.0
Precipitated silica flour	1.0	2.0	2.0
Kaolinite	4.0	1.5	1.5
Illite	4.0	2.0	2.0
Montmorillonite	1.0	3.0	3.0

Finally, a second microfilter disc was placed on top of the sediment and pushed slightly using the piston. Thereafter, pistons were step loaded until the target effective overburden stress was reached. The load was sustained during 48 to 72 hours. Longer loading periods were avoided to minimize the effects of nutrient deficit and waste accumulation on bacterial survivability.

Finally, the chamber was disassembled to recover the sediment specimen. The periphery of each specimen was aseptically trimmed to reduce the probability of contamination, and approximately 0.5 mL of each specimen was introduced into vials, prepared with 4.5 mL Phosphate Buffered Saline (PBS) solution. Vials were sonicated for 10 to 20 seconds to detach cells from sediment particles and 0.1 mL of the fluid was transferred into agar plates, spread using a sterile tool and incubated for 24 hours at the optimum temperature.

This protocol was designed to prevent contamination. The adequacy of the procedure was corroborated by sterile controls run for all sediments and stress combinations. Furthermore, the complete study was duplicated for verification, obtaining identical results.

Particle-Level Analytical Models

Various geometrical and mechanical interaction models were analyzed to establish boundaries and the effect of effective overburden stress and particle size on bacteria's fate. All models assume initial spherical cell shape, constant cell volume and constant cell wall volume and are available as Appendix A. Relevant geometrical and mechanical properties used in the models are summarized in Table 3.2. Brief comments on each of the models follow (equations in Table 3.3).

Table 3.2 Mechanical and Geometrical Properties of Bacteria

Property	Average value	References
Cell wall elastic modulus, E_{cell}	30 MPa	[Boulbitch <i>et al.</i> , 2000; Thwaites and Surana, 1991; Yao <i>et al.</i> , 1999]
Cell wall tensile strength, σ_t	13 MPa	[Thwaites and Surana, 1991; Thwaites <i>et al.</i> , 1991]
Drag velocity of cells, v	10 $\mu\text{m/s}$	[Astumian and Hanggi, 2002]
Cell radius, R	0.5 μm	[Katz <i>et al.</i> , 2003]
Cell wall thickness, t	50 nm	[Edwards, 1990]

Note: average values for bacteria commonly found in soils.

Habitable Pore Space and Traversable Pore-Throats (Table 3.3, Models a and b)

Cells can loosely fit inside pore spaces without suffering mechanical stresses when $d_{cell} \ll d_{pore}$. For cubic-tetrahedral and simple cubic packing of monosized spherical particles size $d_{sediment}$, the pore size varies from $d_{pore} = 0.26 d_{sediment}$ to $0.37 d_{sediment}$.

Cell Squeezed Between Two Particles (Table 3.3, Model c)

Large platy particles such as kaolinite can be as large as or larger than the cell size. The loading mechanism resembles a sphere being squeezed between two large plates. The deformed cell gains a filled torous shape until the cell wall fails in tension.

Cell Puncture (Table 3.3, Model d)

The thickness of kaolinite and illite clay particles are one or two orders of magnitude smaller than cells, and therefore the loading mechanism resembles a spherical bacteria being “pressed by needles” until they eventually puncture the cell [Sun *et al.*, 2003]. The lower limit for this model corresponds to the smallest particle that can exert the required puncture force without buckling, i.e., when platy sediment particles experience excessive bending before perforating the cell wall.

Cell Squeezed Within the Equivalent Continuum Sediment Skeleton (Table 3.3, Model e)

When sediment particles are much smaller than the cell, e.g., montmorillonite, the cell is effectively submerged in an equivalent continuum, and sediment particles are not strong enough to puncture the cell wall. However, as the burial depth of the sediment increases, particles move closer together by compression of the counterion diffuse layer, reducing the space around the cell. In this case a trapped cell can be axially deformed into a filled torous until its cell wall breaks in tension. For this model, the initial interparticle distance is assumed to be equal to twice the diffuse layer thickness and the limit deformation is established at an interparticle distance of 10 Å. According to this mechanical model and the parameters summarized in Table 3.3, reversed arching takes place within the sediment skeleton and the cell takes more load than the neighboring particles due to the high sediment skeleton compliance. The position of this boundary depends on the lateral effective stress, which is linked to the sediment formation history. Nutrient and waste transport are slow in these fine-grained sediments and may become the limiting factor.

Cell Entrapment and Mobilization inside the Sediment Skeleton (Table 3.3, Model f)

Motile microbial cells can generate a viscous drag force in the order of 0.1-to-10 pN [Astumian and Hanggi, 2002; Miyata *et al.*, 2002]. This force may be sufficient to displace neighboring particles. The boundary for this mechanism in the d_{10} versus depth space is computed with the displacement model presented in Table 3.3 (Model f), which considers the particles self weight and the skeletal force per particle, and disregards electrostatic interactions between cells and fine-grained sediment particles. Note that the model considers the displacement of a single particle rather than the area corresponding to the cell's cross section.

Table 3.3 Models for Bacteria-Sediment Interaction^a

Model	Relevant Equations	Particle Size Range
(a) Habitable pore	$R_{throat} = t_p \cdot \left(\frac{\sqrt{3}}{3} - \frac{1}{2} \right) \approx 0.08 \cdot t_p$ $R_{pore} = t_p \cdot \left(\frac{\sqrt{21}}{6} - \frac{1}{2} \right) \approx 0.26 \cdot t_p$	silts and sands
(b) Traversable pore throats	$R_{throat} = t_p \cdot \left(\frac{\sqrt{2}}{2} - \frac{1}{2} \right) \approx 0.21 \cdot t_p$ $R_{pore} = t_p \cdot \left(\frac{\sqrt{3}}{2} - \frac{1}{2} \right) \approx 0.37 \cdot t_p$	silts and sands
(c) Squeezing	$H_{max} = \frac{E_{cell}}{\gamma_{eff}} \cdot \frac{9}{\pi} \cdot \frac{\alpha \cdot \varphi \cdot (1 - 2 \cdot \varphi)}{\frac{\pi}{7} - \frac{1}{2} \cdot \varphi} \cdot \left(\frac{\varphi^{1/3}}{1 - \varphi^{1/3}} \right)^2$	$t_p \geq t_{p_critic}$ $t_{p_critic} = \frac{6 \cdot R}{\pi} \cdot \left(\frac{\varphi^{1/3}}{1 - \varphi^{1/3}} \right)$
(d) Puncture	$H_{max} = \frac{81}{4 \cdot \pi} \cdot \frac{E_{cell}}{\gamma_{eff}} \cdot \alpha \cdot \psi \cdot \varphi^{5/2}$	$t_{p_buckling} < t_p < t_{p_critic}$ $t_{p_buckling} \approx 125 \cdot \frac{E_{cell}}{E_{soil}} \cdot \alpha \cdot R \cdot \varphi^{5/2}$
(e) Equivalent continuum	$H_{max} = B \cdot \left(\frac{2 \cdot \pi^2}{(2 - \varphi^{1/3} + \frac{1}{2} \cdot \varphi^{1/3} \cdot \frac{t_p}{\xi})^2} - 1 \right) + \frac{E_{cell}}{\gamma_{eff}} \cdot \frac{9}{16 \cdot \pi} \cdot \frac{\alpha \cdot \varphi \cdot (1 - 2 \cdot \varphi)}{\frac{\pi}{7} - \frac{1}{2} \cdot \frac{\varphi}{(1 - K_0)^2}} \cdot \left(\frac{\frac{\varphi^{1/3}}{1 - K_0}}{1 - \frac{\varphi^{1/3}}{1 - K_0}} \right)^2$ $B = \frac{R_{gas} \cdot T \cdot c_0}{2 \cdot \gamma_{eff}} \quad \xi = \sqrt{\frac{\varepsilon_0 \cdot R_{gas} \cdot \kappa \cdot T}{2 \cdot F_a^2 \cdot c_0 \cdot z^2}}$	$t_p \leq \left(\frac{4}{\varphi^{1/3}} - 2 \right) \cdot \xi$
(f) Single particle displacement	$H_{pushing} = \frac{6 \cdot \pi \cdot \eta \cdot v}{R \cdot \psi^2 \cdot \mu \cdot \gamma_{eff}}$	$t_p \leq t_{p_max\ imm}$ $t_{p_max\ imm} = \sqrt{\frac{36 \cdot \eta \cdot v \cdot R}{\gamma_{grains} - \gamma_w}}$

^a Notation: $\alpha = \frac{t}{R}$, where t is initial cell wall thickness and R is initial cell radius; $\psi = \frac{t_p}{R}$, where t_p is particle thickness and R is initial cell radius; $\varphi = \frac{\sigma_{tensile}}{E_{cell}}$, where $\sigma_{tensile}$ is cell wall tensile strength and E_{cell} is cell wall elastic modulus; R_{pore} and R_{throat} radius of pore and pore throat for a given geometric configuration; H_{max} maximum depth before the cell wall fails; $H_{pushing}$ maximum depth where cell can push sediment particles; $R_{gas} = 8.314 \text{ N}\cdot\text{m}/\text{K}\cdot\text{mol}$; T , absolute temperature; c_0 [mol/m³]; ξ , double layer thickness; permittivity of free space $\varepsilon_0 = 8.85 \times 10^{-12} \text{ F/m}$; real relative permittivity of water $\kappa = 78.5$; Faraday's constant $F_a = 9.6485 \times 10^4 \text{ C/mol}$; z , valence of cations; E_{cell} , elastic modulus of cell wall; γ_{eff} effective unit weight of sediment mass; K_0 , lateral stress coefficient; E_{soil} , elastic modulus of sediment particle; R , radius of bacterial cell; v , velocity of bacterial cell; η , viscosity of pore fluid; μ , friction coefficient; t_p particle size. For Figure 3, $\gamma_{eff} = 10 \text{ kN/m}^3$, $K_0 = 0.2$, $E_{soil} = 5 \text{ GPa}$, $\eta = 1 \times 10^{-6} \text{ g}/\mu\text{m}\cdot\text{s}$, and $\mu = 0.5$.

Results

Results from the data synthesis exercise, the experimental study, and computed with analytical models are presented in the same two dimensional space defined by particle size and equivalent burial depth (which is a surrogate for effective overburden stress level), to identify boundaries for the mechanical limits of microbial activity in deep sediments.

Data Synthesis: Geometric Constraints

Habitable pore space and traversable pore-throat sizes for a 1 μm nominal bacteria size are shown in Figure 3.2. The data show that habitable pores and traversable pore throats are found in coarse sediments, and in some clayey sediments at shallow depth.

Silt and sand grains may crush at large burial depths and cause a reduction in pore and pore-throat sizes. The depth required for crushing is inversely proportional to the particle diameter and directly proportional to the tensile strength of the mineral that makes the grains [McDowell and Bolton, 1998]. The dotted line in Figure 3.1 captures the estimated grain crushing boundary.

Data in Figure 3.2 provides a geometric explanation for the generally observed decrease in microbial abundance with decreasing particle size [Fredrickson *et al.*, 1991; Phelps *et al.*, 1994; Sinclair *et al.*, 1990; Zhang *et al.*, 1998], and the comparatively low microbial diversity found in deep, fine-grained sediments [Marchesi *et al.*, 2001; Newberry *et al.*, 2004; Zhou *et al.*, 2004]. Both can be linked to lack of habitable pore space and hindered mobility across pores.

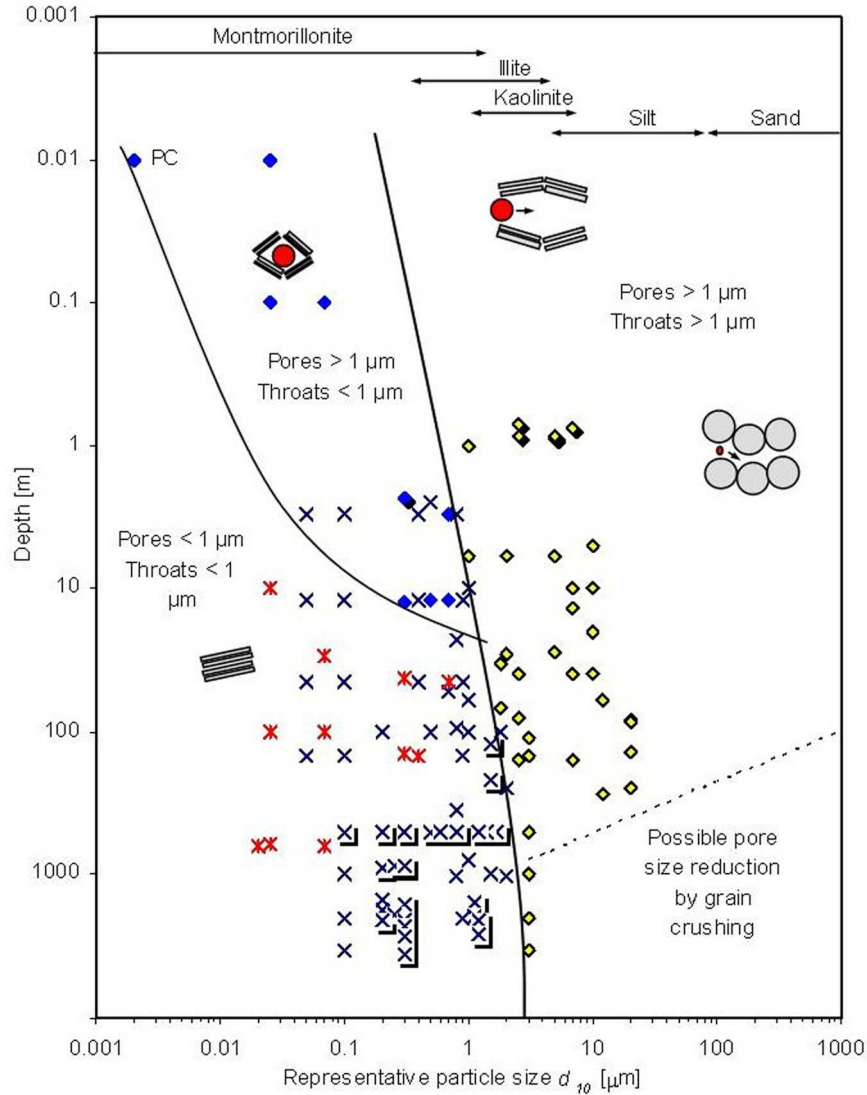


Figure 3.2 Pore and pore-throat size. Habitable pore space (solid diamonds ◆ SEM), traversable pore throat (open diamonds ◇ MIP), nonhabitable pore space (asterisks ✱ SEM), and nontraversable pore throat (crosses ✕ MIP). Lines suggest estimated limits for each geometric configuration, and in the absence of data points, boundaries are extended to reflect expected behavior. Underlined data labels indicate natural samples; all other data points were obtained from artificially compacted specimens (PC: *M. Santagata*, 2005 - *personal communication*). Typical mineral sizes are indicated in the upper part of the plot [*Mitchell*, 1993; *Santamarina et al.*, 2001].

Sources for Figure 3.2 MIP data from [Ahmed *et al.*, 1974; AlMukhtar *et al.*, 1996; Bolton *et al.*, 2000; Cuisinier and Laloui, 2004; Delage and Lefebvre, 1984; Delage *et al.*, 1996; Dewhurst *et al.*, 1998; Dewhurst *et al.*, 1999; Diamond, 1971; Garcia-Bengochea *et al.*, 1979; Griffiths and Joshi, 1989; 1990; Heling, 1970; Horsrud *et al.*, 1998; Juang and Holtz, 1986; Lapierre *et al.*, 1990; Lohnes *et al.*, 1976; Penumadu and Dean, 2000; Simms and Yanful, 2001; 2004; Sridharan and Altschaeffl, 1971; Tanaka *et al.*, 2003; Vasseur *et al.*, 1995; Yang and Aplin, 1998]. SEM pictures from [Delage and Lefebvre, 1984; Griffiths and Joshi, 1990; Hicher *et al.*, 2000; Negre *et al.*, 2004].

Data Synthesis: Presence of Bacteria in Sediments

The compiled data shown in Figure 3.3 emphasize the presence of bacteria in sediments with representative grain size $d_{10} > 1 \mu\text{m}$. Reduced biodiversity is reported in various cases that either involve sediments with $d_{10} < 1 \mu\text{m}$ or high burial depth. Positive reports are predominant for silts and sands. In contrast, there is limited data for finer sediments, and contamination is suspected in some cases (as reported by some of authors). It is important to note that bioactivity at depth may be restricted by other limiting factors such as lack of nutrients. Therefore published data (in the absence of contamination) should be considered as one-way indicators: documented bioactivity suggests that proper conditions exist; however, the absence of bioactivity does not necessarily imply geometric/mechanical limiting conditions.

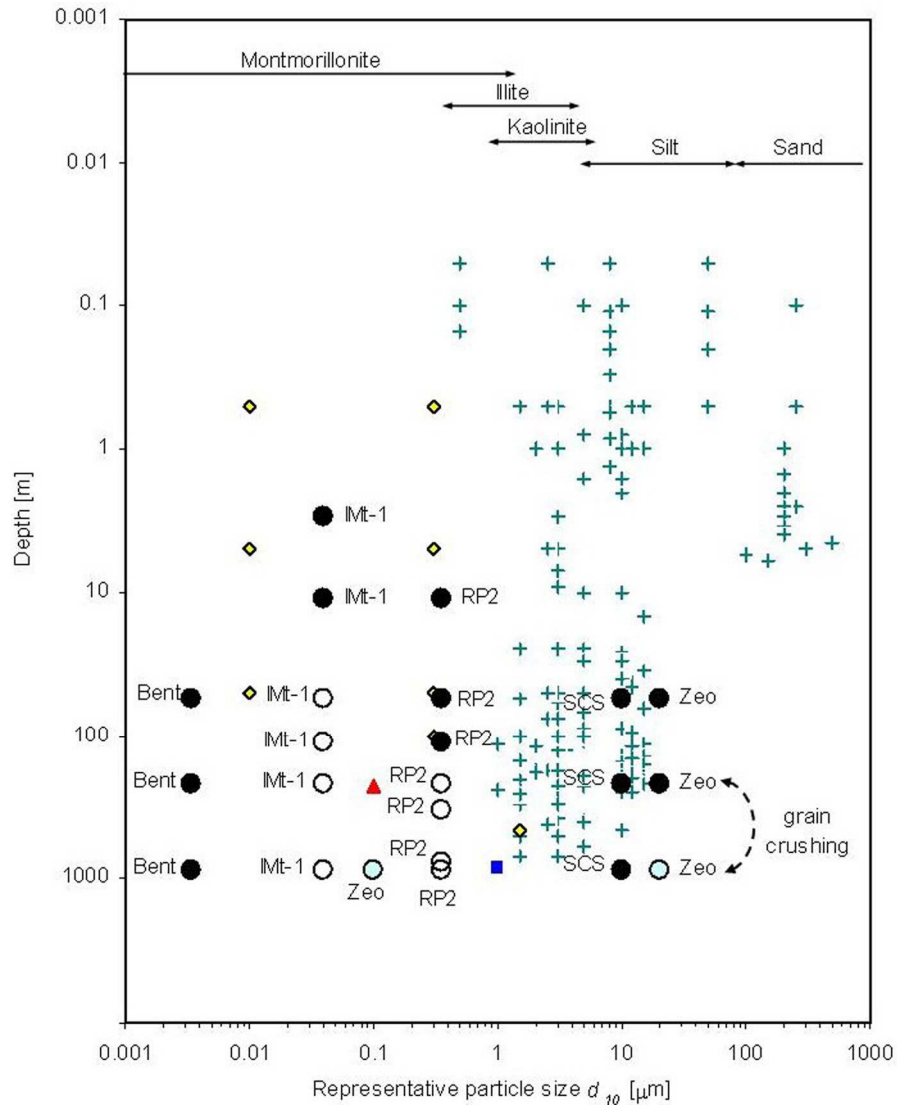


Figure 3.3 Presence of bacteria in sediments. Detected bacteria (crosses +), reduced diversity–nondividing cells (open diamonds ◆), possible contamination (triangle ▲) (as reported by the authors). Lack of reported data in certain regions does not imply impossible living conditions. Experimental data gathered in this study: solid circles, alive; open circles, dead. Dashed curved arrow indicates negative plates in precipitated silica flour after grain crushing at high overburden stresses which causes a particle size reduction from ~20 μm to ~0.1 μm .

Sources for Figure 3.3 [Agnelli *et al.*, 2004; Bird *et al.*, 2001; Blume *et al.*, 2002; Boivin-Jahns *et al.*, 1996; Chen *et al.*, 2003; Cragg *et al.*, 1996; D'Hondt *et al.*, 2004; Dodds *et al.*, 1996; Fierer *et al.*, 2003; Fredrickson *et al.*, 1991; Phelps *et al.*, 1994; Sinclair and Ghiorse, 1989; Sinclair *et al.*, 1990; Wellsbury *et al.*, 1996; Wellsbury *et al.*, 2002; Zhang *et al.*, 1998]. Underlined data labels correspond to unsaturated sediment specimens. Data from [Agnelli *et al.*, 2004; Blume *et al.*, 2002; Chen *et al.*, 2003; Dodds *et al.*, 1996; Fierer *et al.*, 2003; Sinclair and Ghiorse, 1989] do not specify water saturation conditions; the remaining data correspond to presumably saturated sediments.

Experimental Results

The experimental study conducted to gather data for sediments and depths that are poorly constrained by the available field data was designed to provide either of two possible outcomes: “dead” when no colonies formed in culture plates after 24 hours, or “alive” when colonies were present in culture plates after 24 hours. Results are superimposed on Figure 3.3. Average plate counts for each sediment-stress pair are listed in Table 3.4. Note that some species may become non-culturable, yet be alive. This possibility is excluded from the analysis.

Table 3.4 Colony-Forming Units per mL of Sediment (CFU/mL-Sediment) in Specimens

Equivalent depth (m)	Bentonite (Bent)	Illite (IMt-1)	Kaolinite (RP2)	Crushed silica flour (Sil-co-sil)	Precipitated silica flour (Zeo)
3.0		$> 10^5$			
11.0		$> 10^5$	$> 10^5$		
55.2	$> 10^5$	0	$> 10^5$	12×10^3	$> 10^5$
110.3		0	8×10^3		
220.6	5×10^3	0	0	6×10^3	$> 10^5$
330.9			0		
772.2			0		(crushing)
882.5	2×10^3	0	0	5×10^3	0

Puncture appears as the most critical mechanism affecting the survivability of bacteria in clayey sediments. Possible variations in cell size, wall thickness and tensile strength have a small effect on the position of the boundaries when they are plotted in the large variable range captured in Figure 3.4.

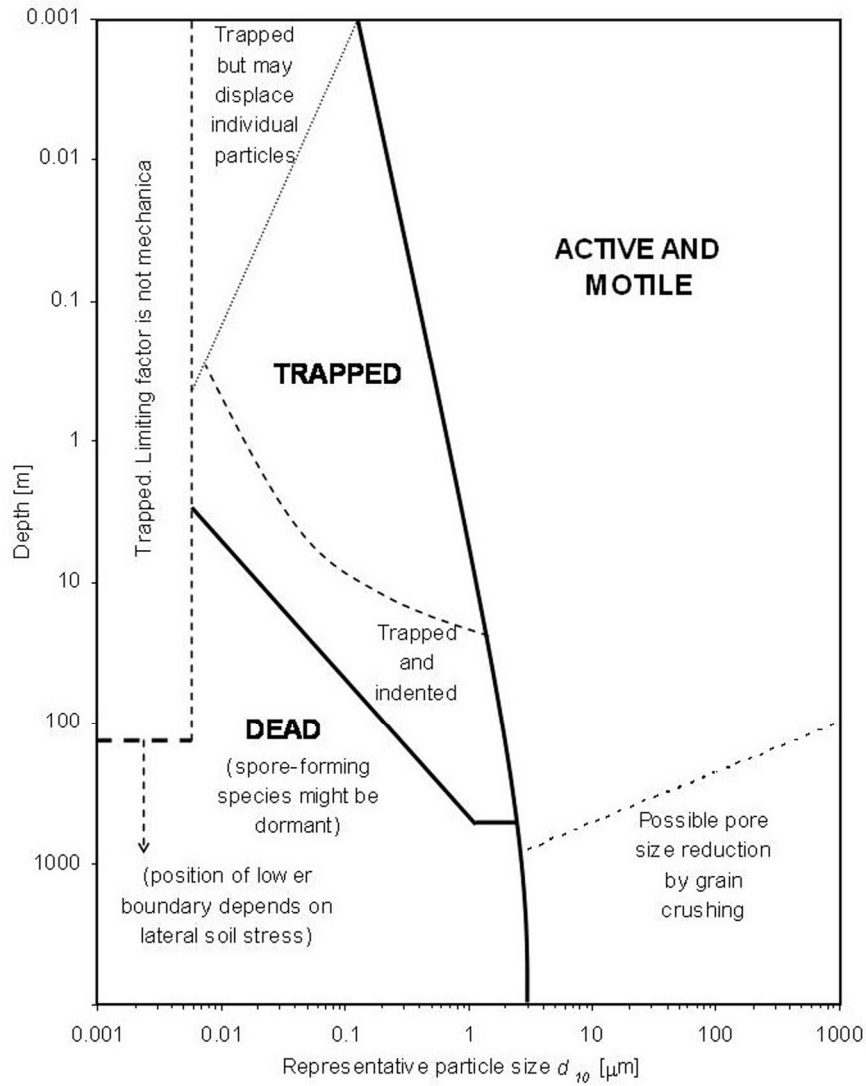


Figure 3.5 Bacteria's fate in sediments. Regions are defined by combining compiled evidence, new experimental data gathered in this study, pore and pore-throat data, and predicted bacteria-sediment mechanical interactions.

Discussion and Conclusions

Combined Effect of Geometric Constraints and Mechanical Interactions

Pore and pore-throat sizes correlate with grain size in silts and sands, where fabric formation is controlled by the particle self-weight and remain quite stable with stress changes. However, fabric formation is determined by electrostatic interactions in fine-grained clayey sediments, and the sediment structure experiences significant volumetric changes with increasing confinement [Bennett *et al.*, 1991; Mitchell, 1993; Santamarina *et al.*, 2001]. Note that pores in clayey sediments can be several times larger than the particles themselves, yet, relatively enclosed.

Regions for Bioactivity

Geometrical constraints and mechanical interactions suggest different regions for bacteria's fate, identified in Figure 3.5. (a) "Active and motile" when pore and pore throats are large so that cells can move through the pore network and find sufficient space for growth and metabolic activity. (b) "Trapped inside pores" when pore throats hinder migration; this zone can be subdivided into three subzones depending on the bacteria's ability to push particles and the size of the habitable pore space. (c) "Dead" when burial depths exceed the puncturing and/or squeezing thresholds; spore-forming species may remain dormant, as illustrated in Figure 3.5. Bacteria in the region that corresponds to very small particle sizes, beyond the buckling limit, may not be mechanically compromised, yet their survivability will be limited by nutrient and waste transport. The geometrical and mechanical constraints to microbial activity identified in Figure 3.5 apply to fracture-free sediments; the pore size distribution and inter-particle forces in the gauge material within fractures may deviate from those imposed by lithostatic stresses assumed in this study.

Summary

The extensive biological activity observed in the near-surface cannot be presumed a priori in deep sediments. Pore and pore-throat sizes restrict habitable pore space and traversable interconnected porosity. Furthermore, sediment-cell interaction may cause puncture or tensile failure of the cell membrane. These results restrict the range of grain size and burial depth where biomediated geochemical processes can be expected in sediments, affect the interpretation of geological processes and the development of engineering solutions such as bioremediation.

CHAPTER 4

MECHANICAL EFFECTS OF BIOGENIC GAS IN SOILS

Introduction

The undrained strength as well as the liquefaction resistance can be enhanced by reducing the contractive tendency of soils (i.e., through densification), increasing their threshold strain (e.g., by injecting foams or plastic fines [*Gallagher and Mitchell*, 2002]), increasing their small strain stiffness (i.e., light cementation to prevent early pore pressure generation [*Ismail et al.*, 2002]), or by decreasing their pore fluid bulk stiffness [*Yang et al.*, 2004; *Yegian et al.*, 2007]. The field application of these alternatives can be restricted by the presence of nearby constructions, high cost, uncertainty of execution, or possible environmental implications.

The fluid bulk stiffness is very sensitive to the presence of gas, and a small volume of bubbles can significantly affect the pore pressure response to loading including the value of Skempton's B parameter, P-wave velocity and liquefaction resistance [*Chaney*, 1978; *Fourie et al.*, 2001; *Ishihara et al.*, 1998; *Kokusho*, 2000; *Tamura et al.*, 2002; *Yegian et al.*, 2007; *Yoshimi et al.*, 1989]. Pore fluid softening by gas injection is limited by the percolation of air bubbles along preferential paths formed by interconnected large pore throats, thus failing to create a homogeneous distribution of small bubbles. On the other hand, methods that cause a relatively homogeneous distribution of air bubbles in the pore fluid, such as gas generation by electrolysis [*Yegian et al.*, 2007], appear effective in reducing the liquefaction potential of soils.

Gas bubbles may also accumulate in otherwise saturated soil matrices through gas dissolution and air trapping during infiltration and/or rapid water table rise [*Constantz et al.*, 1988; *Fayer and Hillel*, 1986] or in-situ anaerobic microbial respiration [*Buttler et al.*,

1991; *Dinel et al.*, 1988]. Previous studies on biogenic gas bubbles in soils are mainly related to the effect of bubbles on compressibility and undrained strength of shallow sediments containing relatively large gas-filled cavities surrounded by a matrix of saturated soil [*Sills et al.*, 1991; *Sills and Gonzalez*, 2001]. The influence of relatively small biogenic gas bubbles on the undrained response of sediments and their potential effects in liquefaction resistance and P-wave velocity requires further research.

The purposes of this study are to review known bacterial metabolisms that generate gas as a by-product, to conduct an experimental study to improve the understanding of the process of biogenic gas generation in soils, and to analyze the data using poroelastic models that capture the influence of gas bubbles on P-wave velocity and Skempton's B parameter.

Review on Biogenic Gas Bubbles

Biogenic Gas

Biologically mediated processes can lead to the production of gases in porous media, as shown in Table 4.1 [*Adams et al.*, 1990; *Soares et al.*, 1988; *Wheeler*, 1988]. Table 4.1 summarizes the conditions and species involved in biogenic gas generation in previous studies reported in the literature. Gas production tends to mimic bacteria population growth rates, and therefore can be controlled by limiting bacterial activity through nutrient availability, and environmental conditions such as temperature, among other factors [*Sills and Gonzalez*, 2001]. Pore scale geometric limitations also apply [*Rebata-Landa and Santamarina*, 2006].

Table 4.1 Previous studies on biogenic gas generation

Species	Remarks	Gases	Reference
Indigenous bacteria from two mine soils in East Texas, USA	NO ₃ ⁻ added No NO ₃ ⁻ added NO ₃ ⁻ + H ₂ O added	N ₂ O N ₂	[Johns <i>et al.</i> , 2004]
Indigenous bacteria from interstitial waters of sulfate-depleted marine sediments	After sulfate depletion Rate of ~ 13 µmole/liter/day	CH ₄	[Martens and Berner, 1974]
Indigenous bacteria from a Brookston loam	NO ₃ ⁻ added	N ₂ O N ₂	[Firestone <i>et al.</i> , 1980]
<i>Methanobacterium thermoautotrophicum</i>	Methane production started after 1 hour lag and ceased after 5 hours	CH ₄ H ₂	[Daniels <i>et al.</i> , 1980]
Indigenous bacteria from soils used for tomato plants	After a lag phase of ~20 hours, gas was produced for 75 hours	H ₂	[Logan <i>et al.</i> , 2002]
Mixed anaerobic bacteria	Gas production inversely proportional to SRT. Total gas production ranged from 4 to 10 liter/day	CH ₄ H ₂	[Nakamura <i>et al.</i> , 1993]
<i>Clostridium acetobutylicum</i>	Vigorous gas production	CO ₂ H ₂	[Behlulgil and Mehmetoglu, 2002]
Indigenous bacteria from soil at an experimental site	Maximum gas production started after 71 hours	N ₂ O N ₂	[Cardenas <i>et al.</i> , 2003]
Mixed denitrifying bacteria	Nitrogen gas (N ₂) was present almost entirely in the gas phase	N ₂ O N ₂ CO ₂	[Chung and Chung, 2000]
Indigenous bacteria from an estuarine clayey silt	Gas produced after 21 days and held in the sediment bed for the next 17 days	CH ₄ CO ₂	[Sills and Gonzalez, 2001]
Indigenous bacteria from a wood compost bed medium	NO _x removal (and presumed N ₂ production) was rapidly performed in batch studies	N ₂ N ₂ O	[Barnes <i>et al.</i> , 1995]
Indigenous bacteria from a fluvic hypercalcaric cambisol	Ratio N ₂ O/(N ₂ O+N ₂) was around 0.54 in all cases	N ₂ O N ₂ CO ₂	[Cannavo <i>et al.</i> , 2004]

The most common biogenic gases found in near-surface soils are CO₂, H₂, CH₄ and N₂. Carbon dioxide CO₂ has high solubility in water causing low residency time; methane CH₄ is a green house gas; and both methane and hydrogen are combustible. On the other hand, nitrogen gas N₂ presents several advantages within the scope of this investigation: it is neither explosive nor a greenhouse gas and its solubility in water is very low (as indicated by Henry's values in Table 4.2), therefore less gas is needed to produce bubbles and bubbles will remain undissolved for longer periods of time.

Table 4.2 Common metabolisms that generate gas as a byproduct

Metabolism	Bio-mediated reaction	Generated gas	Henry's constant k_h [m/atm] ¹
Aerobic respiration	$\text{CH}_2\text{O} + \text{O}_2 \rightarrow \text{CO}_2 + \text{H}_2\text{O}$	Carbon dioxide CO ₂	3.4×10^{-2}
Fermentation	$\text{CH}_2\text{O} \rightarrow 0.333 \text{ CH}_3\text{COOH} + 0.333 \text{ CO}_2 + 0.667 \text{ H}_2$	*hydrogen H ₂	7.8×10^{-4}
Denitrification	$\text{CH}_2\text{O} + 0.8 \text{ NO}_3^- + 0.8 \text{ H}^+ \rightarrow \text{CO}_2 + 0.4 \text{ N}_2 + 0.35 \text{ H}_2\text{O}$	* nitrogen N ₂	6.5×10^{-4}
Methanogenesis	$\text{CH}_2\text{O} \rightarrow 0.5 \text{ CH}_4 + 0.5 \text{ CO}_2$	* methane CH ₄	1.4×10^{-3}

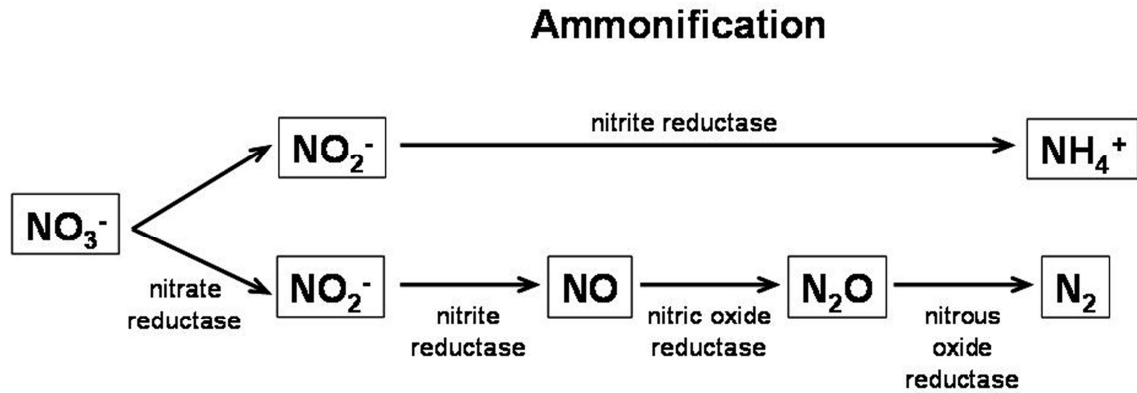
* besides CO₂.

¹ [Wilhelm *et al.*, 1977]

Nitrate Reduction and Respiratory Denitrification in Soils

Nitrate can be reduced in the environment through the direct path of ammonification in which the product is ammonia, or take the indirect path of respiratory denitrification in which products can be nitric oxide, nitrous oxide and nitrogen gas; the two paths are shown in Figure 4.1. The relative contribution of denitrification and nitrate ammonification is a function of the carbon-to-nitrate ratio [Tiedje *et al.*, 1982]. While denitrification dominates in environments rich in nitrate but relatively deficient in electron donors, ammonification is largely favorable in electron-rich environments where

only low concentrations of nitrate are available [Cole and Brown, 1980; Forsythe et al., 1988].



Respiratory denitrification

Figure 4.1 Nitrate and nitrite reduction - Enzymes involved. Pathway $\text{NO}_3^- - \text{NO}_2^- - \text{NH}_4^+$ corresponds to nitrate/nitrite ammonification, while $\text{NO}_3^- - \text{NO}_2^- - \text{NO} - \text{N}_2\text{O} - \text{N}_2$ corresponds to respiratory denitrification [Mohan et al., 2004; Moura and Moura, 2001; Richardson et al., 2001; Simon, 2002].

In respiratory denitrification, nitrate is reduced to dinitrogen through a battery of reactions catalyzed by specific enzymes, as indicated in Figure 4.1 [Mohan et al., 2004; Moura and Moura, 2001; Richardson et al., 2001; Simon, 2002]. Denitrification not always reaches the last step of N_2 formation with 100% efficiency (lower branch in Figure 4.1); hence, the produced gas is a combination of N_2O and N_2 at variable ratios [Barnes et al., 1995; Chung and Chung, 2000; Davidson et al., 1993; Firestone et al., 1980; Johns et al., 2004]. The most relevant factors influencing the ratio $\text{N}_2\text{O}/\text{N}_2$ include: the presence of specific genes encoding the required enzymes in the bacterial species involved in the process, the ratio C/N [Chung and Chung, 2000], the soil acidity and aeration [Barnes et al., 1995; Firestone et al., 1980; Johns et al., 2004], the soil texture and nutrient status [Johns et al., 2004], and the soil moisture [Davidson et al., 1993]. The reduction of N_2O to N_2 is more effective under alkaline conditions since the activity of

denitrifiers is higher when the surroundings pH ranges from pH 6 to 8. In soils with very high moisture, N_2 can be a significant end-product of denitrification, while in relatively dry soils N_2 production by denitrification is generally rare and N_2O becomes the dominant end-product [Davidson *et al.*, 1993]. It is important to highlight that this is a proof-of-concept study: nitrate and other by-products of denitrification are EPA regulated contaminants and no action to increase their concentration could be applied in the field.

Gas Bubble Nucleation

Biogenic gases dissolve in the pore fluid, i.e., gas molecules occupy cavities between water molecules, until the fluid reaches the supersaturation threshold that prompts bubble nucleation [Ronen *et al.*, 1989]. Spontaneous bubble nucleation, can result from: (1) depressurization below the vapor pressure of the pure liquid, (2) temperature increase until the vapor becomes more stable than the pure liquid, or (3) by gas dissolution from a supersaturated liquid when the supersaturation exceeds certain threshold values [Hemmingsen, 1975; 1977; Lubetkin, 2003].

Supersaturation thresholds for homogeneous nucleation in the bulk liquid are a function of molecular interactions between the liquid and the dissolved gas, however, the presence of mineral surfaces tends to favor heterogeneous bubble nucleation at substantially lower supersaturations [Blander, 1979; Gerth and Hemmingsen, 1980; Pease and Blinks, 1947]. Nucleation centers in porous media, include microcavities, irregularities and impurities at mineral surfaces [Dominguez *et al.*, 2000].

Once supersaturation is reached, the pore water pressure u approaches the pressure in the gas p_g (partial pressure when a single gas specie is taken into account), and bubbles form unless the pressure in the fluid increases. The concentration of gas in the aqueous phase c_a is related to the gas pressure through Henry's constant k_H as captured in Henry's Law:

$$k_H = \frac{c_a}{p_g} \quad \text{Henry's Law} \quad (4.1)$$

Henry's constant depends on the gas species (see Table 4.2 for typical values). The tiny bubbles or “embryos” that form at bubble nucleation sites are stable only after reaching a critical size [Finkelstein and Tamir, 1985; La-Mer, 1952; Ward *et al.*, 1970]. The critical radius $r_{critical}$ is defined as [Lubetkin, 2003]:

$$r_{critical} = \frac{2 \cdot T_s}{\sigma \cdot u} \quad (4.2)$$

where T_s is the surface tension (~ 0.072 N/m for water at 20°C), σ is the supersaturation and u is the pressure at which bubbles nucleate. Notice that surfactants are generated as a product of bacterial metabolism, and they can decrease the surface tension of water to a value as low as 0.027 N/m; the following calculations assume $T_s = 0.072$ N/m to compute lower-bound estimates of bubble impact on bulk stiffness. Bubbles smaller than $r_{critical}$ tend to re-dissolve into the pore fluid. On the other hand, stable bubbles $r > r_{critical}$ can migrate and/or coalesce to form larger bubbles that can eventually become trapped at pore throats defining Laplacian capillary surfaces (i.e. water-vapor interfaces that satisfy Laplace's equation). When Henry's Law applies, supersaturation is defined as:

$$\sigma = \frac{c_{gen}}{c_{eq}} - 1 \quad (4.3)$$

where c_{gen} is the gas concentration in the fluid, c_{eq} is the gas concentration soluble in the liquid under the prevailing experimental conditions.

In most cases, theoretical arguments predict much higher supersaturations than experimentally found [Lubetkin, 2003]. These differences point to the use of macroscopic values for surface tension to analyze very small clusters representing subcritical and critical nuclei [Lubetkin, 2003], the reduction of free energy needed to create a critical bubble nucleus due to geometrical imperfections [Wilt, 1986], the existence of “active sites” on a heterogeneous surface that can be chemically, structurally or geometrically

inhomogeneous and therefore more catalytic than others [Deutscher and Fletcher, 1990; Kozisek *et al.*, 2000], inhomogeneous supersaturation away from thermodynamic equilibrium [Li and Yortsos, 1994], and secondary nucleation, whereby pre-existing bubbles behave as nucleation centers for new bubbles [Bergman and Mesler, 1981].

A compilation of experimentally determined supersaturation values for different gases is presented in Table 4.3 [Lubetkin, 2003]. These values, combined with Equation 4.2, can be used to estimate the range of critical size of bubble nuclei for a specific gas species. Figure 4.2 shows the range of critical size of bubble nuclei for nitrogen gas.

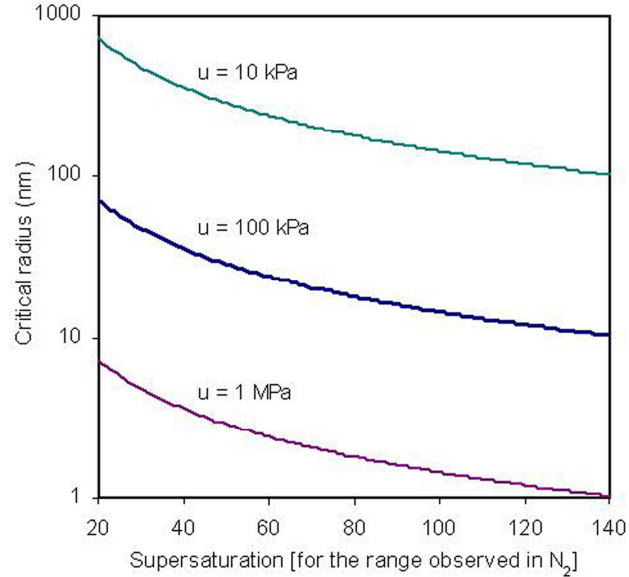


Figure 4.2 Critical radius for N_2 bubble nucleation under different bubble nucleation pressures and supersaturation values, calculated using Equation 4.2. Supersaturation range corresponds to the one observed experimentally in the literature (Table 4.3). The bubble nucleation pressure for experiments in this study can be considered equal to atmospheric pressure (~ 100 kPa, thickest line in the plot).

Table 4.3 Measured values of supersaturation needed to cause bubble nucleation in aqueous solutions. Compiled from [Lubetkin, 2003]

Gas	Measured supersaturation needed
Carbon dioxide CO ₂	4.62 – 20
Hydrogen H ₂	80 – 90
Nitrogen N ₂	19 – 140
Methane CH ₄	80

Note: Supersaturation is defined as: $\sigma = (c_{gen}/c_{eq}) - 1$, where c_{gen} is the gas concentration in the fluid, c_{eq} is the gas concentration soluble in the liquid under the experimental conditions used.

Experimental Study

This experimental study aimed to evaluate the ability of *Paracoccus denitrificans* to generate gas inside different soil types, to monitor gas bubble nucleation inside the soil matrix, and to assess the evolution of P-wave velocity in time. Additionally, the effects of nutrient availability and fines content on gas generation and P-wave velocity were also explored. As shown later, P-wave velocity was chosen due to the controlling effect of bulk stiffness on the behavior of materials near saturation. The study was limited to low-confinement, and most tests were conducted under no nutrient-recharge conditions.

Materials and devices

Sediments

Seven sediments were chosen for their particle size and compatible solution pH: Ottawa 20-30 sand (Ottawa, $d_{10} = 0.5$ mm, $d_{50} = 0.72$ mm, $C_u = 1.15$), F110 sand (F110 $d_{10} = 90$ μ m, $d_{50} = 0.12$ mm, $C_u = 1.62$), crushed silica flour (Sil-co-sil, $d_{10} = 10$ μ m, $S_a = 0.113$ m²/g), precipitated silica flour (Zeo; $d_{10} = 20$ μ m, $S_a = 6$ m²/g), RP2 kaolinite (RP2, $d_{10} = 0.36$ μ m, $S_a = 33$ m²/g Wilkinson), SA1 kaolinite (SA1, $d_{10} = 0.4$ μ m, $S_a = 36$ m²/g Wilkinson) and montmorillonite (Bent, $d_{10} = 0.0034$ μ m, $S_a = 200$ m²/g). Grain-size information was obtained following ASTM D 422, and the specific surface S_a was

measured using methylene blue [Santamarina *et al.*, 2002]. In addition, clayey-sand mixtures were prepared by combining these sediments.

Bacterial Species

The selected strain is *Paracoccus denitrificans* (ATCC 13543), a non-motile coccoid soil organism from the alpha subdivision of the proteobacteria. It is able to reduce nitrate to dinitrogen under anaerobic growth conditions (denitrification – Figure 4.1). The four oxido-reductases required for the denitrification pathway [Mohan *et al.*, 2004; Moura and Moura, 2001; Richardson *et al.*, 2001; Simon, 2002], along with their corresponding structural, accessory and regulatory genes, have been well characterized in *P. denitrificans* [Baker *et al.*, 1998].

Cells were grown in solid agar plates (Nutrient agar, Defco - Fisher Scientific) and incubated at their optimum temperature. Culture broth (Nutrient broth, Defco - Fisher Scientific) vials were inoculated with fresh colonies, grown for several days until reaching the late exponential phase (as verified in a previous study by the authors - results not shown), harvested, washed in saline solution and resuspended in a different culture broth (Nitrate broth Defco - Fisher Scientific) to enhance their denitrification potential. Previous studies using *P. denitrificans* and nitrate-rich broth corroborate the generation of nitrogen gas (*P. Sobecky*, 2007 - *personal communication*). The resuspended mixture will be referred to as the “bacterial inoculum”. In all tests, cells were resuspended immediately before specimen assemblage to prevent cell aging and deterioration.

Devices

The system consists of a set of square Nalgene bottles sealed using rubber stoppers with two exit ports (Figure 4.3). A capillary tube fitted through one port was used to determine the volume of produced gas. The other port was used to expel excess

air during the specimen assemblage and it was closed after assemblage (except in tests when it was used to inject additional nutrient at different time intervals).

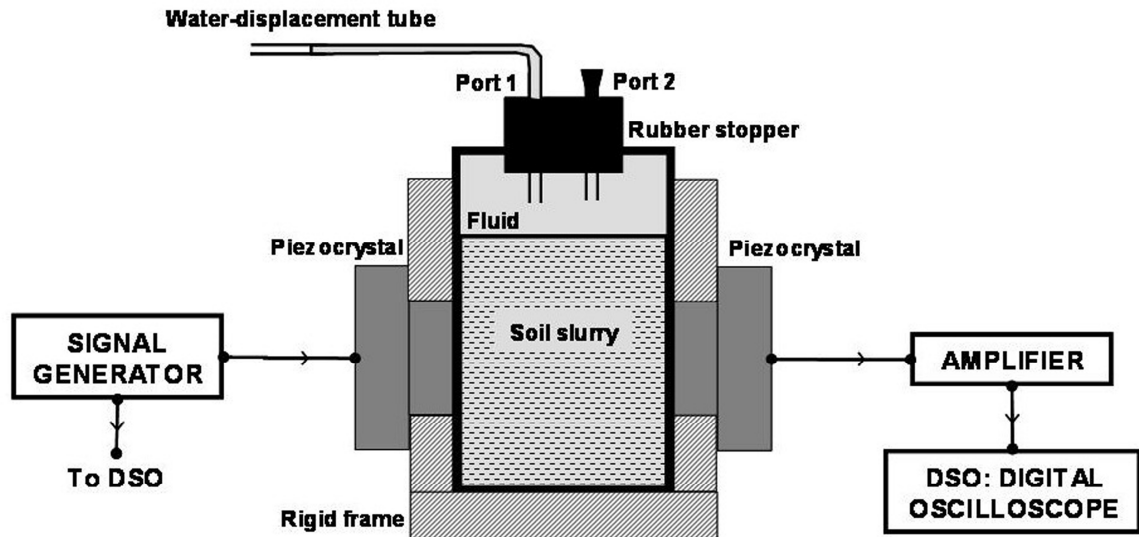


Figure 4.3 Experimental device and peripheral electronics.

P-wave velocity measurements across the specimens were performed using a set of piezocrystals (50 mm in diameter, resonant frequency of 50 kHz), that were externally coupled to the Nalgene bottles. The standard peripheral electronics used involved a pulse generator, amplifier, analog filter and oscilloscope.

Test Procedure

Specimen Preparation

All materials and equipment in contact with the bacterial inoculum (broths, agar, soils, water, capillary tubes, rubber stoppers and bottles) were sterilized using a steam autoclave at 124°C and 125 kPa for 35 min prior to assemblage. All assemblage processes were conducted under aseptic conditions.

Table 4.4 Tested Specimens - Preparation

Study	Soil	Soil (g)	Inoculum (mL)	Nutrient (mL)	Water (mL)
Study #1 and #2	Bent	49.7	10	200	200
	SA1	227.08	10	200	200
	RP2	223.67	10	200	200
	Zeo	66.01	10	200	200
	Sil	575.67	10	200	50
	F110 (1 st trial)	637.21	10	200	0
	F110 (2 nd trial)	640	10	200	0
Study #3	Ottawa	728.58	10	200	0
	Sil (a)	576	10	200	50
	Sil (b)	576	10	200	50
	F110 + 1% Bent	646.4	10	200	0
	F110 + 3% Bent	618	10	200	0
Study #4	F110 + 9% Bent	327	10	200	0
	F110 + 10% Bent	363	10	200	50
	F110 + 15% Bent	281.8	10	200	50
	F110 + 3% RP2	618	10	200	0
	F110 + 9% RP2	545	10	200	0
	F110 + 15% RP2	575	10	200	0

*Total soil weight. Mixtures are reported in percentage by weight.

Soil slurries were prepared by mixing specific amounts of each soil (or mixtures), bacterial inoculum and fresh nitrate broth, as indicated in Table 4.4. Slurries were poured into individual Nalgene bottles, subjected to vacuum to ensure initial saturation and filled to the top with deionized, sterile and deaired water. Rubber stoppers were set in place

along with the water-displacement capillary tube. Initial assessments of P-wave velocity were made, when the initial P-wave velocity values were lower than ~1400 m/s, additional vacuum was applied to remove any remaining gas to ensure that the initial soil saturation was $S \approx 100\%$.

Measurements

The P-wave velocity and the volume of produced gas (water displaced in the capillary tube) were recorded daily for a period of one month for all specimens. On day 30, some of the specimens were subjected to a step increase in pore fluid pressure of 20 kPa for 12 to 24 hours to monitor the partial recovery of P-wave velocity.

Study #1: Sterile Control

A parallel set of all seven soils was tested during 30 days using heat-killed bacteria instead of vegetative cells to verify that gas bubbles did not form and that the P-wave velocity remained constant under abiotic conditions.

Study #2: Single-grained Soils

The selected soils were tested with nutrient added only at time zero. All seven specimens were used for the additional pore fluid pressure step increase after 30 days.

Study #3: Nutrient Availability Effect

Two additional bottles containing Sil-co-sil were used, to study the influence of nutrient availability on P-wave velocity and generated gas evolution. Initial conditions were identical to those in Study #2. After the first measurement, one bottle (A) was injected with 1 mL of fresh Nitrate broth daily, while the other bottle (B) was injected again 10 and 20 days after assemblage with 10 mL of fresh Nitrate broth each time.

Study #4: Mixed soils – Effects of fines content

Eight bottles containing F110 sand with different amounts and types of fines were tested to explore the role of mineral surfaces and gas entrapment. Bottle A contained only F110 sand, bottles B, C, D, and E contained 3%, 9%, 10% and 15% bentonite respectively, and bottles F, G and H contained 3%, 9% and 15% RP2 kaolinite respectively. Bottles C and G (containing 9% bentonite and 9% RP2 kaolinite respectively) were also used for the pore fluid pressure step test.

The complete data set and results for these studies can be found in Appendix B and C. Specific results and observations follow.

Results and Observations

Typical sets of P-wave signatures are presented in Figure 4.4 for F110 sand mixed with different percentages of RP2 kaolinite. Similar results were observed when F110 sand was mixed with bentonite. Figure 4.5 shows the evolution of P-wave velocity and generated gas volume versus time for F110 sand mixed with different percentages of bentonite. Analogous results were observed when F110 sand was mixed with RP2 kaolinite. Once again, parallel measurements were gathered for all specimens. These results suggest a strong correlation between biogas volume generation and P-wave velocity evolution.

The P-wave velocity remained unchanged and no gas was generated in all sterile controls (Study #1 - data not shown here); therefore we can assume that all changes observed in Figures 4.4 and 4.5 are due to the biogenic gas generation inside the sediment.

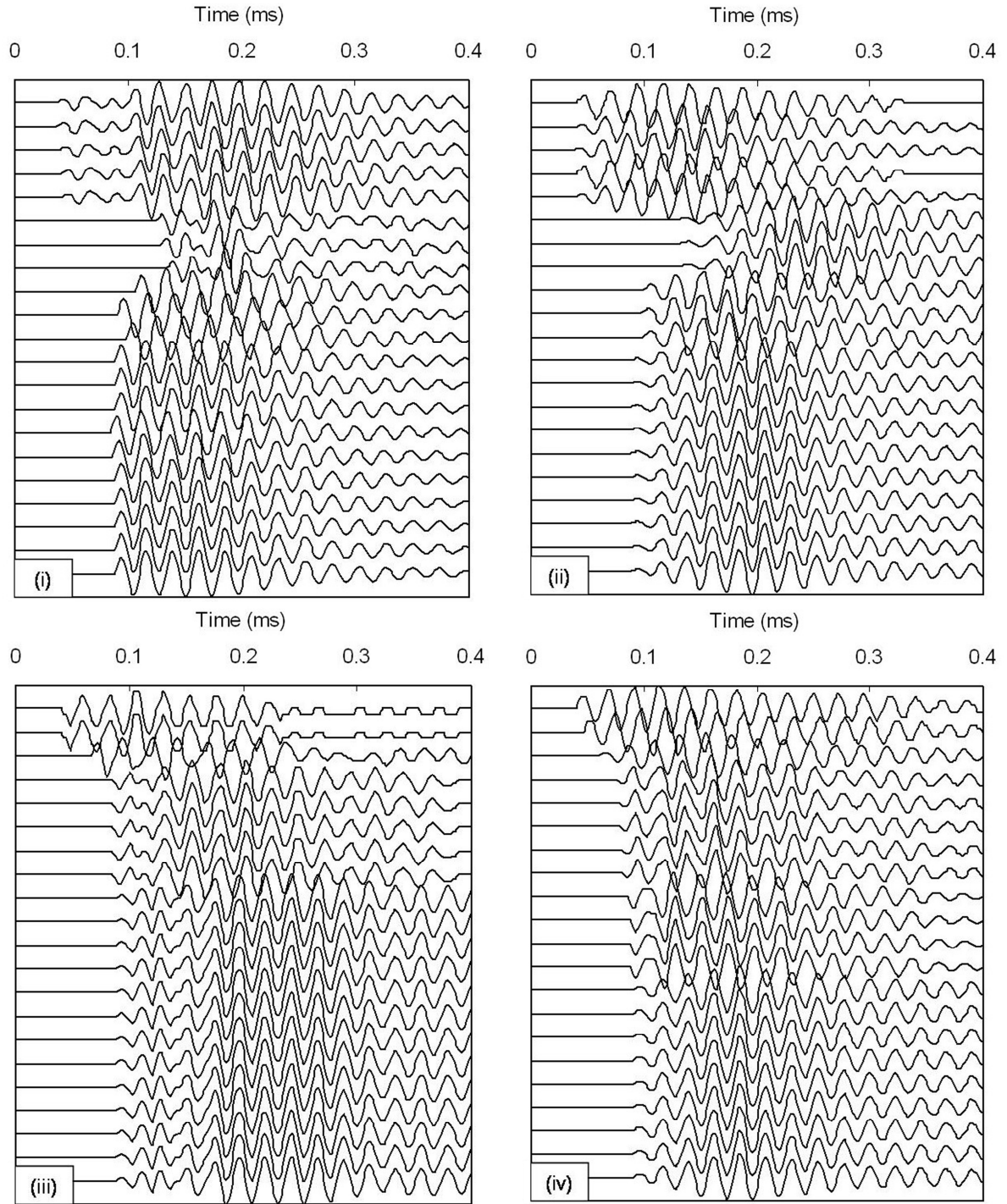


Figure 4.4 Evolution of P-wave signatures during biogenic gas formation. (i) F110 sand without fines. (ii) F110 + 3%RP2. (iii) F110 + 9%RP2. (iv) F110 + 15%RP2. The first signal in each sequence was gathered immediately after the initiation of the test. Successive signals were captured every day thereafter.

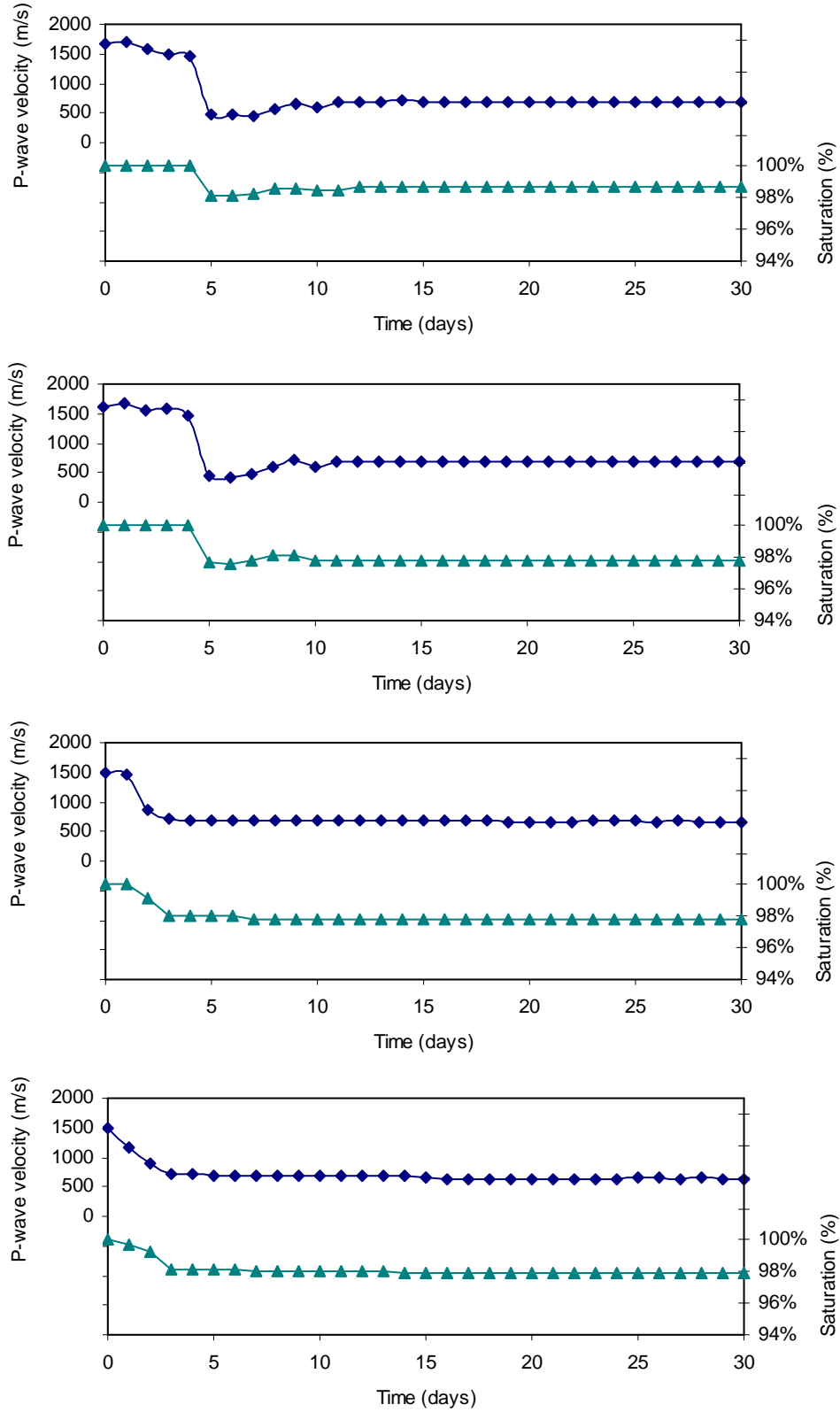


Figure 4.5 P-wave velocity and saturation for (i) pure F110 sand, (ii) F110 + 3% bentonite, (iii) F110 + 9% bentonite and (iv) F110 + 15% bentonite.

The initial ($t \sim 0$) and final ($t \sim 30$ days) values of P-wave velocity for all specimens are plotted versus specific surface in Figure 4.6. In all cases, P-wave velocity seems to stabilize around $V_p = 500$ - 600 m/s. Results summarized in Figure 4.6 also indicate that P-wave velocity can be further modified by consecutive nutrient injections (Study #3). This suggests that the minimum P-wave velocity is not necessarily a boundary imposed by the system but a limitation due to nutrient exhaustion, and thus, nutrient availability could be used as a tool to control the extent of biogas generation in the soil.

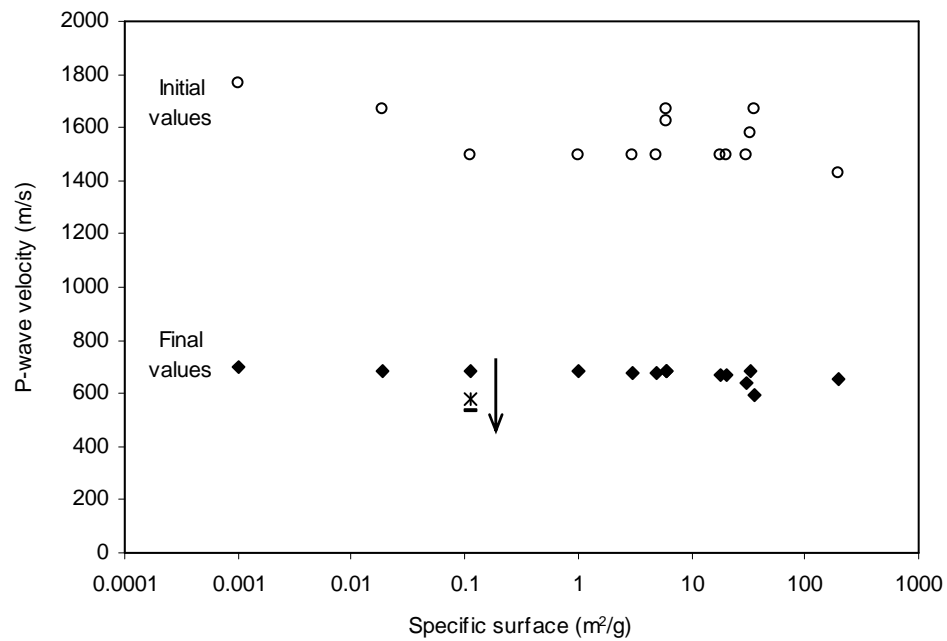


Figure 4.6 Initial ($t = 0$) and final ($t = 30$ days) steady-state P-wave velocity for all specimens, both single-grained soils and mixtures, as a function of the specific surface. The arrow (data for Sil-co-sil) shows the effect of nutrient injections on final P-wave velocity. Original specimens appear as a solid diamond. The two specimens that received nutrient injections daily and every 10 days are shown as an asterisk and a dash respectively.

Figures 4.4 and 4.5 show that changes in P-wave velocity and gas generation are triggered earlier in specimens with higher fines content (Studies #2 and #4). When the percentage of fines is lower than 9% (both kaolinite and bentonite), abrupt changes in P-wave velocity and generated gas volume are followed by a partial recovery to finally reach a stable value. This transient is not observed in soils with higher fines content.

Pore Fluid Pressure Step

The time-dependent increase in P-wave velocity for the nine tested specimens is plotted in Figure 4.7. Note that while the 20 kPa increase in pore fluid pressure is applied almost instantaneously, it takes about 15 hours for the P-wave velocity to stabilize.

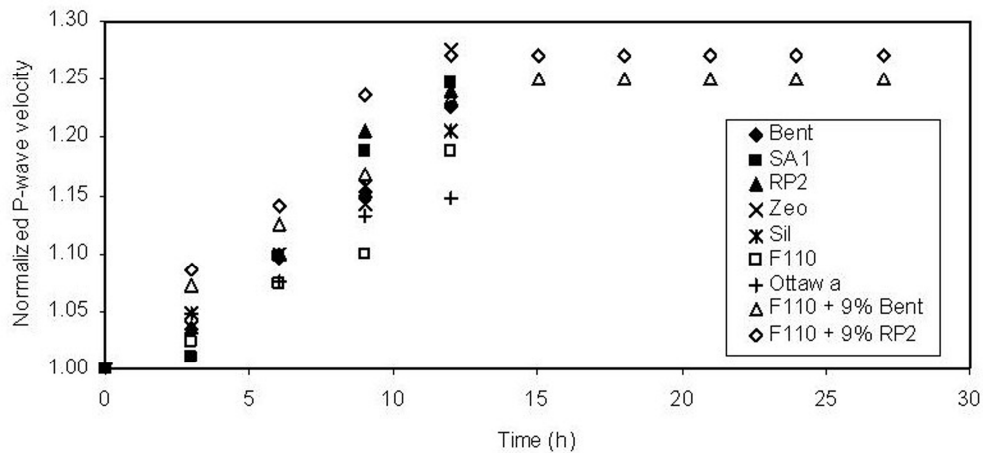


Figure 4.7 P-wave velocity recovery as a function of time after the step increase in the pore fluid pressure. The pressure was increased from the initial value equal to the atmospheric pressure to a constant value of $u = 20$ kPa above the atmospheric pressure.

Dismantling Specimens

All bottles were sealed and vigorously shaken by hand before disposal. Gas bubbles coalesced and formed larger bubbles that could be seen by the naked-eye and raised towards the surface. Specimens with high fines content required significantly more

shaking than those with low fines content to release the gas, clearly showing the role of fines in gas entrapment.

Analysis and Discussion

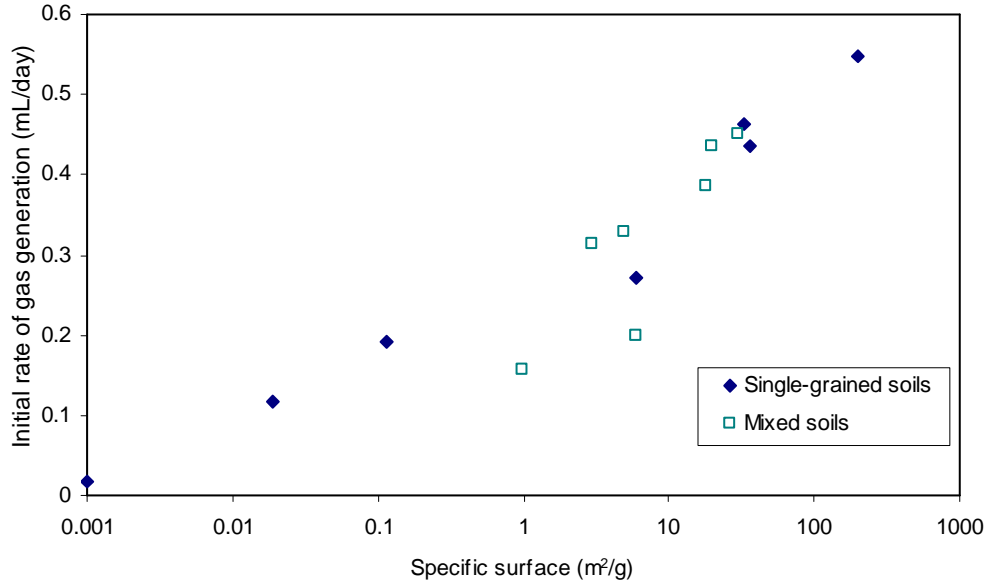
Low Pore Fluid Pressure Effect

These tests were performed at very low pore fluid pressures. In field conditions where higher pore fluid pressures are expected (10 – 100 kPa above atmospheric pressure), gas bubble generation would require production of higher amounts of gas due to higher solubility according to Henry's Law (Equation 4.1) and to higher pressures (less volume of bubbles for the same mass of gas).

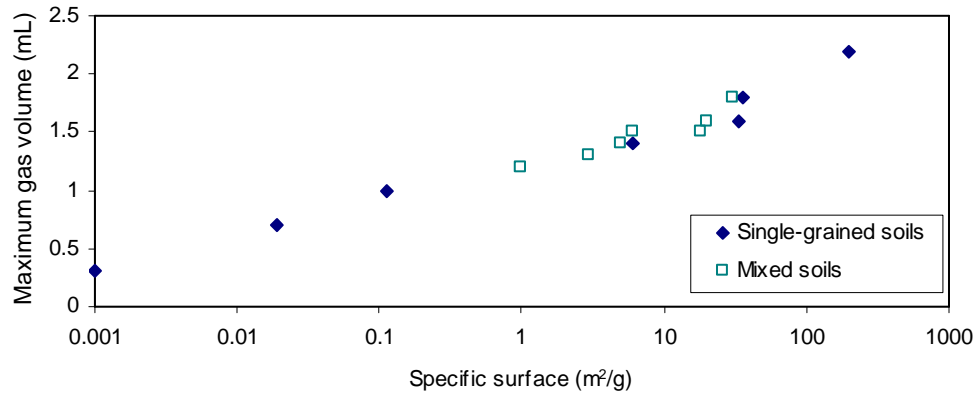
Fines Content Effect

No transient was observed in the P-wave velocity versus time data (Figure 4.4) for soils with some fines content. Apparently, fines hinder the motion of gas bubbles which remain trapped in the soil matrix. On the contrary, bubbles can escape in the absence of fines and the P-wave velocity partially recovers, causing the observed transient in the data.

The initial gas generation rate and the maximum volume of generated gas is plotted versus specific surface in Figure 4.8. The strong correlation observed for all tested sediments suggests that biogas bubble formation develops as heterogeneous nucleation and it is directly linked to the availability of nucleation sites on mineral surfaces, which in turn, also affects the degree of attainable supersaturation.



(a)



(b)

Figure 4.8 (a) Initial rate of gas generation and (b) maximum volume of generated gas versus specific surface. For clarity, the cases with additional nutrient are not included.

Gas Bubbles and Bulk Stiffness – Bubble Size

Bubbles much smaller than soil particles can fit within the pore space without distorting the soil structure; thus, the presence of gas bubbles only changes the compressibility of the pore fluid [Wheeler, 1988]. Even relatively small size bubbles are

sufficient to significantly change the pore fluid bulk stiffness [Sparks, 1963]. The pore fluid bulk stiffness κ_f depends on the degree of saturation S , the bulk stiffness of water κ_w (~2.2 GPa) and the bulk stiffness of gas bubbles κ_b . Relevant mixture formulas are summarized in Table 4.5.

Table 4.5 Bulk stiffness, mass density and propagation velocity (extracted from [Santamarina et al., 2001]).

Parameter	Equation
(a) Fluid bulk stiffness	$\kappa_f = \frac{1}{\frac{S}{\kappa_w} + \frac{1-S}{\kappa_b}}$
(b) Bulk stiffness of a soil suspension	$\kappa_{sus} = \frac{1}{\frac{n}{\kappa_f} + \frac{1-n}{\kappa_g}}$
(c) Bulk stiffness of a fluid-filled soil*	$\kappa_{soil} = \kappa_{sk} + \kappa_{sus} = \kappa_{sk} + \frac{1}{\frac{n}{\kappa_f} + \frac{1-n}{\kappa_g}}$
(d) Mass density	$\rho_{soil} = (1-n) \cdot \rho_g + n \cdot S \cdot \rho_w$
(e) P-wave velocity	$V_P = \sqrt{\frac{\kappa_{soil} + \frac{4}{3}G_{soil}}{\rho_{soil}}}$
(f) S-wave velocity	$V_S = \sqrt{\frac{G_{soil}}{\rho_{soil}}}$

Where n is the porosity, S is the degree of saturation, κ_{soil} , κ_{sk} , κ_{sus} , κ_g , κ_f , κ_w and κ_b are the bulk stiffness of the mixture, the soil skeleton, the soil suspension, the soil particle (material that forms the grains ~ 37 GPa), the pore fluid, the water (~2.2 GPa) and the gas bubbles, respectively, V_P and V_S are the P-wave and S-wave velocity, respectively, G_{soil} is the shear stiffness of the soil mass and ρ_{soil} is the mass density of the soil mass.

*Applicable to near surface soils at low confinement, where $\kappa_g \gg \kappa_{sk}$ otherwise the Gassmann equation must be used instead.

The bulk stiffness of bubbles can be estimated by defining bulk stiffness as:

$$\kappa_b = \left| \frac{\partial P}{\partial V/V_0} \right| \quad (4.4)$$

where the volume V of a bubble is a function of its radius r :

$$V = \frac{4}{3} \cdot \pi \cdot r^3 \quad (4.5)$$

and the gas pressure inside the bubble P , under the assumptions that: (a) the bubbles are isolated, (b) there is a continuous water phase and (c) the vapor-water interface is not in contact with the mineral surfaces, is related to the pressure in the surrounding water u_w and the surface tension T_s according to Laplace's equation:

$$P = u_w + \frac{2 \cdot T_s}{r} \quad (4.6)$$

Therefore the bubble bulk stiffness is:

$$\kappa_b = \frac{2 \cdot T_s}{3 \cdot r} \quad (4.7)$$

Combining Equation (a) from Table 4.5 and Equation 4.7, the fluid bulk stiffness becomes:

$$\kappa_f = \frac{1}{S \frac{1}{\kappa_w} + (1-S) \frac{3 \cdot r}{2 \cdot T_s}} \quad (4.8)$$

On the other hand, the bulk modulus of a suspension of mineral particles in a fluid κ_{sus} takes into account the volumetric changes in grains due to changes in pore fluid pressure, as indicated in Equation (b) in Table 4.5. In addition, when particles come into contact with each other, the granular skeleton shares the load with the fluid, resulting in Equation (c) in Table 4.5. These equations can be sequentially combined to obtain a general expression for the bulk stiffness of sediments in the presence of disseminated gas bubbles:

$$\kappa_{soil} = \kappa_{sk} + \frac{1}{n \left[S \frac{1}{\kappa_w} + (1-S) \frac{3 \cdot r}{2 \cdot T_s} \right] + \frac{1-n}{\kappa_g}} \quad (4.9)$$

In laboratory and field applications, the global bulk stiffness of the soil κ_{soil} and its skeletal stiffness κ_{sk} can be inferred from P and S wave velocity measurements, as indicated in Table 4.5. Then, these expressions permit estimating the average bubble radius as a function of P and S-wave velocity and degree of saturation (for $S < 1$):

$$r = \frac{2 \cdot T_s}{3 \cdot (1-S)} \cdot \left[\frac{1}{n} \left[\frac{1}{\rho_{soil} \left(V_p^2 - \left(\frac{4}{3} + \alpha \right) \cdot V_s^2 \right)} - \frac{1-n}{\kappa_g} \right] - \frac{S}{\kappa_w} \right] \quad (4.10)$$

where α depends on the Poisson's ratio of the skeleton ν_{sk} and varies between $\alpha = 0.92$ and $\alpha = 1.33$ for $\nu_{sk} = 0.1$ to $\nu_{sk} = 0.2$ respectively.

The evolution in average bubble radius was estimated for each experiment using this expression. Maximum values of average bubble radius ranged from 28 nm to 350 nm. These sizes are larger than the critical radius $r_{critical} = 10$ nm computed for the prevailing experimental conditions (atmospheric pressure, nitrogen gas - Figure 4.2) therefore, they are stable bubbles. No explicit correlation is found between the average bubble radius and the specific surface of the various sediments. In part this may reflect the combined effects of mean bubble size and variability. This is explored in Figure 4.9 where all experimental data are shown. Clearly, similar values of V_p can be obtained for the same saturation for different mean-variability pairs. Another important feature is captured in this plot: very small bubbles do not cause an immediate drop in bulk stiffness as the saturation decreases from 100%.

Microbial surfactants can decrease surface tension of water from 0.072 N/m to about 0.027 N/m. For simplicity, all calculations in this study assumed $T_s = 0.072$ N/m. Lower values of T_s imply even larger reductions in fluid bulk stiffness; therefore these calculations represent an upper-boundary for this process.

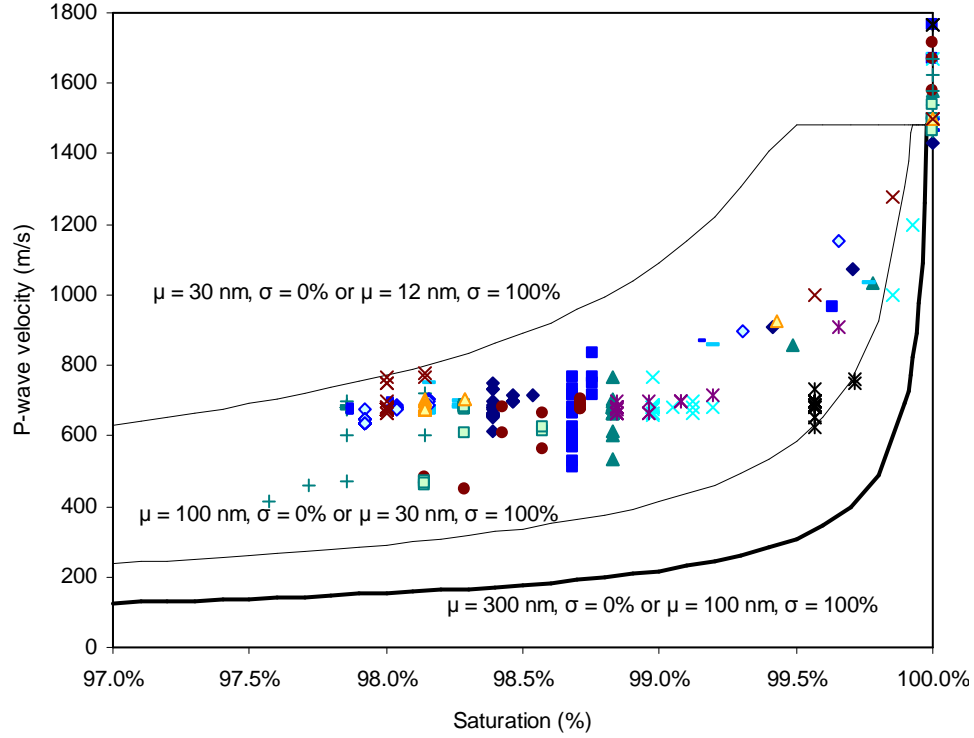


Figure 4.9 Saturation and P-wave velocity data for all tests (dots). Lines correspond to V_P calculated from fluid bulk stiffness ($G = 0$) as a function of saturation, bubble mean size μ , and variability σ (log-normal distributions of bubble size).

Skempton's B-value and P-wave Velocity

Skempton's B -value is the ratio of the change in pore fluid pressure Δu for a change in isotropic confinement $\Delta \sigma$ applied under undrained conditions [Skempton, 1954]:

$$B = \frac{\Delta u}{\Delta \sigma} \quad (4.11)$$

From poroelasticity, the parameter B can be expressed as a function of the bulk stiffness of the mineral that makes the grains κ_g , the granular skeleton κ_{sk} , and the whole soil mass κ_{soil} [Ishihara, 1970]:

$$B = \frac{1 - \frac{\kappa_{sk}}{\kappa_{soil}}}{1 - \frac{\kappa_{sk}}{\kappa_g}} \quad (4.12)$$

Replacing Equation 4.9 in 4.12, the asymptotic solution for B when $\kappa_{sk}/\kappa_g \rightarrow 0$, is [Skempton, 1954]:

$$B = \frac{1}{1 + n \cdot \frac{\kappa_{sk}}{\kappa_f}} \quad (4.13)$$

A convenient expression for Skempton's B parameter can be derived by substituting equations in Table 4.5, Equation 4.8 and Equation 4.10 in Equation 14.3:

$$B = \frac{1}{1 + \alpha \cdot \rho_{soil} \cdot V_s^2 \left[\frac{1}{\rho_{soil} \cdot \left(V_p^2 - \left(\frac{4}{3} + \alpha \right) \cdot V_s^2 \right)} - \frac{1-n}{\kappa_g} \right]} \quad (4.14)$$

While the S-wave velocity in granular media is determined by the skeletal stiffness and it remains practically unchanged during the early stages of unsaturation (i.e., κ_{sk} is not affected at low suction [Cho and Santamarina, 2001]), the P-wave velocity is controlled by the bulk stiffness of the pore fluid and it rapidly decreases as soon as $S < 1$ [Ishihara et al., 1998; Tsukamoto et al., 2002]. Hence, V_p is significantly larger than V_s near saturation ($V_s^2/V_p^2 \sim 0$). The validity of these expressions for B as a function of V_p is corroborated against experimental measurements in Figure 4.10.

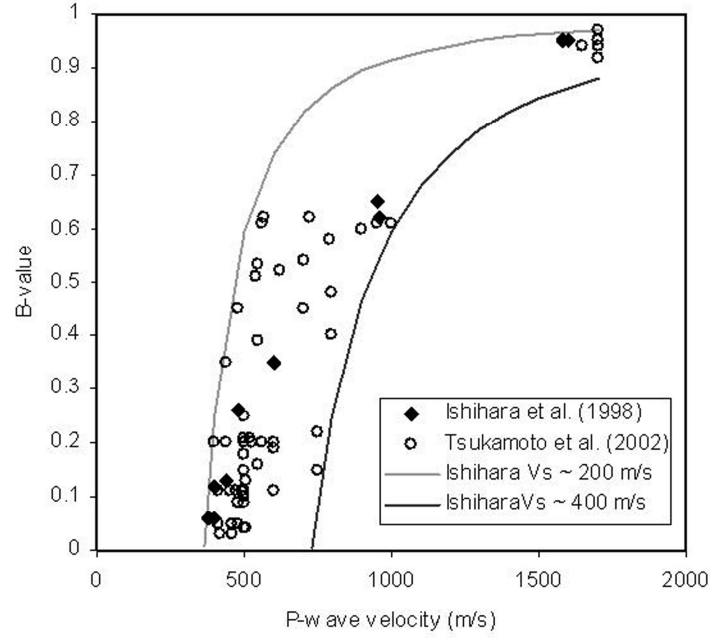


Figure 4.10 Relationship between B-value and P-wave velocity. Experimental data collected from the literature. The lines correspond to Equation 4.12 for two different values of the skeleton bulk stiffness, in terms of shear wave velocity V_S .

Equation 4.14 was used to estimate the value of B for all sediments at the beginning of the test and after 30 days. Calculations consider that V_S is a power function of the mean effective stress σ'_o [Santamarina et al., 2001]:

$$V_S = \delta \cdot \left(\frac{\sigma'_o}{1 \cdot kPa} \right)^\beta \quad (4.15)$$

$$\beta \approx 0.36 - \frac{\delta}{700 \cdot m/s} \quad (4.16)$$

For this particular experimental setup, the mean effective stress confinement is very low ($\sigma'_o \sim 0.02 - 0.2$ kPa) and the emphasis is placed on the bulk stiffness of the pore fluid. Empirical values for the δ -factor and the β -exponent range from $\delta = 25$ m/s and $\beta = 0.32$ for clays to $\delta = 75$ m/s and $\beta = 0.25$ for sands. Therefore, V_S values are in the order of 10 to 50 m/s. Consequently, the skeleton bulk stiffness k_{sk} is very low and the value of B decreases slightly even in the presence of gas bubbles and low V_P values, as shown by

experimental results in Figure 4.11. However, the same volume of gas and bubble size can have a pronounced effect on B values in field conditions where higher V_S values are expected. Computed B -values for soils with $V_S = 200$ m/s and $V_S = 400$ m/s are also included in Figure 4.11.

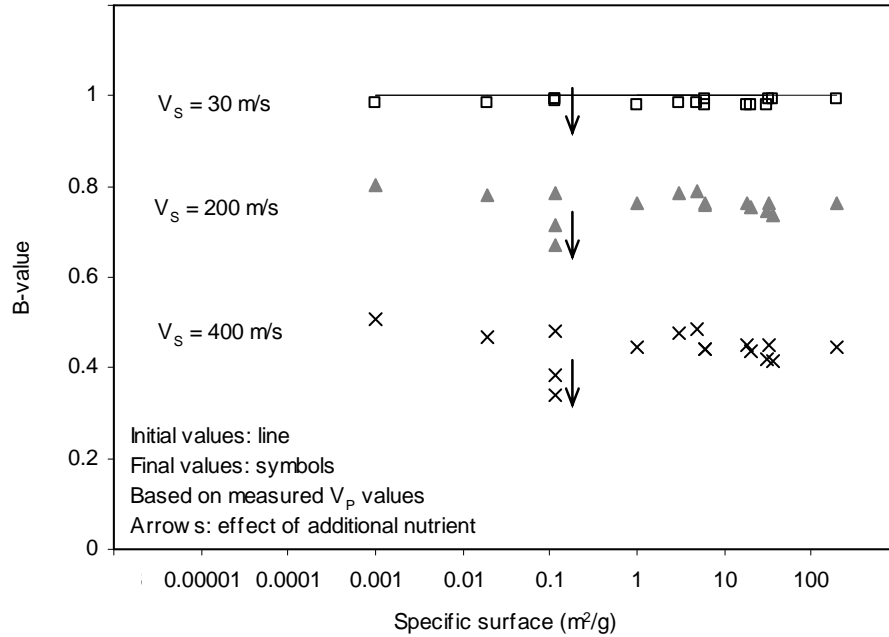


Figure 4.11 Initial and final (steady-state) value of Skempton's B parameter computed for all single-grained soils and mixtures as a function of specific surface. Compiled using Equation 4.14 and assuming $V_S = 30$ m/s and $\alpha \sim 1$. Additional results shown for higher shear-wave velocities assuming that gas bubbles are generated in the same proportions as in the experimental study.

As noted earlier, B -values can be further reduced by consecutive nutrient injections as gas generation is conditioned by nutrient availability in the medium.

The Effect of Biogenic Gas on Liquefaction Resistance

The number of cycles required to attain liquefaction considerably increases as the value of B decreases [Ishihara *et al.*, 1998; Sherif *et al.*, 1977; Tsukamoto *et al.*, 2002;

Yang, 2002; Yoshimi *et al.*, 1989]. Published results are summarized in Figure 4.12 (upper part). For this limited dataset, the liquefaction resistance experiences the most significant improvement when B decreases below $B \sim 0.5$.

From the point of view of field applications, a correlation between V_P and the cyclic stress ratio is particularly convenient. This correlation is supported by the causal link between saturation, and fluid bulk stiffness with both B -value and P-wave velocity, as shown above. This is explored in Figure 4.12 using published results. It can be concluded that the cyclic stress ratio increases by about 20% when the P-wave velocity decreases from $V_P = 1500$ m/s to $V_P = 600$ m/s and exhibits a dramatic improvement when the P-wave velocity drops below $V_P \sim 500$ m/s.

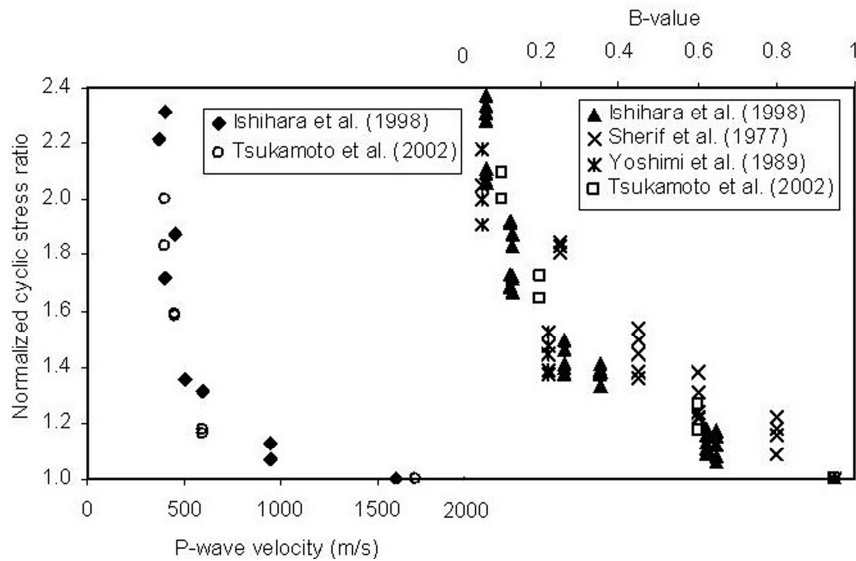


Figure 4.12 Variation in Normalized cyclic stress ratio (NCSS) with respect to P-wave velocity (left) and B-value (right). $NCSS = (CSR)_{actual} / (CSR)_{saturated}$. Data collected from the literature.

These observations, in combination with results shown in Figures 4.5 and 4.6, suggest the potential use of biogenic gas generation (nitrogen gas in this study) to increase the liquefaction resistance of soils subjected to cyclic loading. There are few trade-off: on one hand, presence of fines facilitate gas nucleation and also increase

liquefaction resistance by itself; on the other hand, presence of fines hinders bacterial transport and activity in the soil matrix.

Effect of Pore Fluid Pressure Fluctuations in Bubble Dissolution.

The results from the pore fluid pressure step tests (Figure 4.7) suggest time-dependent bubble dissolution. In other words, gas bubbles compress immediately as the fluid pressure is increased and latter experience diffusion-limited dissolution to reach the new equilibrium condition. This phenomenon may be relevant to tidal or water surge events.

Conclusions

Biogenic gas generation (nitrogen gas in this study) effectively reduces the bulk stiffness of the pore fluid and the P-wave velocity, suggesting potential effects in Skempton's B parameter and the susceptibility to liquefaction. Ultimately, the type, quantity and rate of biogenic gas production may be “designed” to address specific engineering needs.

Controlled nutrient injection can be used to regulate the process; otherwise, biogenic gas generation is expected to be temperature dependent due to the inherent nature of bacterial growth dynamics.

There is no response in any of the sterile controls. In contrast, consistent changes in P-wave velocity and gas volume were observed in inoculated sediments. Therefore, the generated gas is bio-mediated and cannot be explained by chemical effects associated to the addition of nutrients to the soil.

Biogenic gas appears to form sub-micron size bubbles which are disseminated throughout the soil mass in contrast to air injection which tends to concentrate along

percolation paths. Thus, the biogenic gas alternative may be more effective at preventing the local triggering of liquefaction. This hypothesis needs further evaluation.

Soil grain size affects the early evolution of bio-mediated gas generation by contributing nucleation sites as well as entrapment. Soils with small percentages of fines may fail to trap bubbles and show a transient decrease in P-wave velocity, followed by a partial recovery to the final stable value. When the fines content increases, the transient does not take place, and soils reach a stable P-wave velocity faster than in “clean” soils.

The effects of spatial variability have been explored for the case of cementation on Chapter 6. The conclusions are also valid for biogas generation in soils.

Bacteria and nutrients must be properly selected so that the generated gases are environmentally safe, have low solubility in water, facilitate bubble formation, and experience relatively long residency time. Although nitrogen gas appears to exhibit all these characteristics, possible by-products in an incomplete denitrification pathway are environmentally inadequate and should be further analyzed.

P-wave propagation provides insightful information that can be effectively used to monitor biogenic gas generation in laboratory applications. Furthermore, this geophysical method is readily applicable in the field. Pore fluid pressure step experiments and theoretical arguments suggest that biogas generation effects will require longer time under higher pore fluid pressure field conditions, and may be affected by rapid changes in pore fluid pressure.

CHAPTER 5

BIOLOGICAL CLOGGING OF SOILS UNDER RADIAL FLOW

Introduction

Microorganisms can reduce the hydraulic conductivity of soils and fractured rocks, alter fines migration, clog filters, enhance hydrodynamic dispersion, and increase chemical retardation in soils [Allison, 1947; Avnimelech and Nevo, 1964; Baveye *et al.*, 1998; Chang *et al.*, 1974; Daniel and Bouma, 1974; Frankenberger *et al.*, 1979; Gupta and Swartzendruber, 1962; Kristiansen, 1981; McCalla, 1950; McCoy *et al.*, 1981; Mitchell and Nevo, 1964; Nevo and Mitchell, 1967; Oberdorfer and Peterson, 1985; Raiders *et al.*, 1986; Swartzendruber and Gupta, 1964; Taylor and Jaffe, 1990; van Beek and van der Kooij, 1982; van Beek, 1984; Vandevivere and Baveye, 1992a; b; c; Wood and Bassett, 1975].

The biological clogging of soils has been extensively studied, often in the context of detrimental effects such as plugging of sewage infiltration ponds [Mitchell and Nevo, 1964], unwanted plugging near the well bore in both injection and production wells [Cunningham *et al.*, 1991; Kalish *et al.*, 1964; van Beek, 1984], and diminished ground water recharge [Nevo and Mitchell, 1967]. However, controlled soil bioclogging can be applied for selective plugging in enhanced oil recovery [Cusack *et al.*, 1992; Kim and Fogler, 2000; Lappin-Scott *et al.*, 1988; MacLeod *et al.*, 1988], bio-barrier formation and in situ bioremediation [Kim and Fogler, 2000], and rock fracture bio-healing [Ross *et al.*, 2001]. In all these cases, the extensive literature on soil bioclogging is limited to one-dimensional fluid flow situations, in which the velocity is constant along the specimen. In these cases, the most common difficulty experienced is the development of clogging at the inlet, close to the source of nutrient [Chang *et al.*, 1974; de Vries, 1972; Mitchell and

Nevo, 1964; Oberdorfer and Peterson, 1985; Paulsen, 1995; Rice, 1974; Vandevivere and Baveye, 1992a].

The main purposes of this chapter are to review the factors that affect biological clogging of soils, to examine biofilm-fluid flow interaction at the pore scale, and to explore the development of bioclogging in typical field-type radial flow conditions.

Literature Review

Soil Clogging

Clogging is the reduction in the capacity of a soil to conduct fluids due to a decrease in pore or pore-throat sizes or loss in interconnectivity. Underlying processes are of chemical, physical or biological origin [*Baveye et al., 1998*]. Physical clogging results from fines migration and entrapment [*Oberdorfer and Peterson, 1985; Okubo and Matsumoto, 1983; Rice, 1974; Valdes and Santamarina, 2005*], progressive nucleation of dissolved gas to form bubbles or segregation of immiscible liquids [*Allison, 1947; Gupta and Swartzendruber, 1962; 1964; Shaw et al., 1985*]. Chemical clogging combines pore geometry, the chemical properties of the percolating fluid (electrolyte concentration, organic compounds, pH and redox potential) and the mineralogical composition of the soil grains; these characteristics control dissolution and precipitation processes [*Baveye et al., 1998; Oberdorfer and Peterson, 1985; Rice, 1974*].

Biological clogging is the result of several interacting pore-level phenomena: bacterial transport and attachment, bacterial growth, biomass accumulation, the development of micro-colonies and biofilms on mineral surfaces, reduction in pore space, shear detachment of biomass from mineral surfaces, mechanical filtration at pore throats, excreted extracellular polymers, and entrapment of poorly soluble biogenic gas bubbles at pore throats [*Allison, 1947; Baveye et al., 1998; Bonala and Reddi, 1998; Vandevivere*

and Baveye, 1992a; b; c]. The evolution of bioclogging can be controlled through the addition of growth substrate, carbon and energy sources, such as plant residues, monosaccharides, disaccharides, alcohols and minerals [Allison, 1947; Baveye *et al.*, 1998; Frankenberger *et al.*, 1979; McCalla, 1950]. Bioclogging self-regulates through mechanisms such as the balance between the rate of biomass generation and the rate of removal, which increases with the increase in hydraulic gradient across the clogging zone, as well as through the decrease in nutrient transport with increased clogging [Cunningham *et al.*, 1991].

Physical, chemical and biological processes often co-participate in soil clogging. Pure biological clogging can be distinguished from non-biological clogging by applying treatments that suppress biological activity [Baveye *et al.*, 1998], such as sterilization with phenol, ethylene oxide or steam [Allison, 1947; Frankenberger *et al.*, 1979; Gupta and Swartzendruber, 1962], and/or low temperatures [Gupta and Swartzendruber, 1962; McCalla, 1950].

Factors that Affect the Biological Clogging of Soils

The main factors that affect the biological clogging of soils are the size distribution of soil particles [Baveye *et al.*, 1998; Kalish *et al.*, 1964; Raiders *et al.*, 1986], the type of bacteria [Frankenberger *et al.*, 1979; Gupta and Swartzendruber, 1962; Kalish *et al.*, 1964; Vandevivere and Baveye, 1992a; b; c], soil moisture level, nutrient and energy sources [Frankenberger *et al.*, 1979], fluid injection rate [Kalish *et al.*, 1964] and depth of bacteria penetration [Kalish *et al.*, 1964; Lappin-Scott *et al.*, 1988; MacLeod *et al.*, 1988].

Bacterial transport and retardation within the interconnected porous network of a soil mass is controlled by relative size (pore throat relative to a single bacteria or bacterial aggregations), electrical interactions, surface roughness and cell shape.

A major mechanism for bacterial attachment to surfaces is the development of biofilms, which starts with the attachment of microbial cells to soil particles [Donlan, 2002; Duddridge *et al.*, 1982]. Controlling factors are reviewed next.

Substratum

The extent of microbial colonization increases with surface roughness [Characklis and Marshall, 1990], probably because rougher surfaces provide higher surface areas and hinder shear forces [Donlan, 2002]. Electrical interactions between bacteria and mineral surfaces reflect the pH and ionic concentration dependence of bacterial and mineral surface charges and the balance between repulsion and van der Waals attraction between them. Finally, preferential attachment takes place onto surfaces that are nutritionally advantageous [Mueller, 1996].

Conditioning Films

Soil particles are coated or conditioned by polymers present in the pore fluid as soon as they become in contact. This phenomenon modifies the surface chemistry and facilitates microbial attachment [Loeb and Neihof, 1975; Ofek and Doyle, 1994].

Pore Fluid Hydrodynamics

The hydrodynamic boundary layer is the zone of negligible flow immediately adjacent to the solid-liquid interface and acts as a limiting factor in cell-soil particle attachment [Characklis and Marshall, 1990; Donlan, 2002; Rijnaarts *et al.*, 1993; Zheng *et al.*, 1994]. Its thickness is inversely proportional to the fluid velocity so that biofilm development tends to decrease as velocity increases [Duddridge *et al.*, 1982].

Pore Fluid Composition

Nutrient levels, ionic strength, pH, and temperature of the pore fluid affect microbial attachment to soil particles [Cowan *et al.*, 1991; Donlan *et al.*, 1994; Fera *et al.*, 1989; Fletcher, 1988].

Cell Characteristics

Attached cells are linked to the surface by fine extracellular polymeric fibrils of anionic nature in most cases [Beech and Gaylarde, 1989; Fletcher *et al.*, 1991; Zottola, 1991]. Cell fimbriae provide hydrophobic aminoacid residues while the cell hydrophobicity helps overcome the electrostatic repulsion barrier between the cell and the mineral surfaces.[Bullitt and Makowski, 1995; Corpe, 1980; Rosenberg *et al.*, 1982; Rosenberg and Kjelleberg, 1986]. Motile cells adhere to surfaces during pore fluid flow conditions and form biofilms more effectively than non-motile strains [Korber *et al.*, 1989].

There are two phases in bacterial attachment to surfaces: the “reversible” phase is related to the maximum “initial stickiness” of the bacterium, and the “irreversible” phase which is linked to the adhesive strength of the polymer-stabilized attachment [Duddridge *et al.*, 1982].

Compilation and Analysis of Published Results

Hydraulic conductivity data was collected from the literature and plotted in a $k_{initial}$ versus k_{final} space in Figure 5.1.

Most reported results correspond to with initial hydraulic conductivity in the range of $k_{initial} > 10^{-6}$ cm/s to $k_{initial} < 10^{-3}$ cm/s, i.e. silts and fine sands. A possible explanation for the “de facto” lower boundary is that biologically mediated hydraulic conductivity reduction can only be achieved when the environmental conditions favor

cell growth and reproduction. When pore sizes are smaller than $\sim 1 \mu\text{m}$, geometrical and mechanical conditions hinder microbial life [Rebata-Landa and Santamarina, 2006] and consequently prevent biofilm formation that leads to biological clogging of soils.

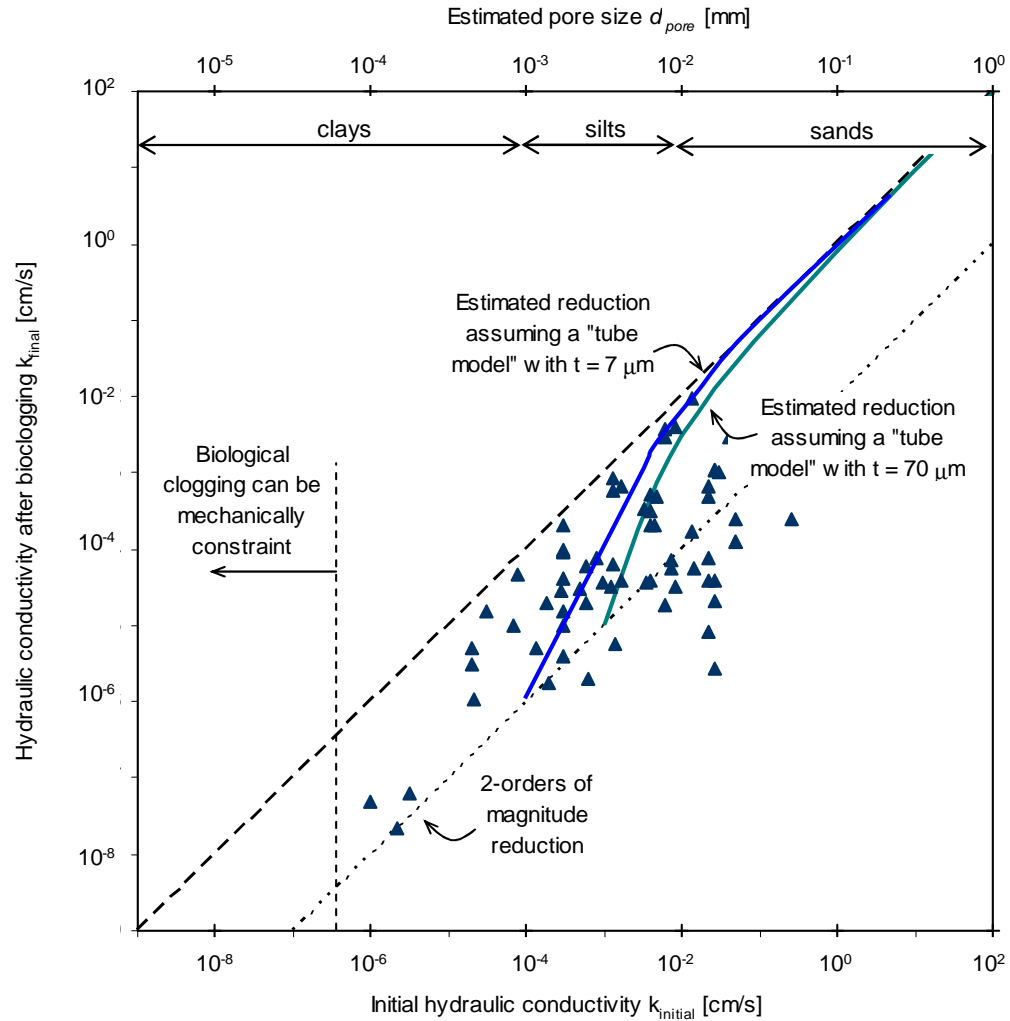


Figure 5.1 Bioclogging effectiveness versus soil type. Compilation of published hydraulic conductivity data [Allison, 1947; Cerini *et al.*, 1946; Chang *et al.*, 1974; Cunningham *et al.*, 1991; Cusack *et al.*, 1992; Dennis and Turner, 1998; Frankenberger *et al.*, 1979; Gupta and Swartzendruber, 1962; 1964; Kalish *et al.*, 1964; Lappin-Scott *et al.*, 1988; McCalla, 1950; Okubo and Matsumoto, 1983; Raiders *et al.*, 1986; Rice, 1974; Sarkar *et al.*, 1994; Shaw *et al.*, 1985; Swartzendruber and Gupta, 1964; Taylor and Jaffe, 1990; Thomas *et al.*, 1966; Vandevivere and Baveye, 1992a; b; c].

The upper boundary appears to reflect the inefficiency of bioclogging in large pores within coarse soils. A “tube” model is assumed to represent pores. The ratio between initial and final hydraulic conductivities for the “tube” model is estimated from the Hagen-Poiseuille equation:

$$\frac{k_{final}}{k_{initial}} = \frac{(d_{pore} - 2 \cdot t)^2}{d_{pore}^2} = \left(1 - \frac{2 \cdot t}{d_{pore}}\right)^2 \quad (5.1)$$

where t is the thickness of the biofilm. This trend is superimposed in Figure 5.1 by relating pore size d_{pore} to particle size $D_{particle}$ as $d_{pore} = D_{particle}/6.4$ (dense packing).

The “tube” model predicts smaller reductions in hydraulic conductivity in the coarser sands than experimentally observed. This indicates that biological clogging is more complex than uniform coating of soil particles.

Experimental Studies

Complementary experimental studies are conducted to gain a better understanding of bioclogging phenomena in radial flow. First, a pore-scale study is conducted to identify fluid flow velocity effects on biofilm accumulation on pore wall surfaces in order to improve the current understanding of biofilm attachment to particle surfaces. Second, a radial flow study is implemented to identify the effects of velocity-dependent bioclogging to field applications such as injection or extraction from wells.

The selected strain for these studies is *Pseudomonas fluorescens*. This is a mesophilic, non-spore forming species naturally present in soils, grown in batch cultures at 25°C in Luria-Bertani (LB) broth (Fisher Scientific).

Viscosity Evolution: Broth and Inocula

The viscosity of a mixture of inocula and Luria-Bertani broth was measured at different time intervals and at different speeds using a Brookfield DV-E viscometer.

Inocula was a late exponential growth phase culture to provide about 10^8 colony forming units per mL (previous study by the authors, data not shown). The mixture was stored at 20°C and the measurements were repeated at 15, 30, 60, 120, 240 and 1440 minutes.

Results and Analysis

Viscosity measurements presented in Figure 5.2 show that the mixture between inocula and LB broth used in these experiments behaves as a Newtonian fluid. Furthermore, the viscosity does not change over time. Therefore, any changes in hydraulic conductivity must be attributed to real changes in pore diameter or interconnectivity and not to changes in fluid viscosity.

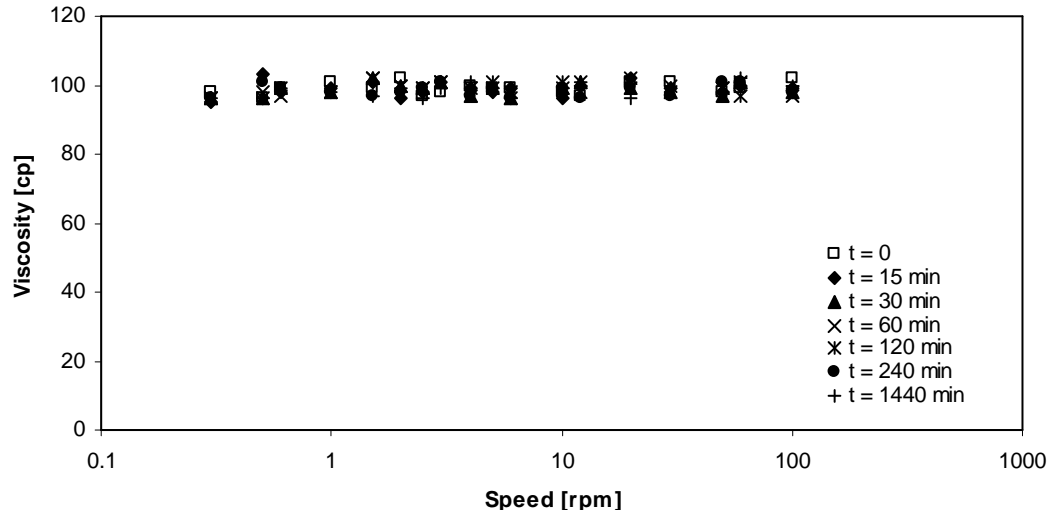


Figure 5.2 Viscosity measurements. Inocula and LB broth mixture (same mixture used in subsequent experiments reported here).

The viscosity of a suspension η_{sus} is related to the pure fluid η_0 and the volume fraction of suspended particles c as predicted by Einstein's equation [Ward and Whitmore, 1950]:

$$\eta_{sus} = \eta_0 \cdot (1 + 2.5 \cdot c) \quad (5.2)$$

For a late exponential phase, the cell concentration is around 10^8 cells/mL; the cell volume is $\sim 5.2 \times 10^{-5}$ mL (1 μ in diameter sphere); so, the volume fraction is $c = 5.2 \times 10^{-5}$. For this volume fraction, the viscosity of the suspension is only 0.01% higher than the fluid viscosity. This calculation corroborates the small changes observed in experimental results.

Pore-scale study

Pore-scale test device and procedure

A sterile chemical-resistant clear PVC capillary tube 1 mm I.D., 100 cm length (Figure 5.3) was used to simulate flow conditions at the pore scale. Different flow rates inside the capillary tube are applied using a syringe pump BS-8000 with a 50 mL sterile syringe loaded with inocula and fresh LB broth. The inlet pore pressure evolution was monitored every minute for 2 weeks using a pore pressure transducer (Smartec), while the outlet was left at atmospheric pressure. Four different flow rates were used: 0.2, 0.3, 0.5 and 0.8 mL/h. A new piece of sterile tube and fresh inocula was used for each test.

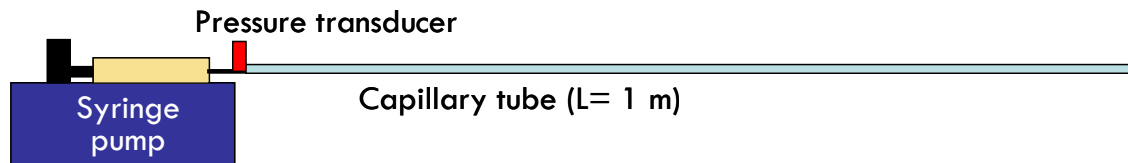


Figure 5.3 Experimental device – Pore-scale test.

Results

The evolution of the inlet fluid pressure with time is presented in Figure 5.4-a for all four flow rates (0.2, 0.3, 0.5 and 0.8 mL/h). While the initial pore fluid pressure increases with increasing flow rate, the asymptotic behavior at $t > \sim 10000$ min shows the

highest final inlet pressure for the lowest flow rate (0.2 mL/h), while the inlet pressure exhibits almost no change for the highest flow rate (0.8 mL/h).

Analysis

The pressure head loss h_{loss} for the fluid flow velocity v in a capillary tube is related to the tube length L and the internal diameter D as prescribed by the Darcy-Weisbach equation:

$$h_{loss} = \lambda \cdot \frac{L}{2 \cdot g \cdot D} \cdot v^2 \quad (5.3)$$

where the Darcy-Weisbach friction coefficient is $\lambda = 64/Re$ for laminar flow when $Re < 2000$. Reynolds number is:

$$Re = \frac{v \cdot D \cdot \gamma_w}{\mu \cdot g} \quad (5.4)$$

where g is the gravitational constant, γ_w is the fluid unit weight, and μ is the dynamic fluid viscosity. The flow rate q is related to the mean flow velocity and the cross-section:

$$q = v \cdot \frac{\pi \cdot D^2}{4} \quad (5.5)$$

These equations can be combined to estimate the evolution of the internal diameter $D(t)$ as a function of the head loss with time $h_{loss}(t)$:

$$D(t) = \sqrt[4]{\frac{128}{\pi} \cdot \frac{\mu}{\gamma_w} \cdot \frac{L \cdot q}{h_{loss}(t)}} \quad (5.6)$$

and the evolution of the mean flow velocity $v(t)$:

$$v(t) = \sqrt{\frac{1}{8 \cdot \pi} \cdot \frac{\gamma_w}{\mu} \cdot \frac{h_{loss}(t) \cdot q}{L}} \quad (5.7)$$

The evolution in flow velocity $v(t)$ is plotted in Figure 5.4-b for the same four cases. The following observations can be made from these results:

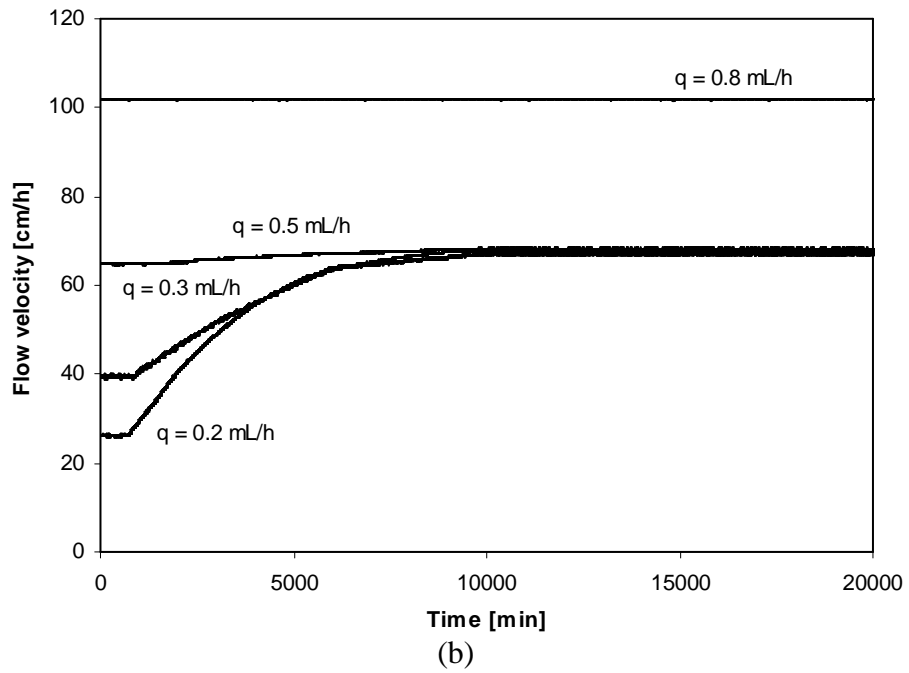
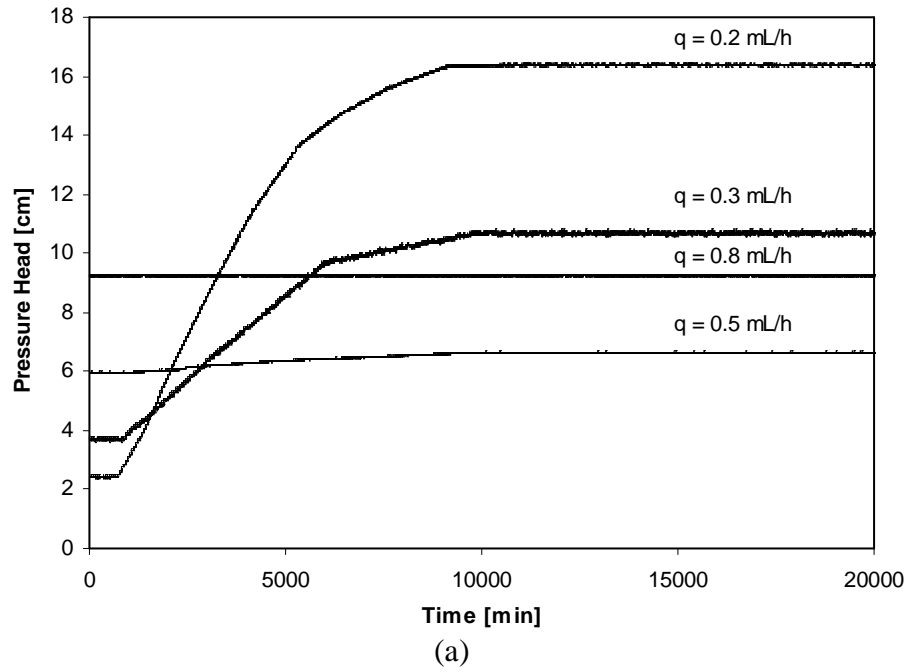


Figure 5.4 Evolution of (a) pressure head in the pore-scale tube test, and (b) mean flow velocity calculated using Equation 5.7.

- Small flow rates facilitate biofilm accumulation and the reduction of the internal diameter. On the contrary, large flow rates hinder biofilm accumulation and may eventually prevent it all together.
- Biofilms accumulate until the flow velocity inside the tube reaches a certain asymptotic value, around $v = 70$ cm/h in this experiment (Figure 5.4-b). Thereafter, the biofilm stops accumulating and the system enter in steady-state flow.
- When the internal flow velocity is above the asymptotic velocity, biofilms cannot accumulate, and all flow parameters remain constant throughout the experiment (pressure head, internal diameter and flow velocity).

Shear stress τ against the wall can be computed from force equilibrium:

$$h \cdot \gamma_w \cdot \frac{\pi \cdot D^2}{4} = \tau \cdot (\pi \cdot D \cdot L) \quad (5.8)$$

to obtain:

$$\tau = \frac{h \cdot \gamma_w \cdot D}{4 \cdot L} \quad (5.9)$$

Experimental results show that biofilm growth can take place when the shear stress is less than $\tau \sim 1$ Pa.

Bioclogging in Radial Flow

Radial Flow Test Device and Procedures

The system consisted of a set of two Plexiglas disks ($D = 40$ cm, $t = 1$ cm) separated by a 3 mm rubber O-ring ($D = 30$ cm) and pressed together around the perimeter using 18 fully threaded stainless steel bolts and wing nuts, so that the effective radial flow zone is 30 cm in diameter and approximately 2 mm thick. Radial drainage ports were carved in the top plate every 5° to allow water to escape and a filter placed over the drainage ports kept sand particles inside the plate (see Figure 5.5). Six pore

pressure transducers (Smartec) were attached to the bottom plate and one to the inlet. Device parts were rinsed thoroughly with Alconox prior to assemblage. Once the equipment was assembled, a perforation located in the bottom plate was used to fill the gap between plates with sterile Ottawa F110 sand selected for its grain size (mean grain size = 110 μm). Continuous in-flow was applied through a central port using a peristaltic pump. The test sequence follows:

1. Sterile and deaired water was pumped continuously for 4 days to attain saturation and constant inlet pressure.
2. Colored sterile water was injected to track the flow front and assess homogeneity using digital imaging at regular time intervals.
3. Bacteria and nutrient were incorporated by injecting 4 pore volumes of inoculum (thereafter, fresh nutrient was injected daily).
4. Deaired water was continuously pumped at a pre-fixed rate for 3 weeks. All seven pore pressure transducers were monitored every minute. The experiment was stopped when asymptotic values in all seven transducers were reached.

The same procedure was followed using three different flow rates q : 100 mL/h, 250 mL/h and 500 mL/h.

Results

Images at different stages of clogging are presented in Figure 5.5. Homogeneous radial flow conditions are preserved after clogging and there are no signs of fingering, local obstruction or desaturation. This indicates that the process is stable and self-homogenizing under the tested conditions.

Hydraulic heads for all seven transducers and all three tests are plotted as a function of time in Figure 5.6. All measurements show an initial “lag phase”, followed by an increase in hydraulic head until it eventually reaches an asymptotic value. The pressure evolution in different flow rate tests can be interpreted as follows:

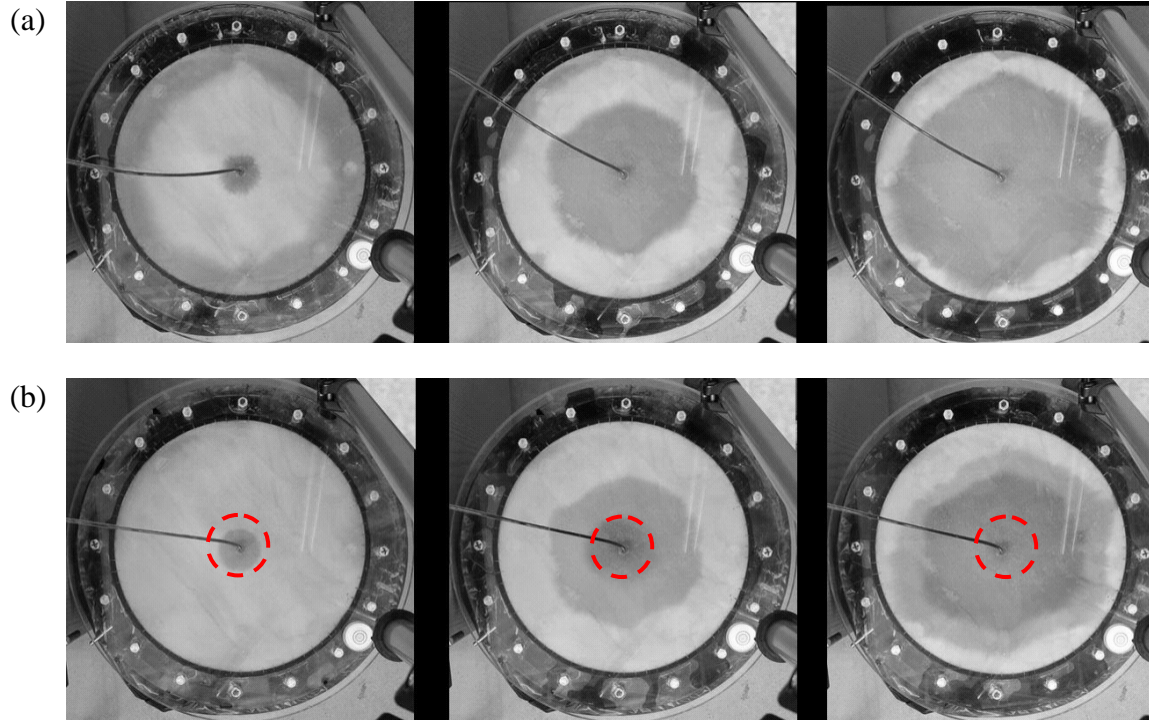
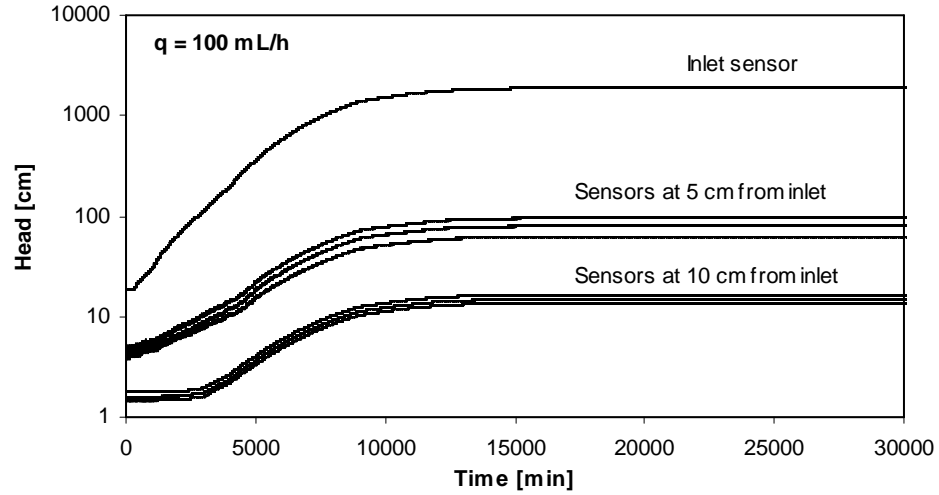
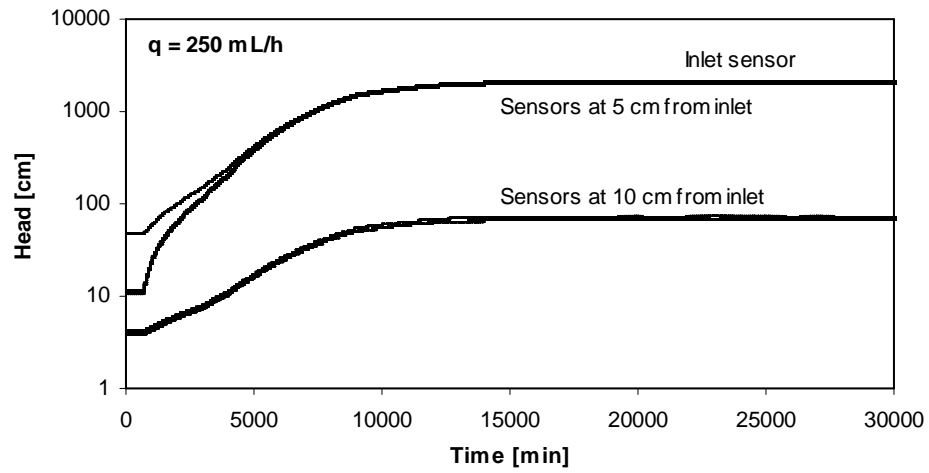


Figure 5.5 Set of images at different stages of clogging, (a) saturated unclogged specimen ($t = 0$), (b) clogged specimen at the end of the test ($t = 30000$ min). Sketch indicates the estimated clogging front.

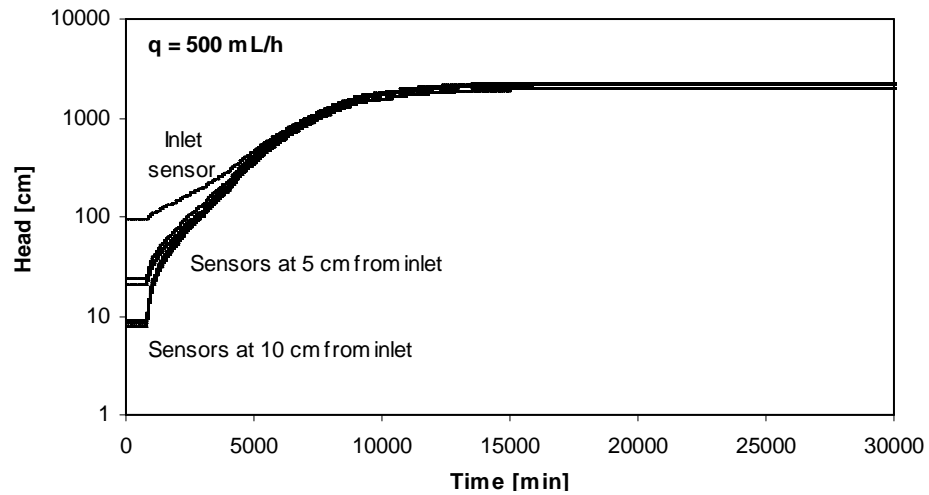
- $q = 100 \text{ mL/h}$. All measurements in Figure 5.6-a collapse onto three trends according to the radial distance suggesting homogeneous clogging.
- $q = 250 \text{ mL/h}$. Steady-state measurements in Figure 5.6-b collapse onto two trends (pressure at the inlet and at 5 cm radius are very similar), which suggests that clogging is occurring at a radial distance larger than 5 cm but smaller than 10 cm.
- $q = 500 \text{ mL/h}$. Steady-state measurements in Figure 5.6-c collapse onto a single trend, which indicates that clogging is taking place between the 10 cm radial distance and the border of the specimen.



(a)



(b)



(c)

Figure 5.6 Bioclogging in radial flow. Evolution of hydraulic head at three radii (inlet, 5 cm and 10 cm) for flow rate (a) $q = 100 \text{ mL/h}$, (b) $q = 250 \text{ mL/h}$ and (c) $q = 500 \text{ mL/h}$.

These observations support the following hypothetical sequence of events: as the seepage velocity decreases away from the inlet, drag forces decrease, bacterial cells attach to soil particles, and biofilms grow. The development of biofilms affects the local fluid velocity which regulates further growth in the vicinity. Gradually, a thick ring-shaped bio-clogged region develops. These hypothetical steps define a highly non-linear process. The situation is aggravated by the complexity of microbial transport mechanisms in porous networks [Abu-Ashour *et al.*, 1994; Fontes *et al.*, 1991; Gannon *et al.*, 1991a; Gannon *et al.*, 1991b; Harvey *et al.*, 1989; Kjelleberg *et al.*, 1983; Rosenberg and Kjelleberg, 1986; Scholl *et al.*, 1990; Stenstrom, 1989; Tim *et al.*, 1988; Yates and Yates, 1987].

Analysis

The pressure field in radial flow for a disc of thickness w satisfies the following differential equation:

$$\partial h = \frac{q}{2 \cdot \pi \cdot w \cdot k} \cdot \frac{\partial r}{r} \quad (5.10)$$

If the hydraulic conductivity is constant between radii r_i and r_f , Equation 5.10 leads to the following expression for the hydraulic conductivity as a function of pressure heads h_f and h_i :

$$k = \frac{q}{2 \cdot \pi \cdot w \cdot (h_f - h_i)} \cdot \ln \left(\frac{r_f}{r_i} \right) \quad (5.11)$$

The goal of this analysis is to solve the inverse problem of inferring $k(r)$ from the measured heads $h(r)$. Given the limited amount of information available in this study, the solution to the inverse problem follows Ockham's Razor Principle of favoring simplicity and is based on the minimum number of unknowns that properly covers the physical reality [Santamarina and Fratta, 1998].

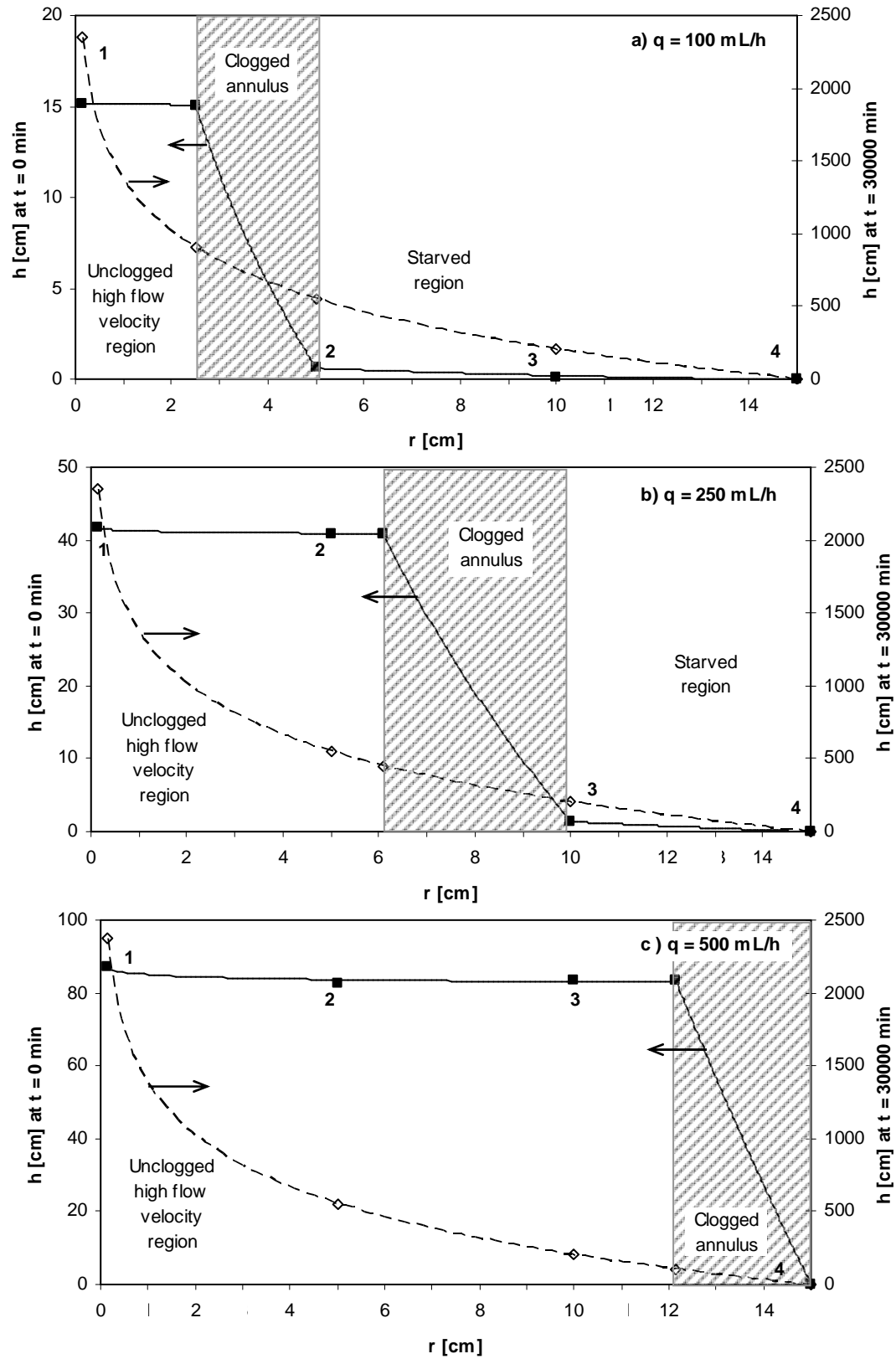


Figure 5.7 Bioclogging in radial flow. Heads at $t = 0$ and at $t = 30000$ min for flow rates (a) $q = 100$ mL/h, (b) $q = 250$ mL/h and (c) $q = 500$ mL/h.

The following assumptions are made: (a) there are at most three “regions” in the specimen, the “unclogged high flow velocity region” near the well, the “clogged annulus”, and the “starved region” in the far field; (b) the transition between the “unclogged high flow velocity region” and the “clogged annulus” is considered to be located at a position linearly proportional to flow velocity and therefore linearly proportional to the flow rate; (c) the transition between the “clogged annulus” and the “starved region” is taken at the nearest transducer; and (d) the hydraulic conductivity in each region is homogeneous and satisfies Equation 5.11.

Figure 5.7 shows heads at time $t = 0$ and after 30000 min for the three cases (flow rates of 100, 250 and 500 mL/h). Clearly, clogging takes place between the inlet and the first set of sensors for $q = 100$ mL/h, between the second and the third set of sensors for $q = 250$ mL/h, and between the third sensor and the border of the specimen for $q = 500$ mL/h. The assumed position and width of the clogged annulus is shown in each case.

The evolution of the inverted hydraulic conductivity for the three regions within each specimen as a function of radial distance r is plotted in Figure 5.8 at four different times. Results indicate that the hydraulic conductivity in the “clogged annulus” can be more than 2 orders of magnitude smaller than the initial value, while the hydraulic conductivity in the “starved region” decreases by only an order of magnitude from the initial value. It is important to recognize that the different regions have been defined arbitrarily to avoid introducing more unknowns; in reality, the “starved region” could start at any point after the “clogged annulus”.

The evolution in inverted hydraulic conductivities for the “clogged annulus” is plotted high time resolution in Figure 5.9. Results show similar induction time and clogging time scale observed in the pore-scale study (Figure 5.4). Furthermore, the hydraulic conductivity in the clogged zone decreases by 2 or 3 orders of magnitude from the initial value, for the three flow rates, in agreement with the pore-scale observations.

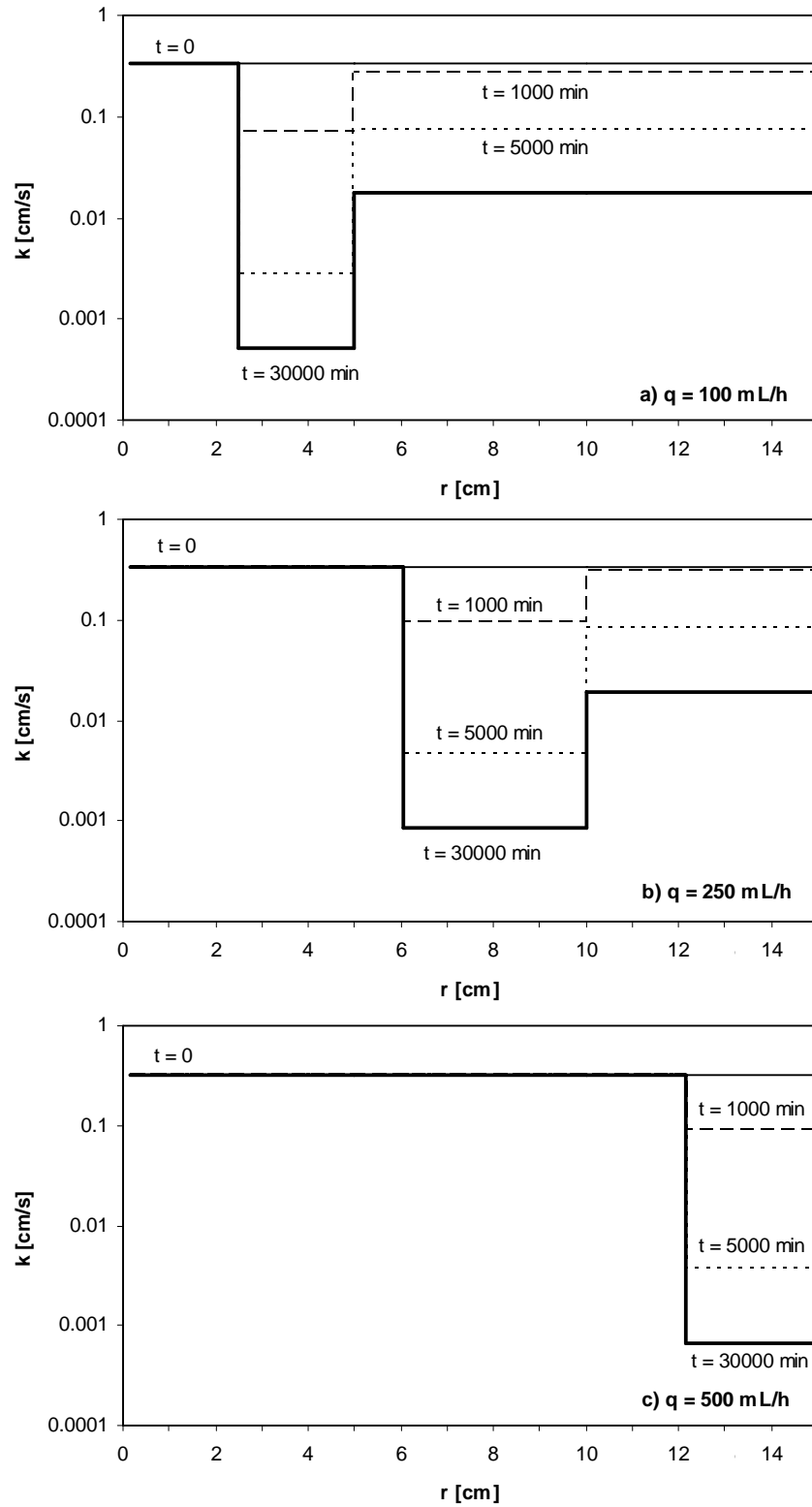


Figure 5.8 Bioclogging in radial flow. Evolution of the hydraulic conductivity within each specimen as a function of radial distance r and time, for flow rates (a) $q = 100$ mL/h, (b) $q = 250$ mL/h and (c) $q = 500$ mL/h.

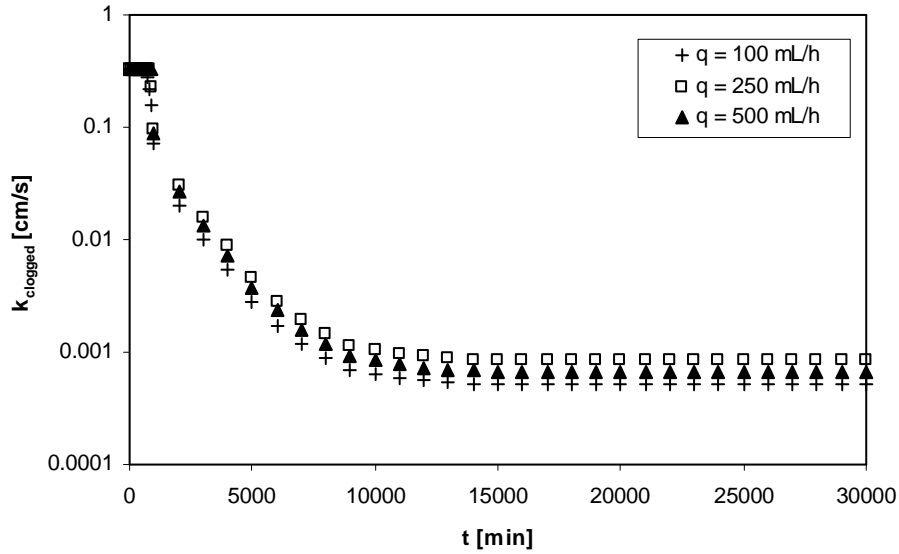


Figure 5.9 Bioclogging in radial flow. Hydraulic conductivities in the “clogged annulus” as a function of time for the three specimens.

Discussion – Coupled Clogging Phenomena

Small mineral particles may not be trapped in the soil mass when pore throats are large. However, the development of biofilms may help stop migratory fines. The result becomes a coupled bio-mechanical clogging process.

An additional test was performed to explore this coupled process. The specimen was prepared as the others and flow rate was set to 100 mL/h. After initial saturation, but before bacterial cells were incorporated, slurry containing 1 g/L bentonite was flushed into the system and the flow pattern was recorded using digital imaging at 1-2 min intervals. Images are similar to those in Figure 5.5: there is a homogeneous flow, the bentonite was flushed away and no clogging developed. Then, the test proceeded as in earlier tests by injecting inocula at $q = 100$ mL/h. Three weeks later, a similar bentonite suspension was flushed and again the flow pattern was recorded using digital images. Selected snapshots are shown in Figure 5.10. The fine particles were no longer able to

cross the pore throats. As the injection pressure increased, the bio-mechanically clogged sand specimen experienced hydraulic fracture.

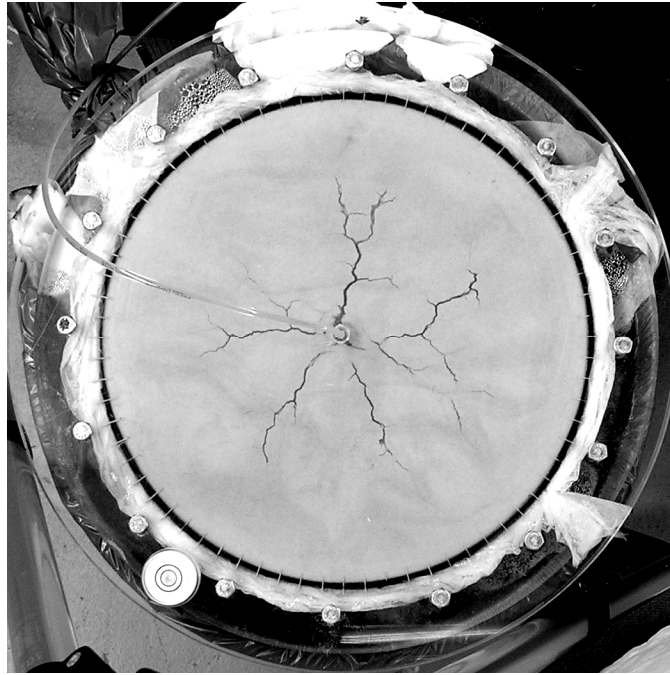


Figure 5.10 Coupled clogging phenomena. Effect of biofilm in fines transport through sand

Conclusions

Biological clogging of soils presents two limiting boundaries related to the pore size. Biological clogging of soils is limited by space availability in the pores. It is presumed that when pore size is smaller than $\sim 1 \mu\text{m}$, bacterial ability to metabolize and generate biofilms is hindered by geometrical constraints and therefore their capacity to reduce the hydraulic conductivity is not as efficient as in coarser soils. On the other hand, when soil particles and pores are too large, biofilm accumulation is limited by pore flow velocity and ensuing shear forces.

The fluid viscosity and the Newtonian response do not change as bacterial counts increase. It is anticipated that viscosity changes for bacterial concentrations as high as

$\sim 10^8$ cells/mL are less than $\sim 1\%$. Thus, any changes in hydraulic conductivity must be attributed to real changes in pore diameter or interconnectivity and not to changes in fluid viscosity.

Biological clogging of soils is a homogeneous and self-homogenizing process. No fingering, local obstruction or local desaturation was observed.

The effects of spatial variability have been explored for the case of biocementation in Chapter 6. The conclusions are also valid biological clogging of soils.

Clogging studies in radial flow eliminate the inlet clogging issue and provide a more realistic representation of most field applications, including fluid injection or extraction.

Radial flow studies show a characteristic radial distance where clogging starts. This radial distance is directly proportional to flow velocity and it is linked to the pore-scale flow velocity that matches the pore-scale experimental data gathered with the 1D tube.

The inversion technique used to estimate hydraulic conductivity values in radial flow appears to properly recover the physical processes in the soil. This suggests that the process is relatively homogeneous in each “zone”. Future work should include a more comprehensive distribution of sensors to verify hypotheses made in this inversion.

Coupling between biological and mechanical clogging could be used as a tool to create a long-term yet reversible solution where lower hydraulic conductivities are needed, or to engineer techniques to stop the unwanted migration of contaminants, including fines.

.

CHAPTER 6

BIOLOGICAL DEPOSITION OF CaCO_3 IN SOILS

Introduction

Advanced crystal engineering concepts can be identified in natural biological systems, such as bones, teeth and shells. In fact, organisms control mineral deposition to tailor mineral type, crystal nucleation, growth, morphology and assembly according to their needs [Heywood *et al.*, 2000]. The interactions between the “bio-organic matrices” and the emerging inorganic solids play a crucial role in these mineral deposition processes [Addadi and Weiner, 1992; Heywood *et al.*, 2000].

Precipitation of calcium carbonate by bacteria has been reported in diverse geological environments, from hot springs to marine environments and caves [Boquet *et al.*, 1973]. Several metabolic pathways can lead to extracellular CaCO_3 precipitation, such as photosynthesis, denitrification, sulphate reduction, ammonification and anaerobic sulphide oxidation [Baskar *et al.*, 2006; Castanier *et al.*, 2000].

The purpose of this study is to gain further insight into bio-mediated CaCO_3 precipitation in soils. Emphasis is placed on precipitation patterns on different mineral substrates, rate effects, pore-grain size effects and the consequences of spatial variability through bio-hydro-chemical coupling.

Literature Review

Biom mineralization

More than 60 types of minerals of biological origin have been identified [Lowenstam and Weiner, 1983]. Most of them involve Ca as the major cation; Fe is the

second most common metal [*Simkiss and Wilbur, 1989*]. Some microorganisms accumulate phosphorites, carbonates, silicates and either iron or manganese oxides; others produce glycocalyx on the cell wall which stays in the environment even after cell death [*Stocks-Fischer et al., 1999*].

Biogenic minerals may be amorphous, paracrystalline or crystalline [*Lowenstam and Margulis, 1980*], may occur as a single unit, numerous individual units or aggregates [*Lowenstam, 1981*], and can be formed intracellularly, intercellularly or extracellularly [*Krampitz and Witt, 1979; Schultze-Lam et al., 1996*]. The morphology of deposits depends on microecological conditions (e.g., pH, salinity, temperature, species present), therefore, a variety of growth rates and crystal morphologies can be found [*Cacchio et al., 2003; Castanier et al., 1993; Cunningham et al., 1995; Ferris et al., 1994*].

Once minerals form at a particular site, they may remain in place, be transferred to other sites, excreted, dissolved and replaced (continuously, periodically or occasionally) [*Lowenstam, 1981*]. Bacterial deposition of carbonates often starts at a single nucleus, which is further grown by the microbial colony, and eventually forms multiple layers [*Cacchio et al., 2003*].

Biogenic mineral formation can be the result of two fundamentally different processes. The first one is “organic matrix-mediated” or active biomineralization and it is characterized by the development of an organic mold into which ions are introduced and induced to crystallize and grow; in this process, mineral type, orientation of crystallographic axes as well as microarchitectures are genetically controlled. The second one is “biologically induced” also known as passive biomineralization, and consists of the creation of bulk extra- and/or intra-cellular mineral deposits that lack organic matrices; the resulting minerals are similar to those produced by inorganic precipitation

[*Lowenstam*, 1981]. Passive mineralization is usually the result of bacterial changes in the system chemistry [*Teng and Dove*, 1997].

Microorganisms are the center of a wide range of mineralization processes, due to their participation in various biochemical pathways and the consequent release of metabolic products to the environment [*Gollapudi et al.*, 1995; *Simkiss and Wilbur*, 1989]. Photosynthetic processes remove carbon dioxide from a solution such as freshwater or seawater containing calcium and bicarbonate ions (carbon dioxide fixation) and cause the precipitation of calcium carbonate [*Parraga et al.*, 1998; *Simkiss and Wilbur*, 1989]. Nitrate reduction by heterotrophs induces calcium carbonate deposition [*Simkiss and Wilbur*, 1989]. Finally, sulfate reduction causes carbonate precipitation in most pedogenic calcretes [*Monger et al.*, 1991].

Several characteristics differentiate biogenic from non-biogenic carbonate deposits [*Folk*, 1993]: (a) the presence of crystal clusters which reflects the bacterial tendency to form colonies, (b) size variations on the deposits that are associated to mixed stages of nutrition, (c) relatively small upper size limit (around $< 2 \mu\text{m}$) and a narrow size range, (d) non-conventional mineral forms that are not observed in abiotically processes (e.g. rod-like or curved), and (e) the presence of Si, Ca, P and/or other minerals commonly found in biogenic minerals.

CaCO₃ Precipitation by Bacteria

Heterotrophic bacterial metabolisms can lead to either passive or active CaCO₃ precipitation [*Castanier et al.*, 1999; 2000]. In passive precipitation, metabolic pathways such as amino acid ammonification, dissimilatory nitrate reduction, urea hydrolysis, and dissimilatory sulfate reduction increase the pH of the surrounding environment and produce both carbonate and bicarbonate ions, facilitating CaCO₃ precipitation [*Castanier*

et al., 1999; 2000]. In active precipitation, carbonates are produced by ion exchange through the cell membrane [*Castanier et al.*, 1999; 2000; *Greenfield*, 1963; *Rivadeneira et al.*, 1994].

CaCO₃ precipitation is controlled by several factors, such as the concentrations of calcium and dissolved inorganic carbon, pH, and the availability of nucleation sites [*Baskar et al.*, 2006; *Kile et al.*, 2000; *Sanchez-Moral et al.*, 1999].

There is a wide variety of calcium carbonate polymorphs which differ in their crystal structure and thermodynamic characteristics. Calcite shows hexagonal-rhombohedral crystal structure and is thermodynamically stable. Aragonite exhibits orthorhombic crystal structure, often like needles, and it is metastable. Vaterite displays hexagonal crystal structure, typically disc-like precipitates, and is it metastable as well. While most calcifying strains are able to produce calcite, the precipitation of other CaCO₃ minerals such as vaterite is not only specie-specific but also temperature-dependent [*Chakraborty et al.*, 1994].

The biogenic precipitation of calcite involves the following steps [*Castanier et al.*, 2000; *Zavarzin*, 2002]: (a) development of an alkaline geochemical barrier, (b) generation of a calcium carbonate supersaturated solution, (c) production of calcite colloids, (d) nucleation of calcium carbonate on bacterial slime containing immobilized Ca²⁺, (e) diagenesis and crystallization of calcium minerals, (6) cementation and consolidation leading to the transformation of sediments in rock.

Urea Hydrolysis and Biogenic CaCO₃ Precipitation

The production of urea in soils can be explained by the bacterial degradation of purines [*Vogels and Drift*, 1976] and arginine [*Cunin et al.*, 1986]. Urea hydrolysis and the subsequent release of free ammonia (urea ammonification) has been widely studied

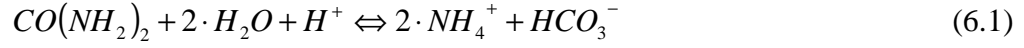
[Pettit *et al.*, 1976; Reynolds *et al.*, 1985; Zantua *et al.*, 1977] and plays an important role in nitrogen cycling following urea fertilization in soils [Xu *et al.*, 1993].

The hydrolysis of urea to form ammonia and carbon dioxide in the last step of nitrogen mineralization is catalyzed by the enzyme urease (urea amidohydrolase) which is a nickel-dependent metalloenzyme [Hausinger, 1993]. Nickel-dependent ureases have been isolated from different types of bacteria including *Bacillus pasteurii* species [Benini *et al.*, 1996], fungi and higher plants [Hausinger, 1993].

Enzymatic effects on reactivity are commonly accepted but not well understood [Estiu and Merz, 2006]. The role of enzymatic catalysis by the reduction of the activation energy is generally recognized [Garcia-Viloca *et al.*, 2004] but the origin of this reduction remains partially unknown [Zhang and Houk, 2005]. In the case of urea hydrolysis, the rate of the uncatalyzed reaction is about 10^{14} times slower than the catalyzed one [Jabri *et al.*, 1995].

Ureases have several roles in the environment. They are utilized by organisms to exploit external and internally generated urea as nitrogen source [Mobley and Hausinger, 1989] and by higher plants as part of their systemic nitrogen transport pathway [Polacco and Holland, 1993]. Medically, they are implicated in the development of infection-induced urinary stones (15-20% of all urinary stones), catheter encrustation, pyelonephritis and hepatic encephalopathy [Mobley and Hausinger, 1989] as well as peptic ulceration and possibly stomach cancer formation [Lee *et al.*, 1993]. This enzyme also catalyzes the hydrolysis of hydroxyurea to hydroxylamine and is used in sickle cell anemia treatment [Lockamy *et al.*, 2003].

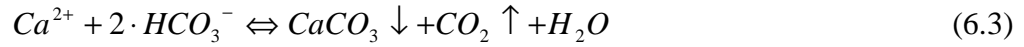
Two bacterial mechanisms related to urease may induce biomineralization. First, urea hydrolysis modifies the local geochemical conditions leading to pH increase [Parraga *et al.*, 1998; Warren *et al.*, 2001]:



Second, bacteria can selectively accumulate Ca^{2+} in their cell walls [Parraga *et al.*, 1998]. Consequently, active urea degradation processes in the presence of calcium can significantly favor carbonate precipitation [Warren *et al.*, 2001]:



The classical model for a heterotrophic bacterium can be expressed as:



For Equation 6.3, the $CaCO_3$ dissolution/precipitation equilibrium constant is defined as:

$$K = [Ca^{2+}] \cdot [CO_3^{2-}] \quad (6.4)$$

where $[Ca^{2+}]$ and $[CO_3^{2-}]$ are the concentrations of Ca^{2+} and CO_3^{2-} in the local environment, respectively.

The solubility product constant in water K_{sp} at any given pressure, salinity and temperature conditions, permits tracking the reactions. When $K = K_{sp}$, the solution is considered to be “exactly saturated”, when $K > K_{sp}$ precipitation of $CaCO_3$ takes place and when $K < K_{sp}$, $CaCO_3$ gets dissolved [Baskar *et al.*, 2006].

The chemical precipitation of calcite requires supersaturation to overcome activation barriers for calcite nucleation and crystal growth. In the case of bio-mediated precipitation of calcite, locally enhanced interfacial calcium ion concentration (produced due to the tendency of bacterial cell walls to adsorb calcium ions) supports the formation of a diffuse bicarbonate/carbonate ions layer, creating $K > K_{sp}$ at a submicron scale [Folk,

1993], which is enough to induce crystallization around bacterial cells [Boquet *et al.*, 1973].

Experimental Studies

Complementary experimental studies are conducted to gain a better understanding of bacterially-induced mineral precipitation on mineral surfaces and within soils. First, a surface-level study is conducted to identify patterns in the evolution of biomineralization on mineral surfaces in order to improve models. Second, three mesoscale tests are implemented to analyze (1) the effects of nutrient and incubation time, (2) the relevance of mineral grain size, and (3) the role of diffusion versus advection of both nutrients and bacterial cells in the efficiency of the bio-cementation phenomenon. Third, a macroscale test is performed to study the coupling between hydraulic conduction and bio-cementation.

Materials and Procedures

The following steps are common to all tests. Sketches for general test setups are shown in Figure 6.1.

Bacterial Species

The selected strain is *Bacillus pasteurii* (*Sporosarcina pasteurii*, ATCC 11859). This bacterium is capable of synthesizing urease, and therefore able to hydrolyze urea to form ammonia and bicarbonate ions.

Solid Media

Cells were resuscitated in solid NH_4 -YE agar: 1L of 0.13 M Tris Buffer (pH 9.0), 20 g yeast extract, 10 g $(\text{NH}_4)_2\text{SO}_4$ and 20 g powder agar; all reagents were analytical

grade from Fisher Scientific. Ingredients were sterilized separately and mixed under aseptic conditions. Then, Petri dishes containing cells and $\text{NH}_4\text{-YE}$ agar were incubated at their optimum temperature ($T = 30^\circ\text{C}$).

Stock Liquid Media

$\text{NH}_4\text{-YE}$ liquid media was used to resuspend cell colonies for stock purposes. It was prepared in similar manner as $\text{NH}_4\text{-YE}$ agar but omitting the powder agar.

Test Liquid Media

Five different Urea- CaCl_2 media were used for the calcium carbonate precipitation experiments. All of them contained 3 g Nutrient broth, 10 g NH_4Cl , and 2.12 g NaHCO_3 per liter of deionized water, but the amounts of urea varied as shown in Table 6.1. These mixtures were adjusted to pH 6.0 and sterilized by autoclaving; then, a filter sterilized solution containing the amount of CaCl_2 indicated in Table 6.1 was added to the previous preparation under aseptic conditions.

Table 6.1 Amounts of Urea and CaCl_2 per liter of solution in the different nutrient combinations used.

Nutrient combination	Urea (g)	CaCl_2 (g)
#1	20	1.4
#2	20	2.8
#3	20	5.6
#4	10	25
#5	15	37.5

Inocula Preparation

Cells grown in stock $\text{NH}_4\text{-YE}$ liquid media were washed in saline solution, harvested and resuspended in Urea- CaCl_2 media or saline solution.

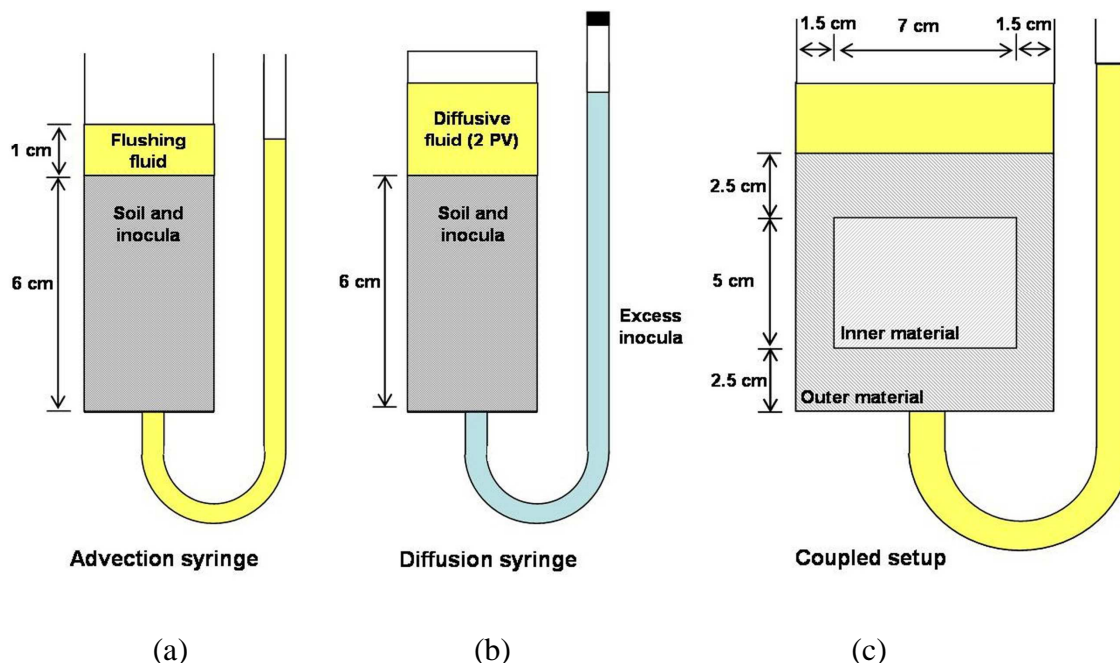


Figure 6.1 Experimental setup: (a) Study #2 and #3, (b) Study #4, (c) Study #5. Details in the text and Table 6.1.

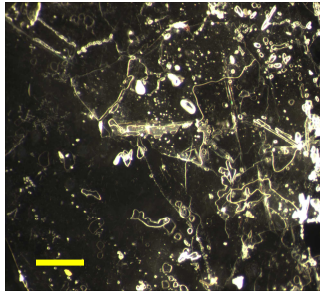
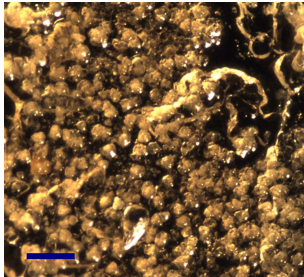
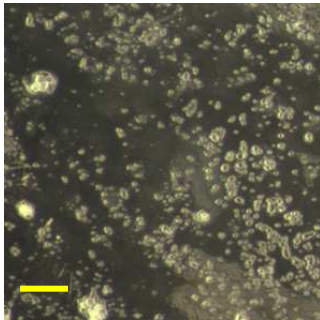
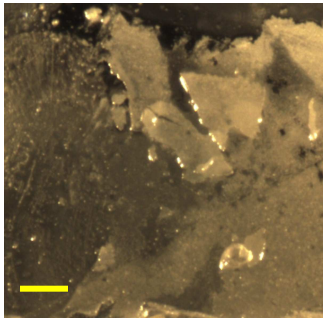
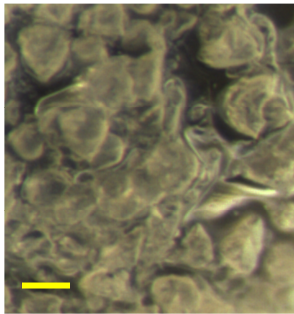
Study #1: Nucleation “Habits”

The purpose of this surface-scale study was to identify patterns in the evolution of biomineralization on mineral surfaces. It involved mica, calcite and quartz as crystal nucleation surfaces. Test liquid media #5 was used for this study (Table 6.1). The inocula was prepared by resuspending cells in Urea- CaCl_2 media.

Test Procedure

Small pieces of mica, calcite, and quartz were disinfected and rinsed thoroughly in warm sterile water. Three specimens of each material were placed in a sterile Petri dish and soaked with the resuspended cells in Urea- CaCl_2 media. All Petri dishes were incubated at the optimum temperature ($T = 30^\circ\text{C}$) for 1, 2 and 4 weeks. Sterile controls were assembled using the same procedure but using sterile Urea- CaCl_2 media.

Table 6.2 Crystal nucleation on mineral surfaces – Main observations

Mineral surface	One week	Four weeks
Mica	<p>Some signs of nucleation.</p>  <p>B Bar = 100 μm</p>	<p>About 90% of the surface is covered by crystals. No uniform coating is observed.</p>  <p>Bar = 100 μm</p>
Calcite	<p>About 10%-30% of the surface is covered with individual nucleation points. Some dendrites are observed.</p>  <p>Bar = 100 μm</p>	<p>100% of the surface is evenly coated by a thin crystal layer: the original calcite surface is transparent and the coating is opaque. Few sporadic crystals are observed, particularly near edges. The layer can be detached when pressed with a point indenter.</p>  <p>Bar = 100 μm</p>
Quartz	<p>About 1% of the surface contains individual nucleation points.</p>	<p>About 70% of the surface is covered by crystals. Edges are preferred. *</p>  <p>Bar = 200 μm</p>

* Note water condensation after exposure to atmosphere.

At the end of each period (1, 2, 4 weeks), one mineral substrate from each series was removed from the Petri dishes, rinsed carefully in alkaline water (pH ~ 9.0) to eliminate excess nutrient without dissolving the crystals, air-dried and examined using optical microscopy.

Results

Table 6.2 shows observations on crystal nucleation evolution on mica, calcite and quartz. It can be observed that:

- Bio-mediated CaCO_3 precipitation starts as individual nucleation points.
- Precipitation evenly coats surfaces that are similar to the crystals (i.e. calcite in this study), however, individual crystal growth is preferred on other mineral surfaces (quartz and mica).

Observations a month after the completion of the test show relatively weak bond of the precipitation on the three different mineral substrates.

Study #2: Effect of Nutrients and Time

It is generally accepted that both nutrient concentration and time play a significant role in bacterial metabolic processes. Urea hydrolysis and consequently calcium carbonate precipitation is not an exemption. The purposes of this test are to analyze the performance of different combination of nutrients (including cases in which CaCl_2 acts as a limiting factor and urea is supplied in excess, and viceversa) and to study the influence of time in the biogenic cementation process.

Several combinations of Urea and CaCl_2 concentrations have been used in the literature to generate detectable biogenic CaCO_3 precipitation [*Nemati et al.*, 2005; *Stocks-Fischer et al.*, 1999]. In this analysis, the 5 combinations summarized in Table 6.1 were tested during 64 days to determine the effect of nutrient concentration, nutrient

volume and incubation time on CaCO_3 precipitation in sands and their influence in sand cementation.

Sand (Ottawa F110, $d_{10} = 90 \mu\text{m}$, $d_{50} = 110 \mu\text{m}$) was selected for this experiment. It was sterilized in autoclave and kept in an aseptic container. The inocula was prepared by resuspending cells in Urea- CaCl_2 media prepared according to Table 6.1.

Test Procedure

A total of 6 specimens were prepared for each of the 5 nutrient combinations listed in Table 6.1. One is the sterile control which was disassembled after 64 days (same nutrient but heat-killed cells instead of vegetative ones). The other 5 were terminated after 2, 8, 16, 32 and 64 days, respectively. For each specimen, inocula was mixed with sand and fresh Urea- CaCl_2 broth and packed in 60 mL plastic syringes connected to a tubing to allow nutrient circulation (sketch Figure 6.1-a). All specimens were incubated at room temperature $T = 20^\circ\text{C}$. A pore volume (PV) of nutrient was introduced in each syringe and the old nutrient was allowed to drain out of the soil every 4 days. The soil remained submerged in the nutrient between flushes. Therefore, specimens terminated after 2, 8, 16, 32 and 64 days had access to 1, 3, 5, 9 and 17 PV of nutrient respectively. The sterile control was fed with the same nutrient as the other specimens during the whole duration of the test (64 days, 17 PV).

The termination of each test involved (a) draining the nutrient, (b) washing with alkaline water $\text{pH} \sim 9$ to remove excess materials in the remaining nutrient (which could precipitate abiotically during drying) without causing dissolution of biological precipitates, and (c) oven drying to stop metabolism. Then, syringes were cut with a mechanical saw to extract the soil. Pictures were taken for qualitative analysis.

The quantitative analysis was designed to determine the percentage by weight of CaCO_3 precipitate as a function of time and nutrient concentration. Specimens were

crushed using a mortar and oven-dried, and the dry weight was recorded, w_{s+p} . Next, the dry soil was washed in HCl solution (0.1 M) to dissolve precipitated carbonates, rinsed, drained and oven-dried. Again, the dry soil weight was recorded w_s . The difference between the two weights is considered to be the weight of the carbonates that were present in the original specimen, $\%CaCO_3 = (w_{s+p} - w_s)/w_s$. The amount of organic carbon was estimated to be less than 0.2 mg in total for these specimens (assuming the dry weight of a bacterial cell to be 0.2 pg and the carbon mass to be 50%). This corresponds to a contribution of less than 0.001% for this study; therefore, organic carbon content was neglected from the calculations.

Results

Pictures for all specimens are arranged in matrix form as a function of time and nutrient concentration in Figure 6.2. The first column corresponds to sterile controls. Each of the subsequent columns corresponds to specimens fed during 2, 8, 16, 32 and 64 days respectively. The first row corresponds to the weakest nutrient concentration (#1 in Table 6.1), and the last one to the strongest one (#5 in Table 6.1). A strong correlation between nutrient concentration, incubation time and apparent cementation of sand can be appreciated.

Carbonate concentration determined for each specimen are plotted in Figure 6.3. The three first nutrients (#1, #2 and #3 in Table 1) yield less than 0.1% carbonates after 64 days, the last two nutrients (#4 and #5 in Table 1) yield 2.4% and 4.0% carbonate.

The cementation efficiency of this experimental procedure is very low. Comparing the maximum amount of $CaCO_3$ that could be generated if all the chemicals in the nutrient reacted and the actual amount generated in the specimens, efficiency ranges between 0% and 0.64% for Nutrients #1, #2 and #3 and between 0.34% and 2.6% for Nutrients #4 and #5. The low efficiency reflects the relatively short time the nutrient stays inside the specimen between flushes.

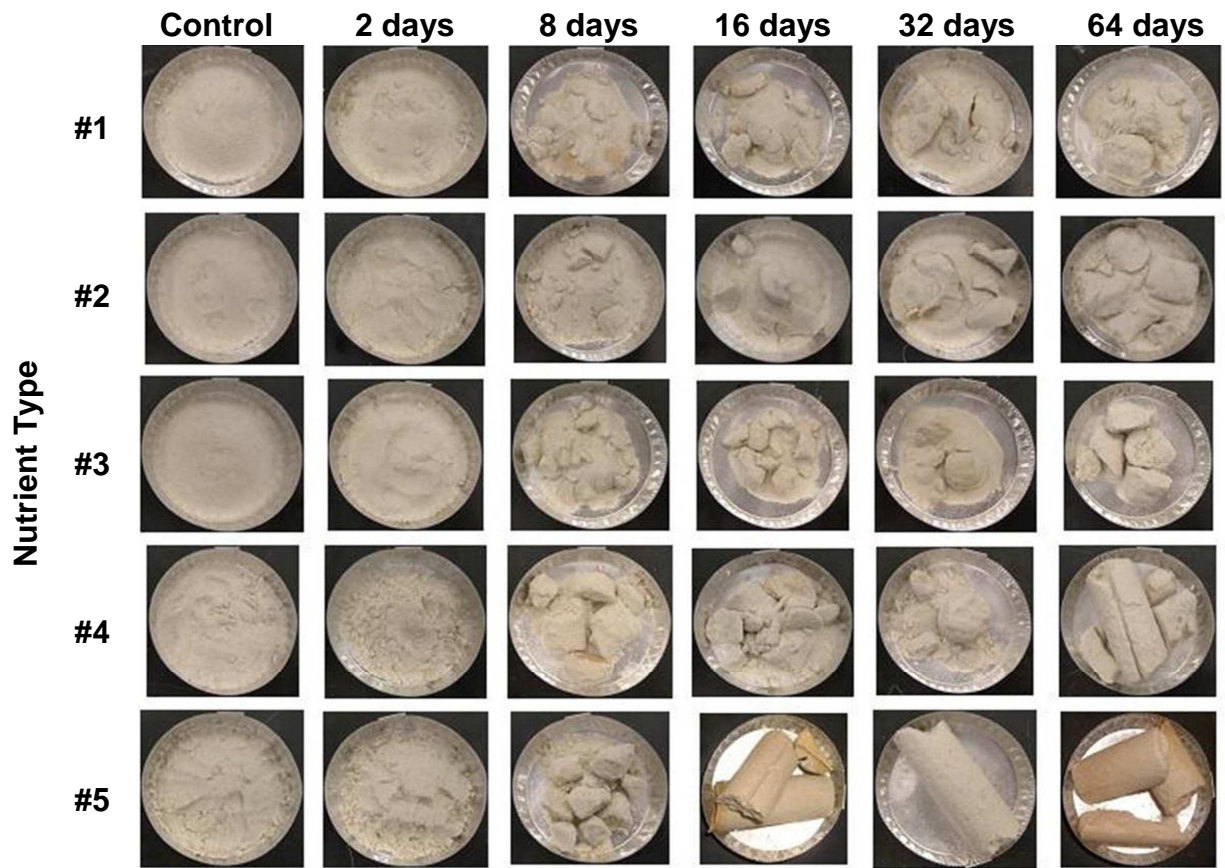


Figure 6.2 Effects of time and nutrient type on biogenic cementation as described in Study #2. Nutrient details in table 6.1.

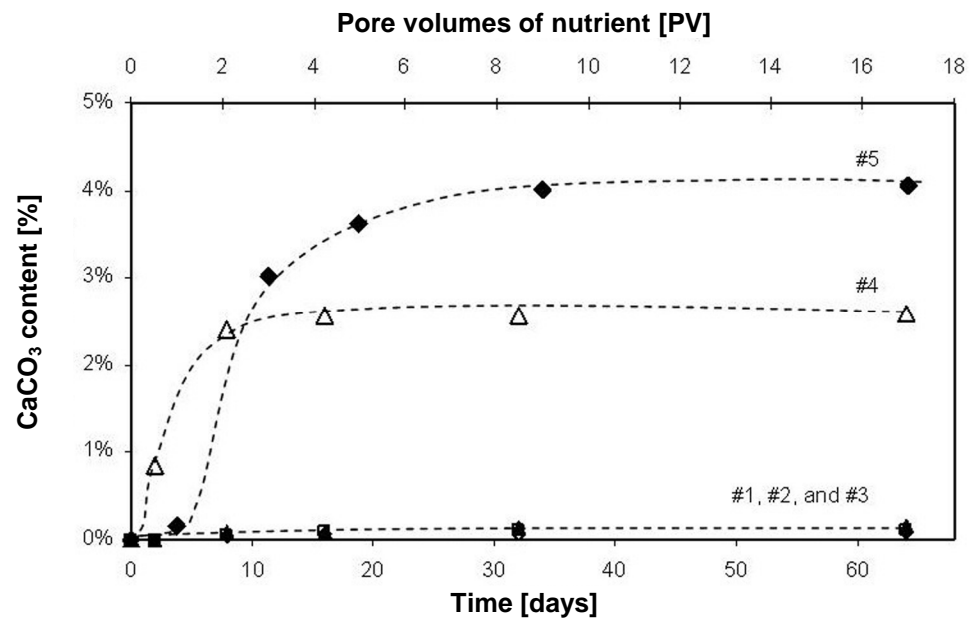


Figure 6.3 CaCO₃ content for specimens in Study #2. For details see Table 6.1.

Study #3: Pore and Grain Size Effects

The objective of this study is to explore the influence of geometry in the effectiveness of biocementation. Several materials were selected to cover a broad spectrum of soil grain sizes. In increasing size: kaolinite (Wilkinson RP2, $d_{10} = 0.36 \mu\text{m}$, $S_a = 33 \text{ m}^2/\text{g}$), silt (Silco-sil, crushed silica flour, $d_{10} = 10 \mu\text{m}$, $S_a = 0.113 \text{ m}^2/\text{g}$), fine sand (Ottawa F110, $d_{10} = 90 \mu\text{m}$, $d_{50} = 120 \mu\text{m}$, $C_u = 1.62$), several sizes of glass beads (GB50, $d_{10} = 50 \mu\text{m}$, $d_{50} = 50 \mu\text{m}$, $C_u = 1$; GB75, $d_{10} = 75 \mu\text{m}$, $d_{50} = 75 \mu\text{m}$, $C_u = 1$; GB250, $d_{10} = 250 \mu\text{m}$, $d_{50} = 250 \mu\text{m}$, $C_u = 1$; GB700, $d_{10} = 700 \mu\text{m}$, $d_{50} = 700 \mu\text{m}$, $C_u = 1$; GB1000, $d_{10} = 1000 \mu\text{m}$, $d_{50} = 1000 \mu\text{m}$, $C_u = 1$; GB5000, $d_{10} = 5000 \mu\text{m}$, $d_{50} = 5000 \mu\text{m}$, $C_u = 1$), coarse sand (S#10, $d_{10} = 4000 \mu\text{m}$, $d_{50} = 5300 \mu\text{m}$, $C_u = 1.48$), and fine gravel (GV#4, $d_{10} = 9000 \mu\text{m}$, $d_{50} = 11500 \mu\text{m}$, $C_u = 1.67$). All materials were sterilized in autoclave and kept in an aseptic container until use. The test liquid media #5 was used for all tests in this study (Table 6.1). The inocula was prepared by resuspending cells in Urea-CaCl₂ media.

Test Procedure

The general assemblage procedure followed the sequence described for Study #2 including termination procedures and data gathering for qualitative and quantitative analyses. Only one syringe was used for each material and all specimens were terminated after 32 days.

Results

The content of CaCO₃ is shown as a function of grain size in Figure 6.4; pictures are superimposed on the figure. Maximum carbonate deposition is observed on grains ~ 100 microns in size. The kaolinite (specimen #1 in Figure 6.4) is uncemented and coarse grains (specimens #9, #10 and #11 in Figure 6.4) readily de-bonded upon manipulation. All other intermediate cases exhibited a well-bonded fabric.

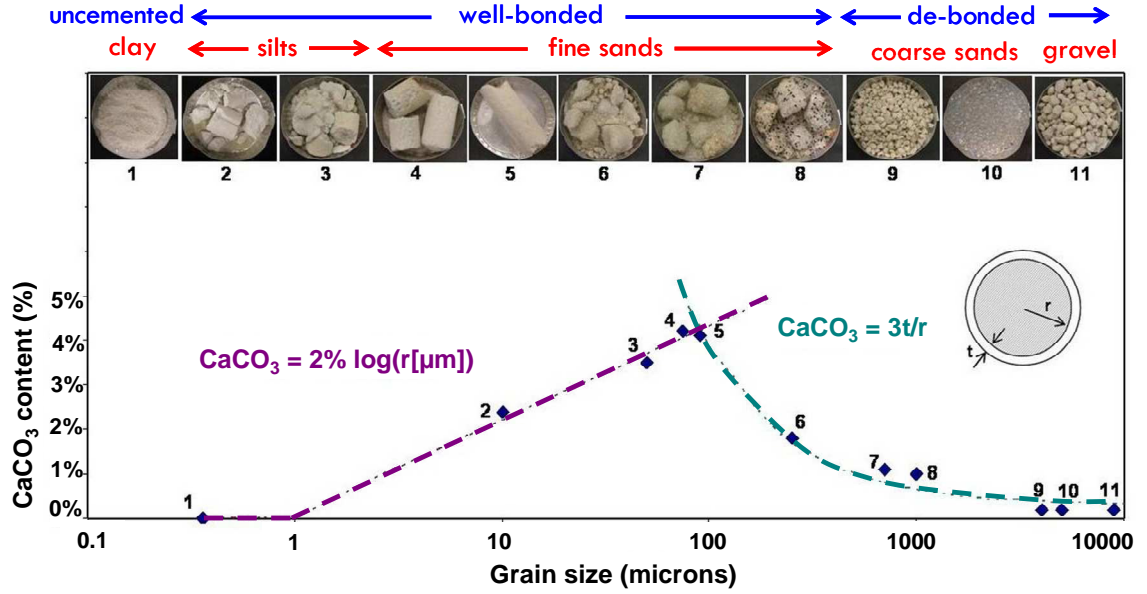


Figure 6.4 CaCO_3 content and models as a function of the grain size, as described in Study #3. Pictures correspond to each data point.

Analysis

The lack of cementation in very fine particles suggests a relationship between bacterial activity, nutrient percolation and mineral precipitation. Bacterial activity is hindered in very fine soils (Chapter 3), therefore their metabolism cannot produce enough calcium carbonate to cement the soil. In field applications the process may also be limited by the slow advection of nutrient throughout the soil mass. On the other hand, the lack of cementation in coarse soils indicate that a thin layer of mineral precipitation is not enough to cement particles together when grains are large or to increase the coordination number of the soil mass.

The mass fraction of carbonate $\text{CaCO}_3(\%)$ as a function of grain size r depends on the thickness t of the precipitate,

$$\text{CaCO}_3(\%) = \frac{4 \cdot \pi \cdot r^2 \cdot t \cdot \rho_{\text{CaCO}_3}}{\frac{4}{3} \cdot \pi \cdot r^3 \cdot \rho_{\text{soil}}} \approx \frac{3 \cdot t}{r} \quad (6.5)$$

This equation properly fits the right portion of the experimental data for a thickness $t \sim 1 \mu\text{m}$ as shown in Figure 6.4. Therefore, this portion of the curve is nutrient and/or time limited.

In view of experimental results, and in agreement with conclusions in Chapter 3, the left hand side of the data in Figure 6.4 is fitted with a log-model starting at $d_{50} \sim 1 \mu\text{m}$:

$$\text{CaCO}_3(\%) = 2\% \cdot \log\left(\frac{r}{1 \cdot \mu\text{m}}\right) \quad \text{for } r \geq 1 \mu\text{m} \quad (6.6)$$

The exponential dependency on size observed for the finer materials suggests geometry-limited bioactivity.

Clearly, both trends in Equations 6.5 and 6.6 apply to the experimental conditions tested herein. However, they reveal the governing limiting effects of pore size, nutrient, and time. Results from this experiment do not deny the possibility of achieving biocementation in coarser soils, but they emphasize that sufficient nutrients and time will be required to create a cemented layer thick enough to overcome skeleton forces that are proportional to the square of the grain size and the effective stresses.

Study #4: Diffusion of Nutrients and Cells

The purpose of this study is to analyze how the diffusion of both bacterial cells and nutrients through the soil mass, affect the biocementation process. Sand (Ottawa F110, $d_{10} = 90 \mu\text{m}$, $d_{50} = 110 \mu\text{m}$) and silt (Sil-co-sil, crushed silica flour, $d_{10} = 10 \mu\text{m}$, $d_{50} = 12 \mu\text{m}$) were selected for this experiment. Soils were sterilized in autoclave and kept in an aseptic container. The test liquid media #5 was used (Table 6.1), and inocula was prepared with cells resuspended in saline solution or in Urea-CaCl₂ media.

Test Procedure

Four 60 mL plastic syringes were packed with soil, two with sand and two with silt. For each soil, specimens differed in the saturation procedure: A-type specimens were saturated with sterile deionized water and a thin film of the water was left on top of the soil to ensure saturation. Then, a pore volume of Urea-CaCl₂ inocula was poured on top of the soil, minimizing mixing and preventing advective flow into the specimen. The B-type specimens were saturated with the saline solution inocula and only fresh Urea-CaCl₂ media was poured on top (see Figure 6.1-b for details). Syringes were incubated at room temperature for 4 weeks without nutrient replacement. At the end of the test, the excess liquid was removed and specimens were terminated as described in Study #2.

Results and Analysis

Both A-type and B-type specimens were cemented and no significant difference was observed among them. These results suggest that diffusion of both bacterial cells and nutrients occur quite efficiently in these two soils.

The chemical diffusion time t_{chem} can be estimated as:

$$t_{chem} = \frac{L^2}{D_{chem}} \quad (6.7)$$

The diffusion coefficient for bacteria D_{bio} assuming unconstrained Brownian motion can be estimated from Einstein's expression ($D_{bio} \propto 1/r_{bio}$). Thus, the time scale for bacterial diffusion is:

$$t_{bio} = \frac{L^2}{D_{bio}} \quad (6.8)$$

Finally, a lower-boundary for bacterial self-transport t_{min} can be estimated as the travel time of a bacterium swimming in straight line through the porous network:

$$t_{min} = \frac{L}{v} \quad (6.9)$$

For $L = 50$ mm and $D_{chem} = 10^{-9}$ m²/s, and $v = 10$ μm/s (Chapter 3), $t_{chem} \sim 29$ days, $t_{bio} \sim 800$ years and $t_{min} \sim 85$ min. Based on these expressions and experimental results, the following observations can be made:

- Chemical diffusion explains the transport of nutrients along the specimens within the length of this study.
- Bacterial diffusion through unconstrained Brownian motion cannot justify test results. If bacteria had been transported by bio-diffusion, the specimens would have been uncemented at the end of the 30 day-long study.
- Published experimental results show the importance of chemotaxis for migration of bacteria towards high-nutrient concentration areas in porous media [*Ford and Harvey*, 2007; *Olson et al.*, 2004; *Sherwood et al.*, 2003]. Note, however, that in this case bacteria are migrating together with the nutrient front i.e., towards low-nutrient concentration areas and against the chemotaxis direction. Therefore the mechanism appears to be related to population growth and volume-exclusion controlled by nutrient availability. Clearly, bacteria does not advance ahead of the nutrient front in this study, hence the biomineralization process was nutrient diffusion controlled.

These analyses suggest the benefits of diffusion for biocementation in natural sands and silts that are not necessarily homogeneous.

Study #5: Coupled Effects – Heterogeneity and Unsaturation

While diffusion acts as a homogenizing process, some forms of spatial variability in natural soils may hinder the evolution of biogenic cementation. The case of imbibition in unsaturated media is explored next.

Sand (Ottawa F110, $d_{10} = 90$ μm, $d_{50} = 110$ μm) and silt (Sil-co-sil, crushed silica flour, $d_{10} = 10$ μm, $d_{50} = 12$ μm) were selected for this experiment. Soils were sterilized

in autoclave and kept in an aseptic container. Test liquid media #5 was used for this study (Table 6.1). Inocula was prepared by resuspending cells in saline solution.

Four 1 L plastic bottles were packed as follows: two with dry sand as a host with a cylindrical dry silt inclusion, and two with dry silt as a host with a cylindrical dry sand inclusion at the center (See Figure 6.1-c for details). A pore volume of the saline solution inocula was slowly poured on top of the specimens. Then, a pore volume of nutrient was added to the top of each bottle. This process was repeated every 3 days allowing the old nutrient to drain out of the soil every time. Specimens were fed approximately 5 PV by the end of the 2 week-long experiments and 10 PV by the end of the 4 week-long tests. At the end of the test, excess liquid was removed, and specimens were terminated as described in Study #2.

Results

Sketches presented in Figure 6.5 capture the degree of cementation observed in the disassembled specimens. The following observations can be made:

- Two weeks: the silt portion was strongly cemented in both specimens. The sand host was lightly cemented at the top, bottom and around the borders of the silt inclusion while the sand inclusion was clearly uncemented.
- Four weeks: no significant changes were observed; both the silt host and silt inclusion were strongly cemented. The top portion of the sand host was significantly more cemented after 4 weeks; however, no significant changes were appreciated in the bottom and sides of the sand host, or in the sand inclusion, compared to the 2 weeks specimens.

Results show that capillary driven fluid flow prevents the penetration of fluid in the sand (either the same inclusion or along the sides of the sand host) which remains

“dry” throughout the test. Instead, capillary driven imbibition prevails in the silt and it becomes rock-like at the end of the tests.

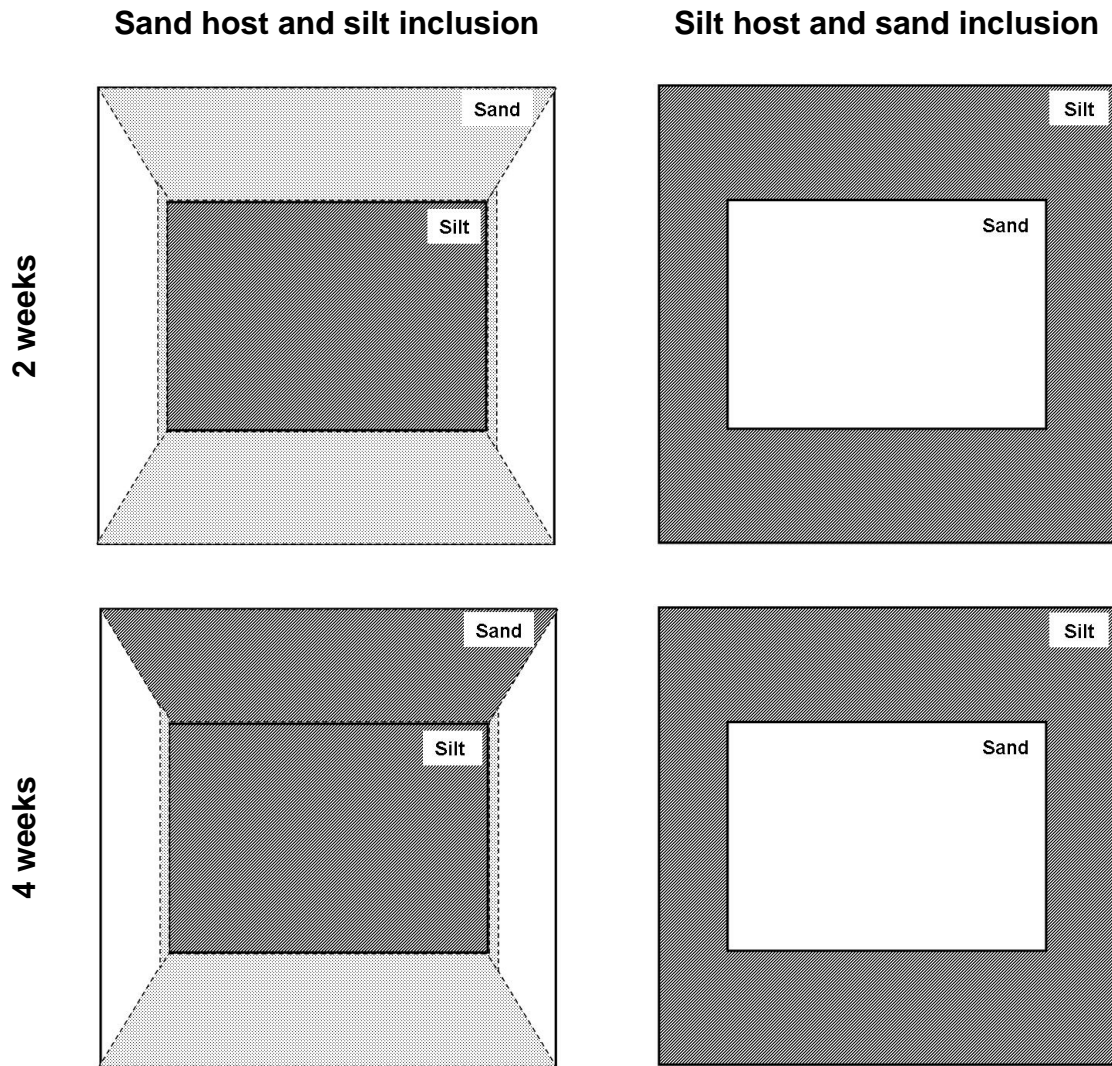


Figure 6.5 Evolution of cementation in unsaturated heterogeneous specimens (Study #5). The darker the color, the higher the degree of cementation (white: no cementation, dark gray: rock-like material).

Discussion and Analysis

Cementation and Soil Stiffness and Strength

The particle-level deformation mechanisms vary with strain level. At small-strains ($\varepsilon < \sim 10^{-5}$), stresses and strains concentrate at contacts. In fact, the normal stiffness of the soil skeleton at small strains E_{tan} depends on the size of contacts r_c , for a particle size r [Santamarina *et al.*, 2001],

$$\frac{E_{tan}}{E_m} = \frac{1}{2 \cdot (1 - \nu_m^2)} \cdot \frac{r_c}{r} \quad (6.9)$$

where E_m and ν_m are the elastic modulus and Poisson's ratio of the material that makes the grains. This equation highlights that a small change in contact area can significantly affect soil stiffness.

The cementation thickness, particle size and cement content can be geometrically related as follows:

$$t = \left((\alpha + 1)^{1/3} - 1 \right) \cdot r \quad (6.10)$$

where t is the cementation thickness, r is the particle size, and α is the relative cement content (W_{cement}/W_{soil}). Combining Equations 6.9 and 6.10 it can be anticipated that even a slight amount of cementation can significantly affect soil stiffness.

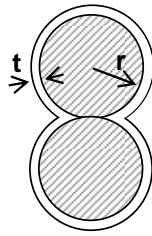
At large strains, bio-precipitated carbonates can add interparticle tensile resistance, increase rotational frustration, and partially fill voids. In turn, these particle level effects cause higher friction and dilative tendency at the macroscale. These particle level mechanisms are summarized in Figure 6.6.

The effects of biogenic cementation in soil stiffness and strength have been reported in recent publications. Soil stiffness evolution with biocementation has been

monitored in sands using shear-wave velocity V_S , and reported data indicates that V_S increases from ~ 180 m/s to ~ 540 m/s due to this process [DeJong *et al.*, 2006]. The soil strengthening effects of biocementation has been corroborated using drained triaxial tests: a maximum compressive strength of ~ 500 kPa was measured for a confining pressure of 50 kPa [Whiffin *et al.*, 2007].

Mechanical Effects

STIFFNESS

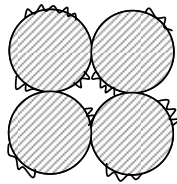


$$\frac{E_{\tan}}{G_g} = \frac{1}{(1-\nu_g)} \sqrt{(CC+1)^{2/3} - 1 + \left[\frac{3 \cdot (1-\nu_g)}{2} \left(\frac{\sigma}{G_g} \right) \right]^{2/3}}$$

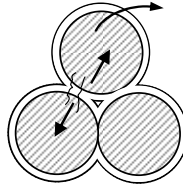
[Fernández & Santamarina, 2001]

STRENGTH

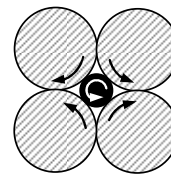
Surface roughness



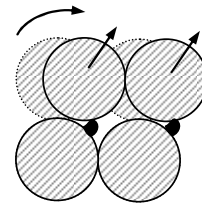
Contact tensile strength



Pore filling and rotational frustration

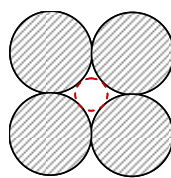


Dilation

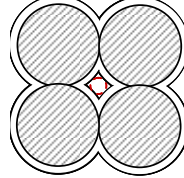


HYDRAULIC CONDUCTIVITY

Uncemented



Reduced pore-throat



$$\frac{k_{final}}{k_{initial}} = \frac{(d_{pore} - 2 \cdot t)^2}{d_{pore}^2} = \left(1 - \frac{2 \cdot t}{d_{pore}} \right)^2$$

Figure 6.6 Effects of biogenic cementation on soil properties.

Metabolic By-Products

Environmentally undesirable metabolic by-products such as ammonia can be deposited into the soil when biocementation takes place through the pathway described in

this study. Further research is needed to adjust the process to attain the desired mechanical impact within an environmentally friendly methodology.

Reversibility

Biocementation is a reversible process. Since CaCO_3 dissolves in $\text{pH} < 7$, precipitates may dissolve as the pore fluid reverses to background conditions prevailing before treatment.

Conclusions

The morphology and timing of biogenic crystal nucleation on mineral surfaces is influenced by the nature of the substrate. Thus, it is expected that biocementation will vary in soils with different mineralogy even if their pore and grain sizes are similar.

The balance between Urea and CaCO_3 content, as well as the residency time of the nutrients must be adjusted to achieve optimal efficiency and minimize waste in the biocementation process.

Pore and grain sizes play a fundamental role in soil biocementation. On the one hand, bacterial activity cannot take place in very fine soils. On the other hand, when grains are large, a thin layer of cementation cannot overcome skeletal forces that are proportional to the square of the grain size and the effective stresses and fails to cement the soil mass. Therefore, longer time and larger amounts of nutrients are needed to increase the stiffness and strength in coarse soils.

Diffusion of nutrients and bacterial cells can be beneficial for biocementation in saturated natural sands and silts, where hydromechanical conditions may bias fluid transport.

Capillary-driven fluid flow in unsaturated soils can prevent penetration of nutrients and bacterial cells in the coarser soil regions and favor biocementation of finer zones within the soil mass.

At small strains, even a slight cementation can significantly increase soil stiffness. At large strains, cementation can add interparticle tensile resistance, increase surface roughness and rotational frustration and partially fill voids, increasing friction and dilative tendencies of the soil mass. In addition, void filling alters the hydraulic conductivity of soils.

CHAPTER 7

GENERAL CONCLUSIONS AND FUTURE WORK

General Conclusions

Mechanical and geometrical interactions between bacterial cells and soil particles play an important role in the design of bio-mediated soil improvement techniques. Grain size and burial depth restrict the range where biomediated geochemical processes can be expected in sediments, affect the interpretation of geological processes and the development of engineering solutions such as bioremediation (Chapter 3).

Geometrical constraints and mechanical interactions suggest different regions for bacteria's fate. (a) "Active and motile" when pore and pore throats are large so that cells can move through the pore network and find sufficient space for growth and metabolic activity. (b) "Trapped inside pores" when pore throats hinder migration; this zone can be subdivided into three subzones depending on the bacteria's ability to push particles and the size of the habitable pore space. (c) "Dead" when burial depths exceed the puncturing and/or squeezing thresholds; spore-forming species may remain dormant. Bacteria in the region that corresponds to very small particle sizes, beyond the buckling limit, may not be mechanically compromised, yet their survivability will be limited by nutrient and waste transport. The geometrical and mechanical constraints to microbial activity apply to fracture-free sediments; the pore size distribution and inter-particle forces in the gouge material within fractures may deviate from those imposed by lithostatic stresses assumed in this study.

Bacterial metabolic activity and by-products can have important effects in the mechanical properties of soils, including the bulk stiffness of the pore fluid hence pore

pressure generation during shear (Chapter 4), hydraulic conductivity (Chapter 5) and small-strain shear stiffness (Chapter 6).

Biogenic gas forms into sub-micron size bubbles which are disseminated throughout the soil mass in contrast to air injection which tends to concentrate along percolation paths. Thus, the biogenic gas alternative may be more effective at preventing the local triggering of liquefaction. Soil grain size affects the early evolution of bio-mediated gas generation by contributing nucleation sites as well as entrapment. Bacteria and nutrients must be properly selected so that the generated gases are environmentally safe, have low solubility in water, facilitate bubble formation, and experience relatively long residency time. Biogenic gas generation (nitrogen gas in this study) effectively reduces the bulk stiffness of the pore fluid and the P-wave velocity, suggesting potential effects in Skempton's B parameter and the susceptibility to liquefaction. P-wave propagation provides insightful information that can be effectively used to monitor biogenic gas generation in laboratory applications.

The effective biological clogging of soils presents two limiting boundaries related to the pore size. Bacterial ability to metabolize and generate biofilms is hindered by geometrical constraints when pore size is smaller than $\sim 1 \mu\text{m}$. On the other hand, when soil particles and pores are too large, biofilm accumulation is limited by pore flow velocity and ensuing shear forces. Radial flow studies show a characteristic radial distance where clogging starts. This radial distance is directly proportional to flow velocity and it is linked to the "pore-scale" flow velocity. Coupling between biological and mechanical clogging could be used as a tool to create a long-term yet reversible solution where lower hydraulic conductivities are needed, or to engineer techniques to stop unwanted contaminants including migratory fines.

Biogenic cementation is influenced by the pore and grain size and mineralogy of the soil particles where crystals nucleate, and the type of nutrient, residency time and flow processes that take place in the soil mass. At small strains, even a slight cementation

can significantly increase soil stiffness. At large strains, biomineralization can add interparticle tensile resistance, increase surface roughness and rotational frustration and partially fill voids, increasing friction and dilative tendencies of the soil mass. In addition, void filling alters the hydraulic conductivity of soils.

Bio-mediated changes of soil properties can be controlled/engineered to modify the mechanical and conduction properties of soils. However, the potential development of bio-mediated soil improvement methods needs to be further analyzed to prevent environmental issues related to the injection of bacterial cells and/or nutrients into the soil mass, and to assess the long-term stability and geochemical equilibrium of the treated soil.

Future Work

Results and conclusions gathered in this study can be augmented to extend the scope and impact of this research. Some suggestions follow.

Chapter 3. A Gram-positive bacterium could be used. Gram-positive bacteria are less common in soils but they have thicker cell wall that may protect them against bursting and puncture under high overburden conditions.

Chapter 4. Only the effects of nitrogen gas on the bulk stiffness of the pore fluid were analyzed. Other metabolisms could be explored to evaluate possible differences. A more detailed analysis of waste-products generated through denitrification, in particular when this metabolic pathway is incomplete is needed for field applications.

Chapter 5. Use a more comprehensive configuration of pore pressure transducers to gather more extensive information in a single test and improve the inversion process. Implement reverse flow and mixed-fluid flow to explore the effect of this common field condition.

Chapter 6. A large-scale test is needed to account for the possible effects of percolation and spatial variability in the efficiency of biocementation. X-Ray diffraction analysis can be used to corroborate the nature of the crystals.

General. Investigate long-term equilibrium conditions, and extend previous studies to explore the effects of mixed-microbial communities.

APPENDIX A

PARTICLE LEVEL ANALYTICAL MODELS

Cell Squeezed Between Two Particles (Table 3.3, Model c)

Since the critical particle size is considered to be the one generating the critical contact area:

t_p	Particle size	
R	Cell radius	
γ_{eff}	Effective unit weight of the soil mass	
σ_f	Internal pressure in the cell at failure	
ε	Axial strain	
α	Ratio initial thickness over initial radius	$\frac{t_i}{R}$
β	Ratio final over initial surface area	
ν	Poisson's ratio of cell wall	
E_{cell}	Elastic modulus of cell wall	
ϕ	Ratio tensile strenght over elastic modulus	
H_{crit}	Maximum depth the cell can survive	
$A_c = \left(\frac{t_{p.crit}}{2} \right)^2 \cdot \pi$	Critical contact area (when cell wall fails)	
$A_{inf} = (2 \cdot R)^2$	Influence area	
$H_{crit} = \frac{\sigma_f}{\gamma_{eff}} \cdot \frac{A_c}{A_{inf}}$	Critical depth for cell wall straining (deeper than this, cell wall fails)	

To obtain the internal pressure at failure, σ_f

$$b = R \cdot (1 - \varepsilon) \quad \text{Deformed radius}$$

Assuming constant volume inside the cell, the deformed contact radius can be obtained:

$$a = \frac{-\pi^2 \cdot R \cdot (1 - \varepsilon)^2 + \sqrt{\pi^4 \cdot R^2 \cdot (1 - \varepsilon)^4 - \frac{32}{3} \cdot \pi^2 \cdot R^2 \cdot [(1 - \varepsilon)^3 - 1]}}{4 \cdot \pi \cdot (1 - \varepsilon)}$$

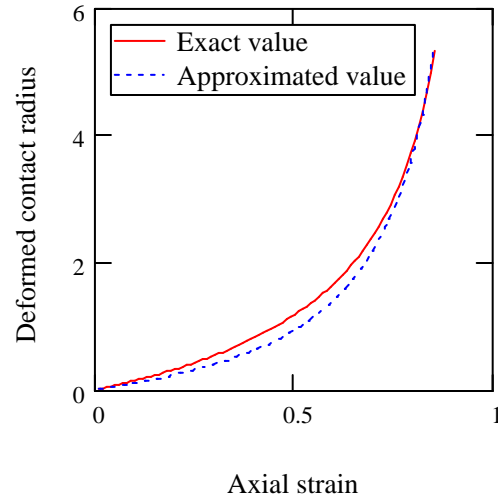
This expression can be approximated by:

$$\varepsilon := 0.01, 0.02 \dots 0.85$$

$$R := 1$$

$$a = \frac{3 \cdot R}{\pi} \cdot \left(\frac{\varepsilon}{1 - \varepsilon} \right)$$

The cell is assumed to deform following the shape of a filled torous



The initial and final surface areas are:

$$A_i = 4 \cdot \pi \cdot R^2 \quad \text{Initial surface area (sphere)}$$

$$A_f = 2 \cdot \pi \cdot a^2 + 2 \cdot \pi^2 \cdot a \cdot b + 4 \cdot \pi \cdot b^2 \quad \text{Final surface area (filled torous)}$$

Assuming thin-walled geometry: $\frac{A_f}{A_i} = \frac{t_i}{t_f} = \frac{\alpha \cdot R}{t_f} = \beta$ $\varphi := 0.1, 0.2 \dots 0.5$

Then, the transversal strain can be defined in terms of β as: $\varepsilon_t = \frac{1 - \beta}{\beta}$

Assuming constant volume in the membrane ($v = 0.5$) the tensile strain is: $\varepsilon_l = \frac{-\varepsilon_t}{2} = \frac{\beta - 1}{2 \cdot \beta}$

Therefore the tensile stress is: $\sigma_l = \varepsilon_l E_{\text{cell}} = \frac{E_{\text{cell}}}{2} \cdot \left(\frac{\beta - 1}{\beta} \right)$

Thus, the maximum deformation the cell can sustain is related to β as: $\varphi = \frac{\beta_{\text{max}} - 1}{2 \cdot \beta_{\text{max}}}$

And therefore, the maximum allowable β is: $\beta_{\text{max}} = \frac{1}{1 - 2 \cdot \varphi}$

Which can be approximated as:

$$\varepsilon_{\max} = \varphi^{\frac{1}{3}}$$

By force equilibrium:

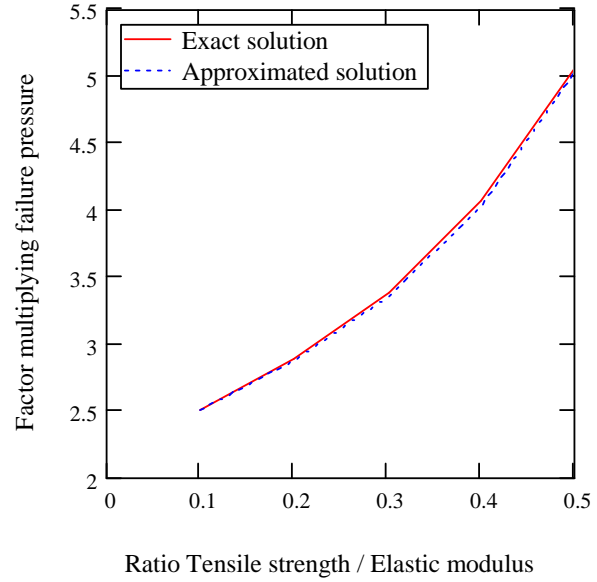
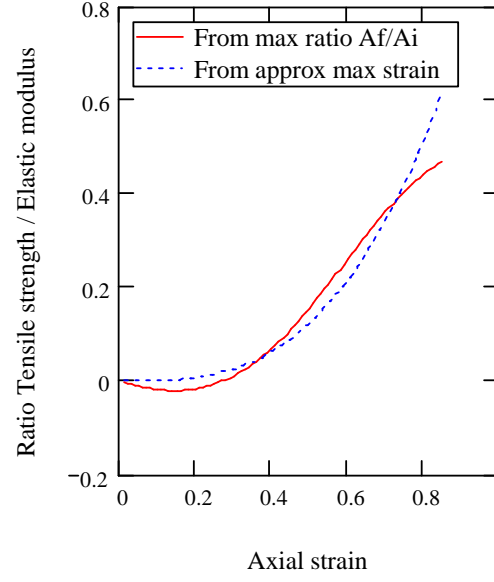
$$\sigma_p = \sigma_I \frac{A_I}{A_p} = \frac{E_{\text{cell}} \alpha \cdot R}{2} \cdot \left(\frac{\beta - 1}{\beta^2} \right) \cdot \frac{4 \cdot a + 2 \cdot \pi \cdot b}{4 \cdot a \cdot b + \pi \cdot b^2}$$

$$\sigma_f = \frac{E_{\text{cell}} \alpha \cdot R}{2} \cdot \left(\frac{\beta_{\max} - 1}{\beta_{\max}^2} \right) \cdot \frac{4 \cdot a_{\max} + 2 \cdot \pi \cdot b_{\min}}{4 \cdot a_{\max} \cdot b_{\min} + \pi \cdot b_{\min}^2}$$

Replacing:
$$\sigma_f = E_{\text{cell}} \alpha \cdot \varphi \cdot (1 - 2 \cdot \varphi) \cdot \frac{\frac{12}{\pi} \cdot \varphi^{\frac{1}{3}} + 2 \cdot \pi \cdot \left(1 - \varphi^{\frac{1}{3}}\right)^2}{\frac{12}{\pi} \cdot \varphi^{\frac{1}{3}} + \pi \cdot \left(1 - \varphi^{\frac{1}{3}}\right)^2} \cdot \frac{1}{1 - \varphi^{\frac{1}{3}}}$$

Which can be approximated as:

$$\sigma_f = E_{\text{cell}} \alpha \cdot \varphi \cdot (1 - 2 \cdot \varphi) \cdot \left(\frac{1}{\frac{\pi}{7} - \frac{1}{2} \cdot \varphi} \right)$$



Finally the critical depth will be:

$$H_{\text{crit}} = \frac{E_{\text{cell}} \cdot \alpha \cdot \varphi \cdot (1 - 2 \cdot \varphi) \cdot \left(\frac{\frac{\pi}{7} - \frac{1}{2} \cdot \varphi}{1} \right) \cdot \left(\frac{t_{\text{p.crit}}}{2} \right)^2 \cdot \pi}{\gamma_{\text{eff}} \cdot (2 \cdot R)^2}$$

but the critical particle thickness is:

$$\frac{t_{\text{p.crit}}}{2} = a_{\text{max}} = \frac{3 \cdot R}{\pi} \cdot \left(\frac{\frac{1}{\varphi^3}}{1 - \frac{1}{\varphi^3}} \right)$$

$$H_{\text{crit}} = \frac{E_{\text{cell}}}{\gamma_{\text{eff}}} \cdot \frac{9}{4 \cdot \pi} \cdot \frac{\alpha \cdot \varphi \cdot (1 - 2 \cdot \varphi)}{\frac{\pi}{7} - \frac{1}{2} \cdot \varphi} \cdot \left(\frac{\frac{1}{\varphi^3}}{1 - \frac{1}{\varphi^3}} \right)^2$$

Cell Puncture (Table 3.3, Model d)

t_p		Particle size	
R	$\underline{R} := 1$	Cell radius	
γ_{eff}		Effective unit weight of the soil mass	
ε	$\underline{\varepsilon} := 0.01, 0.02.. 0.85$	Axial strain	
α		Ratio initial thickness over initial radius	$\frac{t_i}{R}$
λ	$\lambda := 6.8, 6.9.. 25$	Ratio particle radius over deformed contact area radius	
ν		Poisson's ratio of cell wall (equal to 0.5)	
E_{cell}		Elastic modulus of cell wall	
ϕ		Ratio tensile strenght over elastic modulus	
H_{crit}		Maximum depth the cell can survive	
ψ		Ratio particle thickness over cell radius	
w_d		Indentation depth	
a		Deformed radius of contact area	

Following the expressions developed by Sun et al, 2003 for puncturing geometry:

$$\sigma_1 = \frac{-E_{\text{cell}} \cdot w_d^2}{a^2} \cdot \left[\frac{3 - 4\lambda^2 + \lambda^4 + 2 \cdot \ln(\lambda^2)}{(1 - \lambda^2) \cdot (1 - \lambda^2 + \ln(\lambda^2))^2} \right]$$

This expression can be simplified as:

$$\sigma_1 = \frac{E_{\text{cell}} \cdot w_d^2}{a^2} \cdot \left(\frac{\pi}{3\lambda} \right)^2$$

But by definition: $\lambda = \frac{\psi \cdot R}{2 \cdot a}$

$$\sigma_1 = E_{\text{cell}} \cdot \left(\frac{2 \cdot \pi}{3} \cdot \frac{w_d}{\psi \cdot R} \right)^2$$

At failure:

$$w_{d,f} = \frac{3 \cdot \psi \cdot R}{2 \cdot \pi} \cdot \varphi^{\frac{1}{2}} \quad a_f = \frac{3 \cdot \psi \cdot R}{\pi} \cdot \varphi^{\frac{1}{2}}$$

In addition, according to Sun et al, 2003 model:

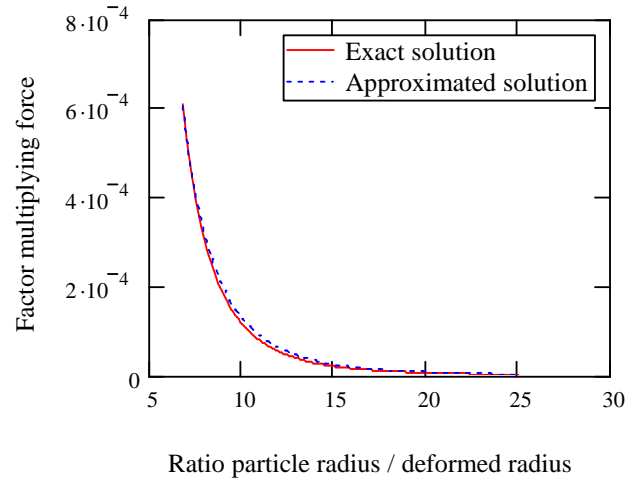
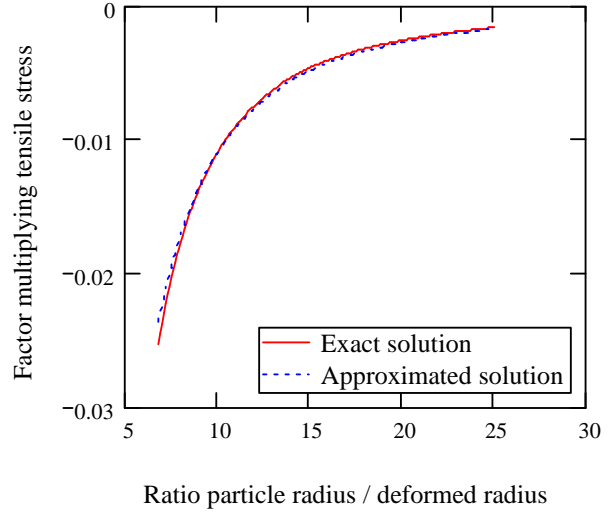
$$F_f = \pi \cdot E_{\text{cell}} \cdot \alpha \cdot R \cdot w_{d,f} \cdot \left[\frac{3 - 4\lambda^2 + \lambda^4 + 2 \cdot \ln(\lambda^2)}{(1 - \lambda^2) \cdot (1 - \lambda^2 + \ln(\lambda^2))^3} \right]$$

Simplifying:

$$F_f = E_{\text{cell}} \cdot \alpha \cdot R \cdot w_{d,f}^5 \cdot \left(\frac{32\pi^4}{3} \right) \cdot \left(\frac{1}{\psi \cdot R} \right)^4$$

Replacing the indentation depth at failure, the critical depth is:

$$H_{\text{crit}} = \frac{81}{4 \cdot \pi} \cdot \frac{E_{\text{cell}}}{\gamma_{\text{eff}}} \cdot \alpha \cdot \psi \cdot \varphi^{\frac{5}{2}}$$



Cell Squeezed Within the Equivalent Continuum Sediment Skeleton (Table 3.3,

Model e)

t_p	Particle size	
R	Cell radius	
γ_{eff}	Effective unit weight of the soil mass	
σ_f	Internal pressure in the cell at failure	
ε	Axial strain	
α	Ratio initial thickness over initial radius	$\frac{t_1}{R}$
β	Ratio final over initial surface area	
ν	Poisson's ratio of cell wall	
E_{cell}	Elastic modulus of cell wall	
ϕ	Ratio tensile strenght over elastic modulus	
H_{crit}	Maximum depth the cell can survive	
ψ	Ratio particle thickness over cell radius	
σ_s	Stress acting in the soil skeleton	
ξ	Diffuse double layer thickness	$\xi = \sqrt{\frac{\varepsilon_0 \cdot R_{gas} \cdot \kappa \cdot T}{2 \cdot Fa^2 \cdot c_0 \cdot z^2}}$
ε_0	Permittivity of the free space	
R_{gas}	Gas constant	
κ	Real permittivity of water	
T	Absolute temperature	
Fa	Faraday's constant	
c_0	Ionic concentration	
z	Valence of cations	
A_h	Hamaker constant	
K_0	Lateral stress coefficient	

In this case, the critical depth includes a component due to the stress in the soil skeleton:

$$A_c = a_{\max}^2 \cdot \pi \quad \text{Critical contact area (when cell wall fails)}$$

$$A_{\inf} = (4 \cdot R)^2 \quad \text{Influence area}$$

$$A_{\text{soil}} = (2 \cdot R)^2 \quad \text{Soil skeleton influence}$$

$$H_{\text{crit}} = \frac{\sigma_f}{\gamma_{\text{eff}}} \cdot \frac{A_c}{A_{\inf}} + \frac{\sigma_s}{\gamma_{\text{eff}}} \cdot \frac{A_{\text{soil}}}{A_{\inf}} \quad \text{Critical depth for cell wall straining (deeper than this, cell wall fails)}$$

To obtain the internal pressure at failure, σ_f : $\varepsilon := 0.01, 0.02 \dots 0.85$ $R := 1$

$$b = R \cdot (1 - \varepsilon) \quad \text{Deformed radius}$$

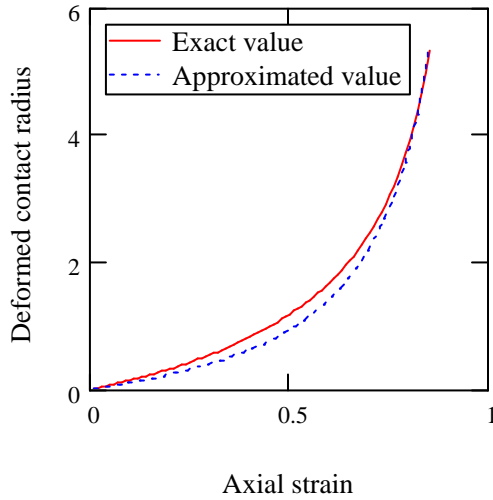
Assuming constant volume inside the cell, the deformed contact radius can be obtained:

$$a = \frac{-\pi^2 \cdot R \cdot (1 - \varepsilon)^2 + \sqrt{\pi^4 \cdot R^2 \cdot (1 - \varepsilon)^4 - \frac{32}{3} \cdot \pi^2 \cdot R^2 \cdot [(1 - \varepsilon)^3 - 1]}}{4 \cdot \pi \cdot (1 - \varepsilon)}$$

this expression can be approximated by:

$$a = \frac{3 \cdot R}{\pi} \cdot \left(\frac{\varepsilon}{1 - \varepsilon} \right)$$

The cell is assumed to deform following the shape of a filled torous



The initial and final surface areas are:

$$A_i = 4 \cdot \pi \cdot R^2 \quad \text{Initial surface area (sphere)}$$

$$A_f = 2 \cdot \pi \cdot a^2 + 2 \cdot \pi^2 \cdot a \cdot b + 4 \cdot \pi \cdot b^2 \quad \text{Final surface area (filled torous)}$$

Assuming thin-walled geometry:

$$\frac{A_f}{A_i} = \frac{t_i}{t_f} = \frac{\alpha \cdot R}{t_f} = \beta$$

Then, the transversal strain can be defined in terms of β as:

$$\varepsilon_t = \frac{1 - \beta}{\beta}$$

Assuming constant volume in the membrane ($\nu = 0.5$) the tensile strain is:

$$\varepsilon_l = \frac{-\varepsilon_t}{2} = \frac{\beta - 1}{2\beta}$$

Therefore the tensile stress is:

$$\sigma_l = \varepsilon_l E_{\text{cell}} = \frac{E_{\text{cell}}}{2} \cdot \left(\frac{\beta - 1}{\beta} \right)$$

Thus, the maximum deformation the cell can sustain is related to β as:

$$\varphi = \frac{\beta_{\text{max}} - 1}{2\beta_{\text{max}}}$$

And therefore, the maximum allowable β is:

$$\beta_{\text{max}} = \frac{1}{1 - 2\varphi}$$

$$\varphi := 0.1, 0.2 \dots 0.5$$

Which can be approximated as:

$$\varepsilon_{\text{max}} = \varphi^{\frac{1}{3}}$$

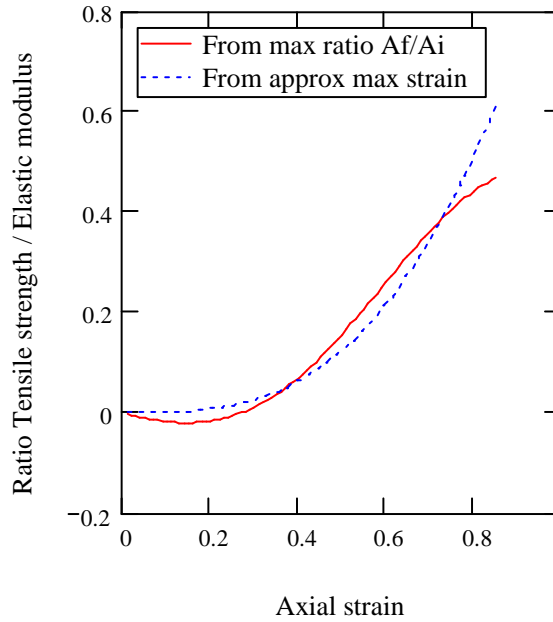
But considering the lateral support of the soil:

$$\varepsilon_{\text{real}} = \varepsilon - \varepsilon_{\text{sup}}$$

$$\varepsilon_{\text{real}} = \frac{\sigma_{\text{ov}}}{E} - K_0 \frac{\sigma_{\text{ov}}}{E}$$

$$\varepsilon_{\text{real}} = \varepsilon \cdot (1 - K_0)$$

$$\text{And therefore: } \varepsilon_{\text{max}} = \frac{\varphi^{\frac{1}{3}}}{1 - K_0}$$



By force equilibrium:

$$\sigma_p = \sigma_l \cdot \frac{A_l}{A_p} = \frac{E_{\text{cell}} \alpha \cdot R}{2} \cdot \left(\frac{\beta - 1}{\beta^2} \right) \cdot \frac{4 \cdot a + 2 \cdot \pi \cdot b}{4 \cdot a \cdot b + \pi \cdot b^2}$$

Pressure inside the cell

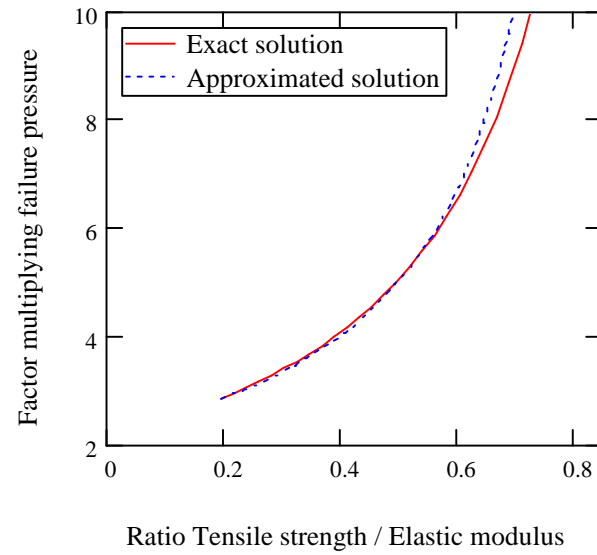
$$\sigma_f = \frac{E_{\text{cell}} \alpha \cdot R}{2} \cdot \left(\frac{\beta_{\text{max}} - 1}{\beta_{\text{max}}^2} \right) \cdot \frac{4 \cdot a_{\text{max}} + 2 \cdot \pi \cdot b_{\text{min}}}{4 \cdot a_{\text{max}} \cdot b_{\text{min}} + \pi \cdot b_{\text{min}}^2}$$

Replacing:
$$\sigma_f = E_{\text{cell}} \cdot \alpha \cdot \varphi \cdot (1 - 2 \cdot \varphi) \cdot \frac{\frac{12}{\pi} \cdot \frac{\varphi^{\frac{1}{3}}}{1 - K_0} + 2 \cdot \pi \cdot \left(1 - \frac{\varphi^{\frac{1}{3}}}{1 - K_0}\right)^2}{\frac{12}{\pi} \cdot \frac{\varphi^{\frac{1}{3}}}{1 - K_0} + \pi \cdot \left(1 - \frac{\varphi^{\frac{1}{3}}}{1 - K_0}\right)^2} \cdot \frac{1}{1 - \frac{\varphi^{\frac{1}{3}}}{1 - K_0}}$$

Which can be approximated as:

$\varphi := 0.1, 0.111, 0.5$

$$\sigma_f = E_{\text{cell}} \cdot \alpha \cdot \varphi \cdot (1 - 2 \cdot \varphi) \cdot \left[\frac{1}{\frac{\pi}{7} - \frac{1}{2} \cdot \frac{\varphi}{(1 - K_0)^3}} \right]$$



To calculate the stress in the soil skeleton, deformation compatibility is used:

$$n_p = \frac{2 \cdot R}{\xi \cdot \left(2 + \frac{t_p}{\xi}\right)}$$

Number of particles in one cell-height, assuming that each particle is surrounded by an amount of water equivalent to one double layer

$$\delta_{\text{cell}} = R \cdot \varepsilon = \delta_{\text{soil}} = n_p \cdot \delta_p$$

Deformation compatibility

$$\delta_p = \frac{\varepsilon}{2} \cdot \xi \cdot \left(2 + \frac{t_p}{\xi}\right)$$

Deformation in one soil particle

$$r = 2 \cdot \xi - \delta_p = \xi \cdot \left[2 - \varepsilon + \frac{\varepsilon}{2} \cdot \left(\frac{t_p}{\xi}\right)\right]$$

Distance the particles are going to be pushed together

By DLVO theory:

$$\sigma_s = R_{\text{DDL}} - A_{\text{tt}}$$

$$R_{DDL} = 2 \cdot R_{\text{gas}} \cdot T \cdot c_0 \cdot \left(\frac{2 \cdot \pi^2 \cdot \xi^2}{r^2} - 1 \right)$$

Repulsion component assuming short interparticle distance

$$A_{\text{tt}} = \frac{A_{\text{h}}}{6 \cdot \pi \cdot r^3}$$

Attraction component for two parallel platy particles

Replacing and simplifying, including the maximum axial strain:

$$\epsilon_{\text{max}} = \frac{\frac{1}{3}}{1 - K_0}$$

$$R_{DDL} = 2 \cdot R_{\text{gas}} \cdot T \cdot c_0 \cdot \left[\frac{2 \cdot \pi^2}{\left[2 - \frac{\frac{1}{3}}{1 - K_0} + \frac{\frac{1}{3}}{2 \cdot (1 - K_0)} \cdot \left(\frac{t_p}{\xi} \right) \right]^2} - 1 \right]$$

$$A_{\text{tt}} = \frac{A_{\text{h}}}{6 \cdot \pi \cdot \xi^3 \cdot \left[2 - \frac{\frac{1}{3}}{1 - K_0} + \frac{\frac{1}{3}}{2 \cdot (1 - K_0)} \cdot \left(\frac{t_p}{\xi} \right) \right]^3}$$

$$\sigma_s = \frac{4 \cdot \pi^2 \cdot R_{\text{gas}} \cdot T \cdot c_0}{\left[2 - \frac{\frac{1}{3}}{1 - K_0} + \frac{\frac{1}{3}}{2 \cdot (1 - K_0)} \cdot \left(\frac{t_p}{\xi} \right) \right]^2} - 2 \cdot R_{\text{gas}} \cdot T \cdot c_0 - \frac{A_{\text{h}}}{6 \cdot \pi \cdot \xi^3 \cdot \left[2 - \frac{\frac{1}{3}}{1 - K_0} + \frac{\frac{1}{3}}{2 \cdot (1 - K_0)} \cdot \left(\frac{t_p}{\xi} \right) \right]^3}$$

Neglecting the attraction component, and calling

$$B = \frac{R_{\text{gas}} \cdot T \cdot c_0}{2 \cdot \gamma_{\text{eff}}}$$

Finally the critical depth will be:

$$H_{\text{crit}} = B \cdot \left[\frac{2 \cdot \pi^2}{\left[2 - \frac{\frac{1}{\varphi^3}}{1 - K_0} + \frac{\frac{1}{\varphi^3}}{2 \cdot (1 - K_0)} \cdot \left(\frac{t_p}{\xi} \right) \right]^2} - 1 \right] + \frac{E_{\text{cell}}}{\gamma_{\text{eff}}} \cdot \frac{9}{16 \pi} \cdot \frac{\alpha \cdot \varphi \cdot (1 - 2 \cdot \varphi)}{\frac{\pi}{7} - \frac{1}{2} \cdot \frac{\varphi}{(1 - K_0)^3}} \cdot \left(\frac{\frac{\frac{1}{\varphi^3}}{1 - K_0}}{1 - \frac{\frac{1}{\varphi^3}}{1 - K_0}} \right)^2$$

When the lateral support is ignored, or $K_0 = 0$, the expression becomes:

$$H_{\text{crit}} = B \cdot \left[\frac{2 \cdot \pi^2}{\left[2 - \frac{\frac{1}{\varphi^3}}{\varphi^3} + \frac{\frac{1}{\varphi^3}}{2} \cdot \left(\frac{t_p}{\xi} \right) \right]^2} - 1 \right] + \frac{E_{\text{cell}}}{\gamma_{\text{eff}}} \cdot \frac{9}{16 \pi} \cdot \frac{\alpha \cdot \varphi \cdot (1 - 2 \cdot \varphi)}{\frac{\pi}{7} - \frac{1}{2} \cdot \varphi} \cdot \left(\frac{\frac{\frac{1}{\varphi^3}}{\varphi^3}}{1 - \frac{\frac{1}{\varphi^3}}{\varphi^3}} \right)^2$$

Cell Entrapment and Mobilization inside the Sediment Skeleton (Table 3.3, Model f)

η	Viscosity of pore fluid
t_p	Particle size
σ	Skeletal stress in the soil mass
γ_{eff}	Effective unit weight of the soil mass
γ_{grains}	Unit weight of soil grains
γ_w	Unit weight of water
$W_{particle}$	Effective weight of a single soil particle
μ	Soil friction coefficient
R	Cell radius
v	Velocity of cell
F_{drag}	Drag force generated by a cell
$t_{p_maximum}$	Maximum particle size that can be displaced by a cell
$H_{pushing}$	Depth of analysis or maximum depth a cell can drag a soil particle

The displacement of a single particle must overcome the normal force associated to the skeleton N , the frictional component between soil grains F_{friction} and the force that a motile cell can exert over a soil particle thanks to the drag it can mobilize F_{drag} .

Taking into account the viscosity of the pore fluid, the velocity that can be achieved by a cell and the typical cell diameters, the drag force a cell can mobilize can be estimated as follows:

$$F_{\text{drag}} = 6 \cdot \pi \cdot \eta \cdot v \cdot R$$

The skeletal component (N) can be obtained from the following expression:

$$N = t_p^2 \cdot \sigma$$

Finally, the frictional component can be calculated as:

$$F_{\text{friction}} = N \cdot \mu = \mu \cdot t_p^2 \cdot \sigma$$

Replacing the definition of σ in the previous expression:

$$\sigma = \gamma_{\text{eff}} \cdot H_{\text{pushing}}$$

$$F_{\text{friction}} = \mu \cdot t_p^2 \cdot \gamma_{\text{eff}} \cdot H_{\text{pushing}}$$

By force equilibrium in the horizontal direction, the maximum depth can be calculated as follows:

$$H_{\text{pushing}} = \frac{6 \cdot \pi \cdot \eta \cdot v \cdot R}{\mu \cdot \gamma_{\text{eff}} \cdot t_p^2}$$

The upper limit of this model corresponds to the case in which the effective self-weight of the soil particle cannot be overcome by the cell drag, and this occurs when:

$$F_{\text{drag}} = W_{\text{particle}}$$

$$W_{\text{particle}} = \frac{4}{3} \cdot \pi \cdot \left(\frac{t_p}{2} \right)^3 \cdot (\gamma_{\text{grains}} - \gamma_w)$$

Therefore:

$$t_{p_maximum} = \sqrt[3]{\frac{36 \cdot \eta \cdot v \cdot R}{\gamma_{\text{grains}} - \gamma_w}}$$

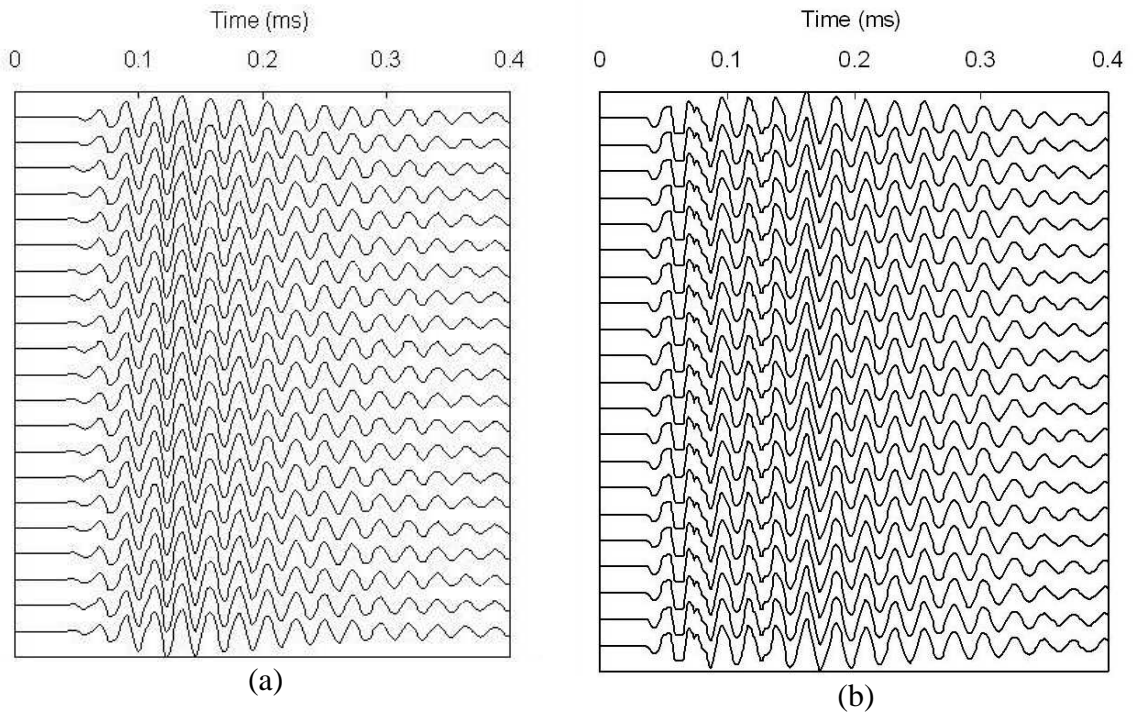
APPENDIX B

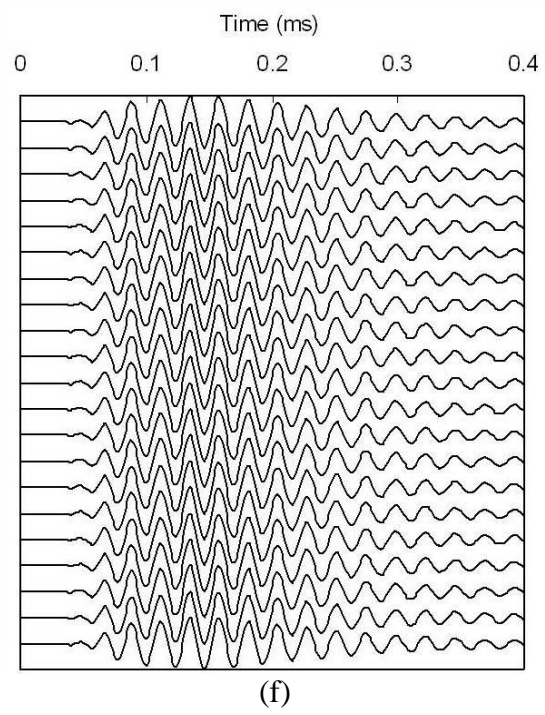
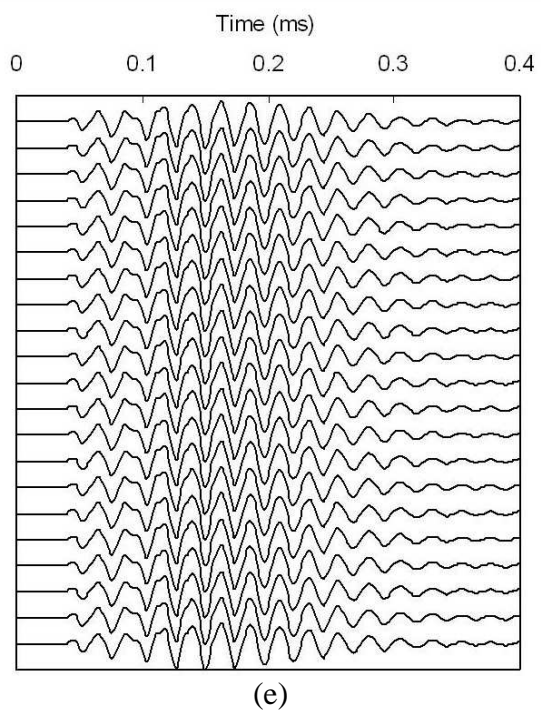
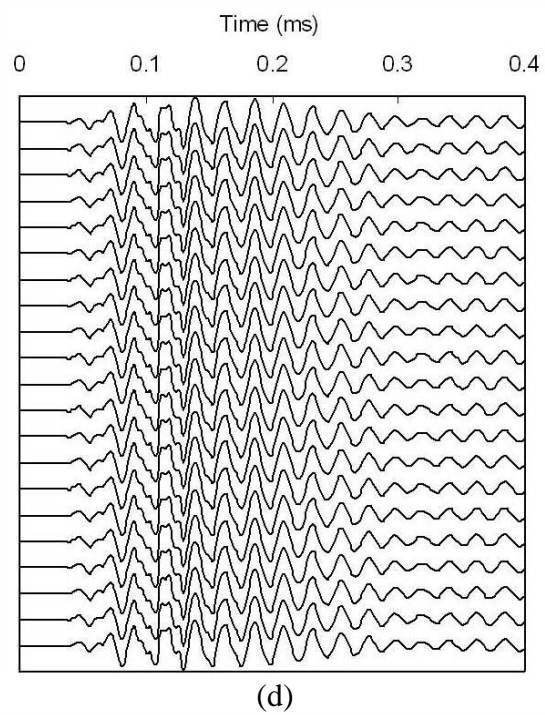
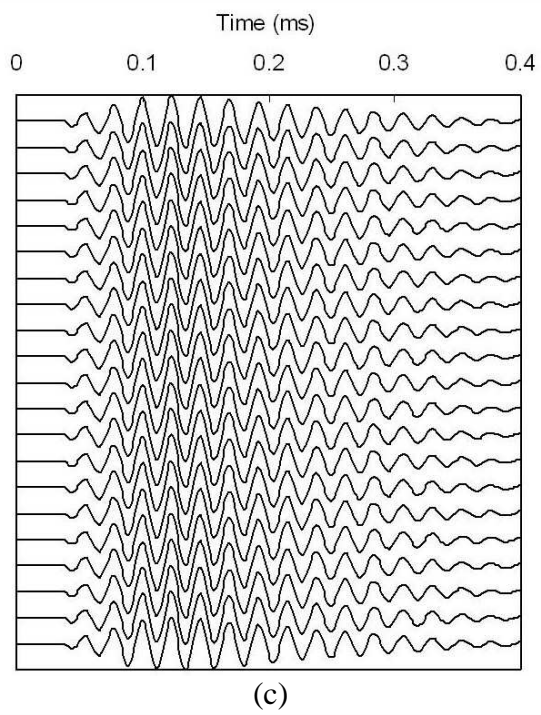
P-WAVE SIGNATURES

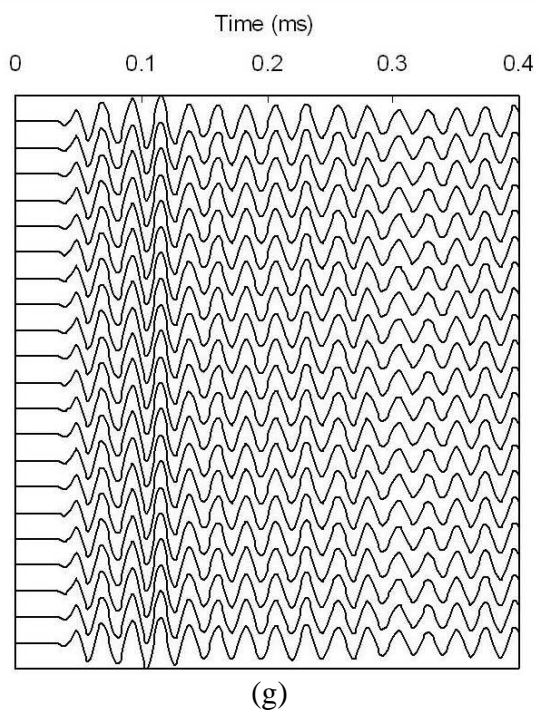
Study #1: Sterile Control

Evolution of P-wave signatures in sterile controls. (a) Bentonite, (b) SA1, (c) RP2, (d) Zeofree, (e) Sil-co-sil, (f) F110 sand and (g) Ottawa sand. The first signal in each sequence was gathered immediately after the initiation of the test. Successive signals were captured every day thereafter.

No measurable changes were observed during the 30 day-long experiment.

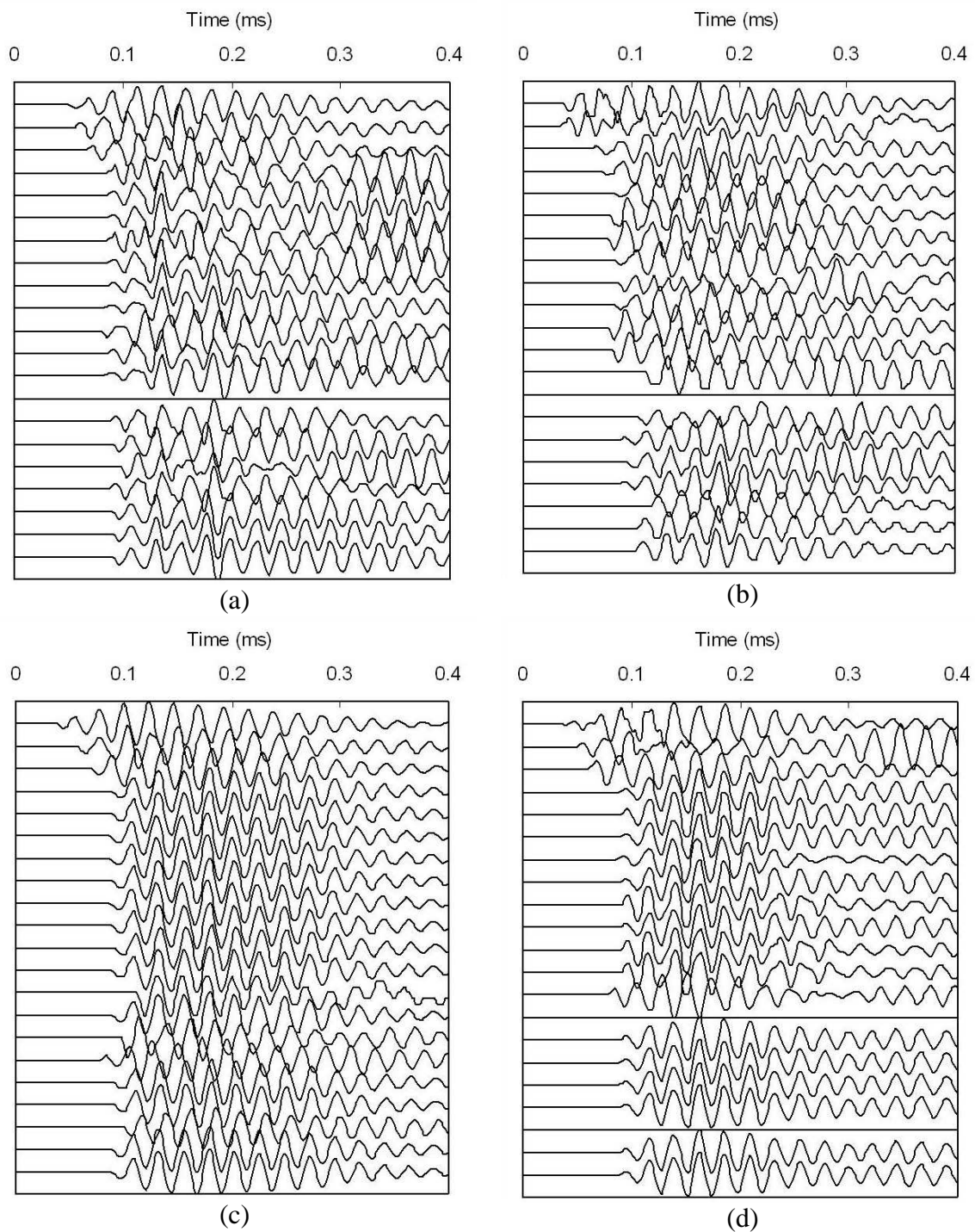


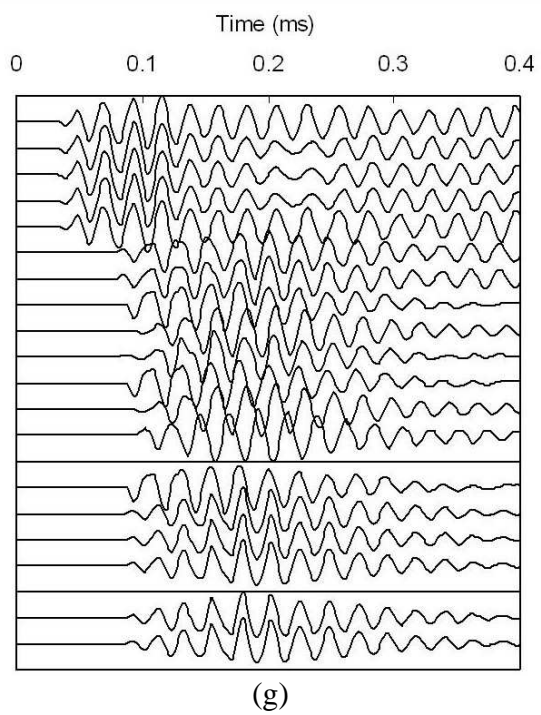
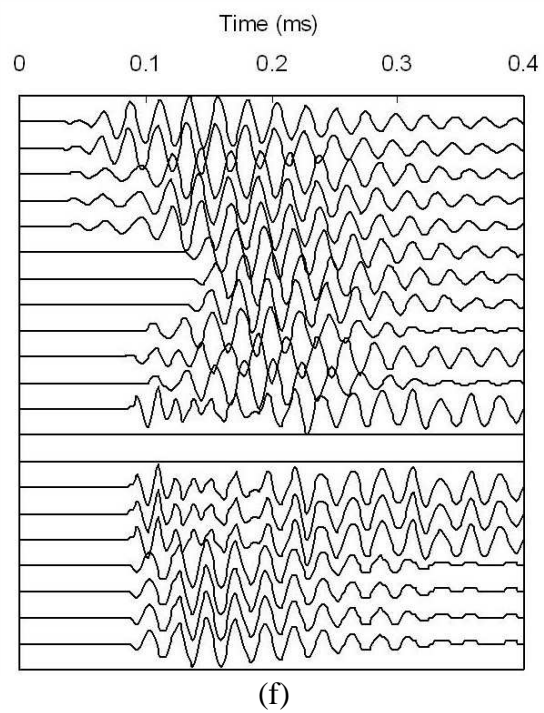
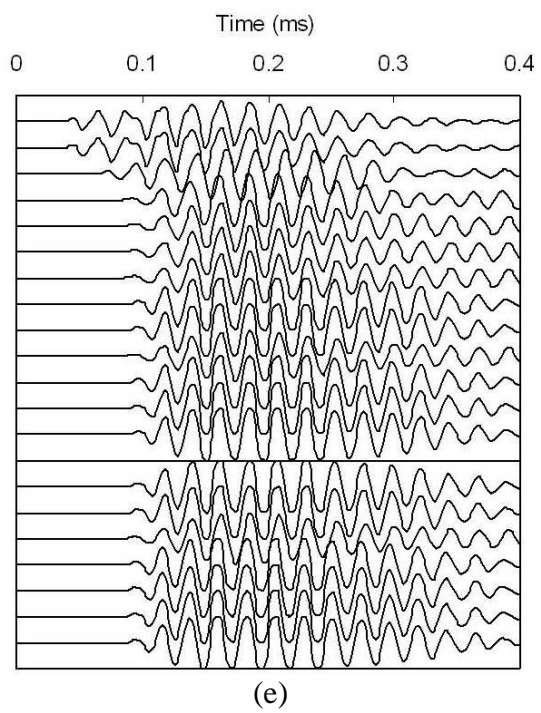




Study #2: Single-grained Soils

Evolution of P-wave signatures during biogenic gas generation. (a) Bentonite, (b) SA1, (c) RP2, (d) Zeofree, (e) Sil-co-sil, (f) F110 and (g) Ottawa.

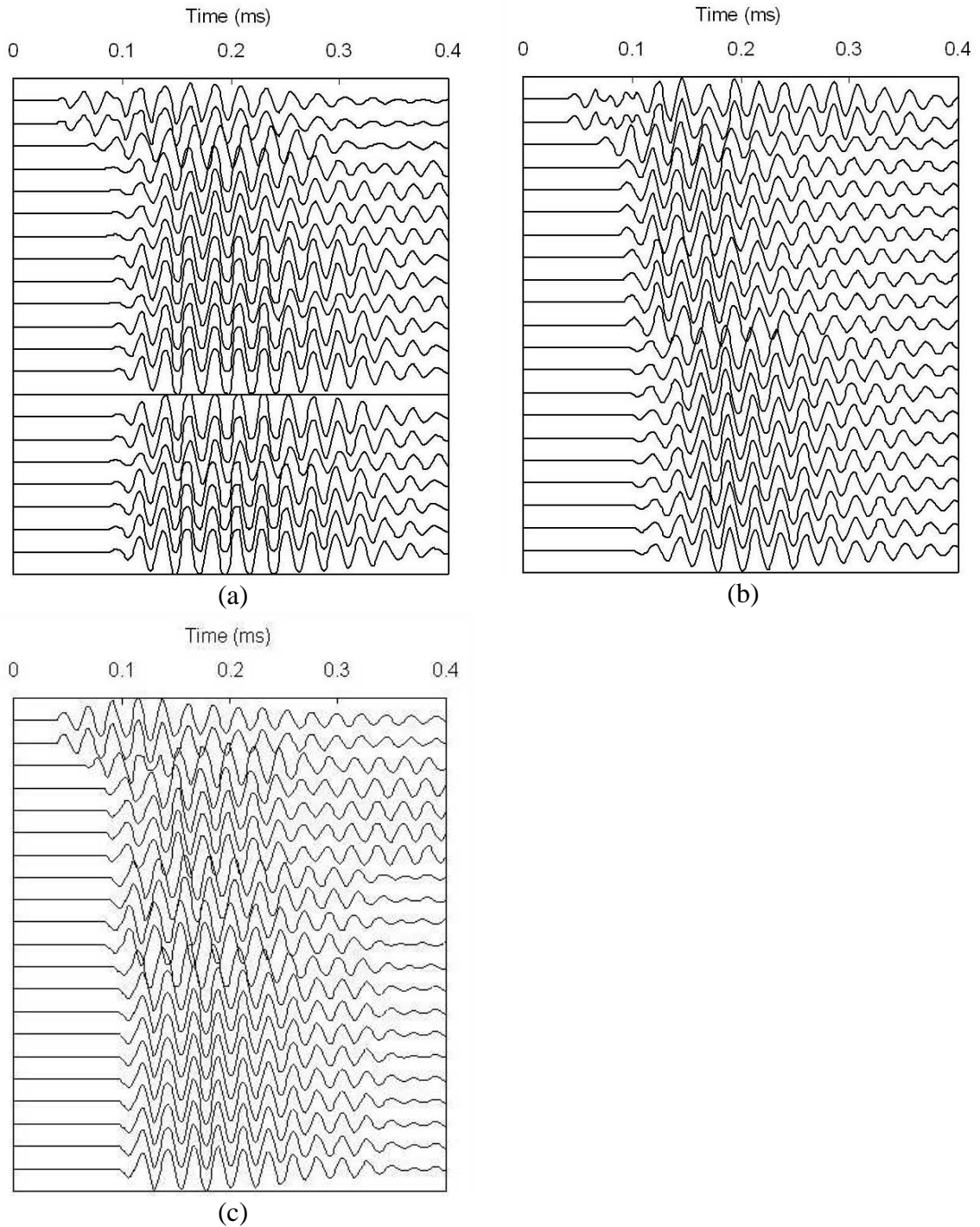




Study #3: Nutrient Availability Effect

Evolution of P-wave signatures in Sil-co-sil during biogenic gas generation. (a)

No extra nutrient added, (b) Nutrient added every day, (c) Nutrient added every 10 days.

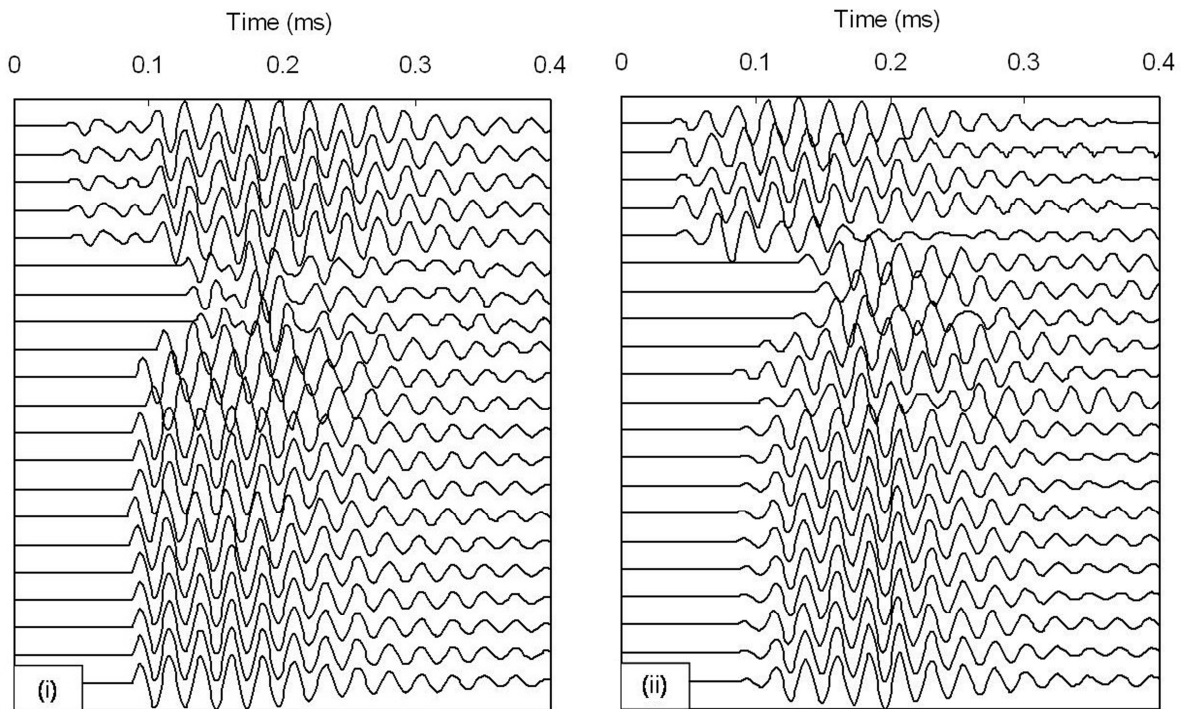


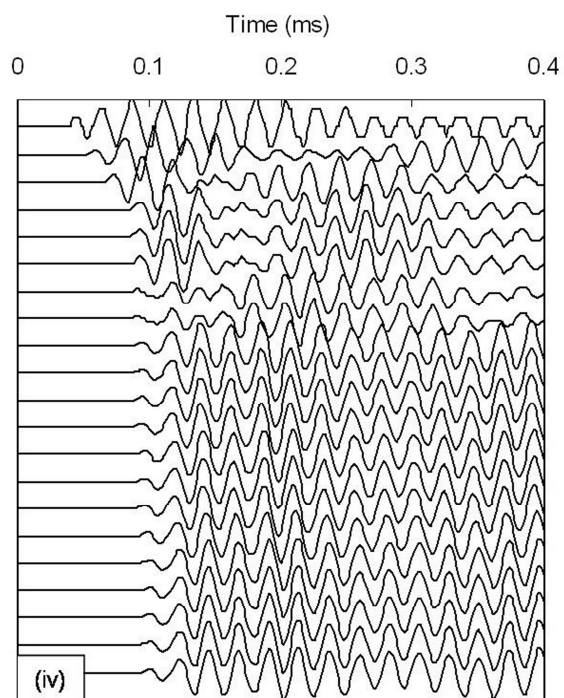
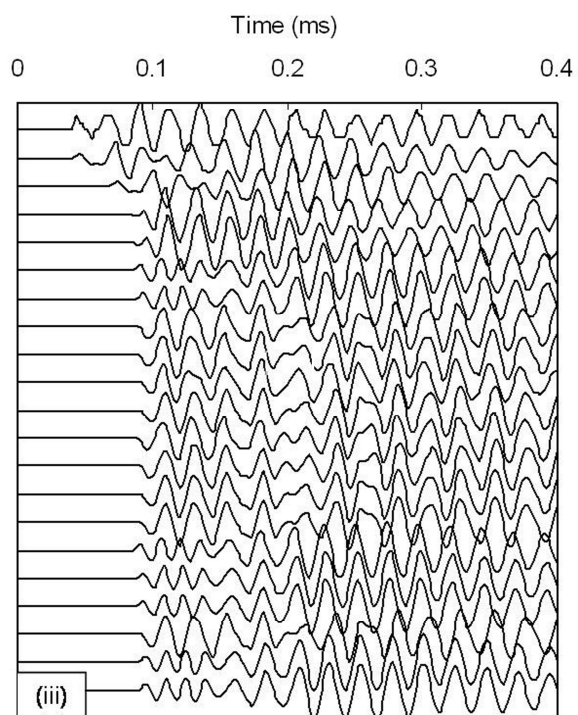
APPENDIX C

COMPLEMENTARY DATA

P-wave Signatures

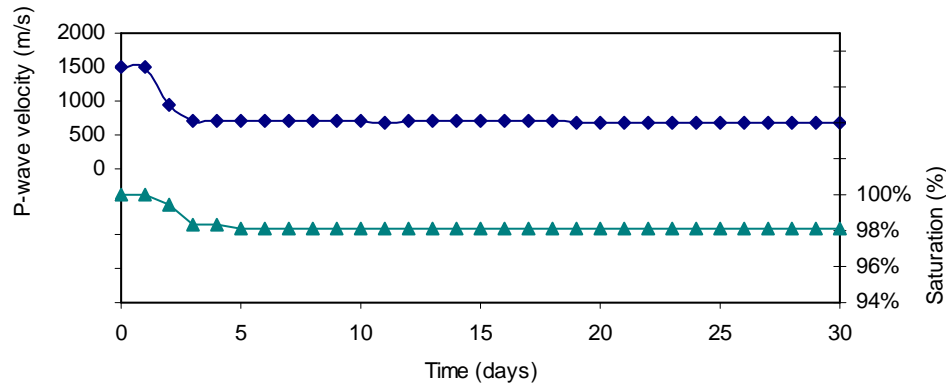
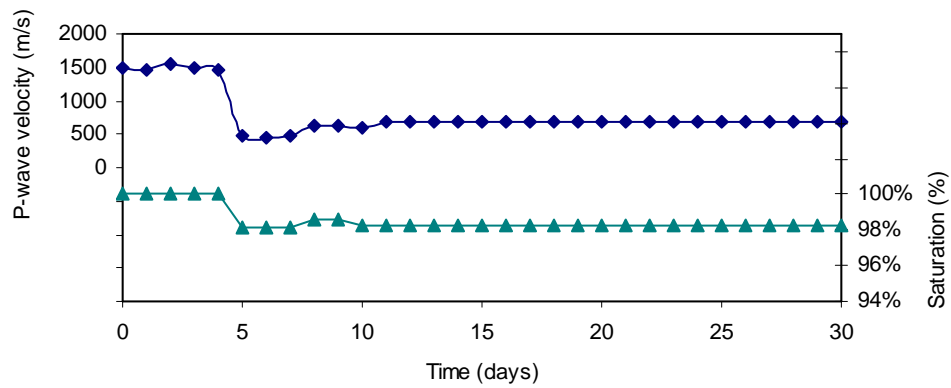
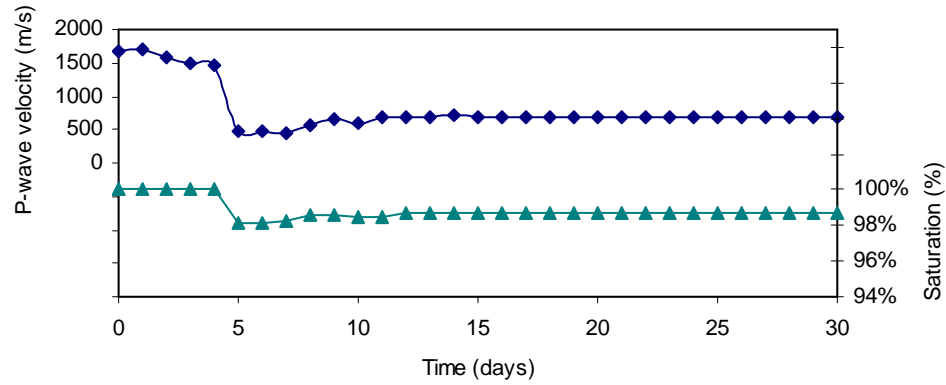
Evolution of P-wave signatures during biogenic gas formation. (i) F110 sand without fines. (ii) F110 + 3% bentonite. (iii) F110 + 9% bentonite. (iv) F110 + 15% bentonite. The first signal in each sequence was gathered immediately after the initiation of the test. Successive signals were captured every day thereafter.

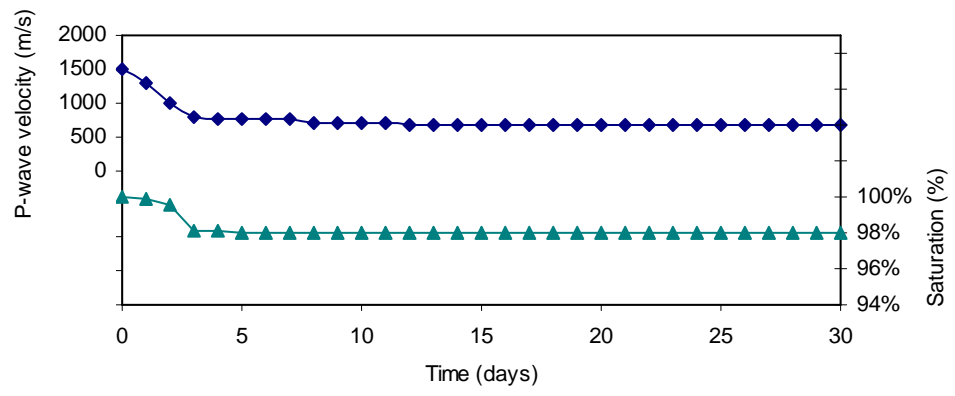




P-wave Velocity and Generated Gas

P-wave velocity and saturation for (i) pure F110 sand, (ii) F110 + 3% RP2, (iii) F110 + 9% RP2 and (iv) F110 + 15% RP2.





REFERENCES

- Abu-Ashour, J., D. M. Joy, H. Lee, H. R. Whiteley, and S. Zelin (1994), Transport of microorganisms through soil, *Water Air and Soil Pollution*, 75(1-2), 141-158.
- Adams, D. D., N. J. Fendiger, and D. E. Glotfelty (1990), Biogenic gas production and mobilization of in-place sediment contaminants by gas ebullition, in *Sediments: Chemistry and toxicity of in-place pollutants*, edited by R. Baudo, et al., pp. 215-236, Lewis Publishers, Inc., Michigan.
- Addadi, L., and S. Weiner (1992), Control and design principles in biological mineralization, *Angewandte Chemie-International Edition in English*, 31(2), 153-169.
- Agnelli, A., J. Ascher, G. Corti, M. T. Ceccherini, P. Nannipieri, and G. Pietramellara (2004), Distribution of microbial communities in a forest soil profile investigated by microbial biomass, soil respiration and DGGE of total and extracellular DNA, *Soil Biology & Biochemistry*, 36(5), 859-868.
- Ahmed, S., C. W. Lovell, and S. Diamond (1974), Pore sizes and strength of compacted clay, *Journal of the Geotechnical Engineering Division - ASCE*, GT4, 407-425.
- Alexander, M. (1961), *Introduction to soil microbiology*, 472 p. pp., Wiley, New York,.
- Allison, L. E. (1947), Effect of microorganisms on permeability of soil under prolonged submergence, *Soil Science*, 63(6), 439-450.
- AlMukhtar, M., N. Belanteur, D. Tessier, and S. K. Vanapalli (1996), The fabric of a clay soil under controlled mechanical and hydraulic stress states, *Applied Clay Science*, 11(2-4), 99-115.
- Astumian, R. D., and P. Hanggi (2002), Brownian motors, *Physics Today*, 55(11), 33-39.
- Atlas, R. M. (1995), *Microorganisms in our world*, xix, 765 p. pp., Mosby-Year Book, St. Louis, MO.

- Audesirk, T., G. Audesirk, and B. E. Byers (2006), *Biology Life on Earth*, 7th edition ed., Academic Internet Publishers.
- Avnimelech, Y., and Z. Nevo (1964), Biological clogging of sands, *Soil Science Society of America Journal*, 98, 222-226.
- Baker, S. C., S. J. Ferguson, B. Ludwig, M. D. Page, O. M. H. Richter, and R. J. M. van Spanning (1998), Molecular genetics of the genus *Paracoccus*: Metabolically versatile bacteria with bioenergetic flexibility, *Microbiology and Molecular Biology Reviews*, 62(4), 1046-+.
- Barnes, J. M., W. A. Apel, and K. B. Barrett (1995), Removal of nitrogen oxides from gas streams using biofiltration, *Journal of Hazardous Materials*, 41(2-3), 315-326.
- Baskar, S., R. Baskar, L. Maucclair, and J. A. McKenzie (2006), Microbially induced calcite precipitation in culture experiments: Possible origin for stalactites in Sahastradhara caves, Dehradun, India, *Current Science*, 90(1), 58-64.
- Baveye, P., P. Vandevivere, B. L. Hoyle, P. C. DeLeo, and D. S. de Lozada (1998), Environmental impact and mechanisms of the biological clogging of saturated soils and aquifer materials, *Critical Reviews in Environmental Science and Technology*, 28(2), 123-191.
- Beech, I. B., and C. C. Gaylarde (1989), Adhesion of *Desulfovibrio desulfuricans* and *Pseudomonas fluorescens* to mild steel surfaces, *Journal of Applied Bacteriology*, 67, 2017.
- Behlulgil, K., and M. T. Mehmetoglu (2002), Bacteria for improvement of oil recovery: A laboratory study, *Energy Sources*, 24(5), 413-421.
- Benini, S., C. Gessa, and S. Ciurli (1996), *Bacillus pasteurii* urease: A heteropolymeric enzyme with a binuclear nickel active site, *Soil Biology & Biochemistry*, 28(6), 819-821.

- Bennett, R. H., W. R. Bryant, and M. H. Hulbert (1991), *The microstructure of fine-grained sediments, from mud to shale*, xxii, 582 p. pp., Springer Verlag, New York.
- Bergman, T., and R. Mesler (1981), Bubble nucleation studies. 1.- Formation of bubble nuclei in superheated water by bursting bubbles, *AIChE Journal*, 27(5), 851-853.
- Bird, D. F., S. K. Juniper, M. Ricciardi-Rigault, P. Martineu, Y. T. Prairie, and S. E. Calvert (2001), Subsurface viruses and bacteria in Holocene/Late Pleistocene sediments of Saanich Inlet, BC: ODP Holes 1033B and 1034B, Leg 169S, *Marine Geology*, 174(1-4), 227-239.
- Blander, M. (1979), Bubble nucleation in liquids, *Advances in Colloid and Interface Science*, 10(Jan), 1-32.
- Blume, E., M. Bischoff, J. M. Reichert, T. Moorman, A. Konopka, and R. F. Turco (2002), Surface and subsurface microbial biomass, community structure and metabolic activity as a function of soil depth and season, *Applied Soil Ecology*, 20(3), 171-181.
- Boivin-Jahns, V., R. Ruimy, A. Bianchi, S. Daumas, and R. Christen (1996), Bacterial diversity in a deep-subsurface clay environment, *Applied and Environmental Microbiology*, 62(9), 3405-3412.
- Bolton, A. J., A. J. Maltman, and Q. Fisher (2000), Anisotropic permeability and bimodal pore-size distributions of fine-grained marine sediments, *Marine and Petroleum Geology*, 17(6), 657-672.
- Bonala, M. V. S., and L. N. Reddi (1998), Physicochemical and biological mechanisms of soil clogging - An overview. Filtration and Drainage in Geotechnical/Geoenvironmental Engineering, *ASCE Geotechnical Special Publication*, 78, 43-68.

- Boquet, E., A. Boronat, and Ramoscor.A (1973), Production of calcite (calcium carbonate) crystals by soil bacteria is a general phenomenon, *Nature*, 246(5434), 527-529.
- Boulbitch, A., B. Quinn, and D. Pink (2000), Elasticity of the rod-shaped Gram-negative eubacteria, *Physical Review Letters*, 85(24), 5246-5249.
- Bullitt, R., and L. Makowski (1995), Structural polymorphism of bacterial adhesion pili, *Nature*, 373, 164-167.
- Buttler, A. J., H. Dinel, M. Levesque, and S. P. Mathur (1991), The relation between movement of subsurface water and gaseous methane in a basin bog with a novel instrument, *Canadian Journal of Soil Science*, 71(4), 427-438.
- Cacchio, P., C. Ercole, G. Cappuccio, and A. Lepidi (2003), Calcium carbonate precipitation by bacterial strains isolated from a limestone cave and from a loamy soil, *Geomicrobiology Journal*, 20(2), 85-98.
- Cannavo, P., A. Richaume, and F. Lafolie (2004), Fate of nitrogen and carbon in the vadose zone: in situ and laboratory measurements of seasonal variations in aerobic respiratory and denitrifying activities, *Soil Biology & Biochemistry*, 36(3), 463-478.
- Cardenas, L. M., J. M. B. Hawkins, D. Chadwick, and D. Scholefield (2003), Biogenic gas emissions from soils measured using a new automated laboratory incubation system, *Soil Biology & Biochemistry*, 35(6), 867-870.
- Castanier, S., M. C. Bernetrollande, A. Maurin, and J. P. Perthuisot (1993), Effects of microbial activity on the hydrochemistry and sedimentology of Lake Logipi, Kenya, *Hydrobiologia*, 267(1-3), 99-112.
- Castanier, S., G. Le Metayer-Levrel, and J. P. Perthuisot (1999), Ca-carbonates precipitation and limestone genesis - The microbiogeologist point of view, *Sedimentary Geology*, 126(1-4), 9-23.

- Castanier, S., G. Le Metayer-Levrel, and J. P. Perthuisot (2000), Bacterial roles in the precipitation of carbonate minerals, in *Microbial Sediments*, edited by R. E. Riding and S. M. Awramik, pp. 32-39, Springer-Verlag, Berlin.
- Cerini, W. F., W. R. Battles, and P. H. Jones (1946), Some factors influencing the plugging characteristics of an oil-well injection water, *Transactions of the American Institute of Mining and Metallurgical Engineers*, 165, 52-63.
- Chakraborty, D., V. K. Agarwal, S. K. Bhatia, and J. Bellare (1994), Steady-state transitions and polymorph transformations in continuous precipitation of calcium carbonate, *Industrial & Engineering Chemistry Research*, 33(9), 2187-2197.
- Chaney, R. C. (1978), Saturation effects on the cyclic strength of sands, *Earthquake Engineering and Soil Dynamics (ASCE)*, 1, 342-258.
- Chang, A. C., W. R. Olmstead, J. B. Johanson, and Yamashit.G (1974), Sealing mechanism of wastewater ponds, *Journal Water Pollution Control Federation*, 46(7), 1715-1721.
- Characklis, W. G., and K. C. Marshall (1990), *Biofilms*, John Wiley & Sons, Ltd., NY.
- Chen, C. R., Z. H. Xu, T. J. Blumfield, and J. M. Hughes (2003), Soil microbial biomass during the early establishment of hoop pine plantation: seasonal variation and impacts of site preparation, *Forest Ecology and Management*, 186(1-3), 213-225.
- Cho, G. C., and J. C. Santamarina (2001), Unsaturated particulate materials - Particle-level studies, *Journal of Geotechnical and Geoenvironmental Engineering*, 127(1), 84-96.
- Chung, Y. C., and M. S. Chung (2000), BNP test to evaluate the influence of C/N ratio on N₂O production in biological denitrification, *Water Science and Technology*, 42(3-4), 23-27.
- Cole, J. A., and C. M. Brown (1980), Nitrite reduction to ammonia by fermentative bacteria: A short circuit in the biological nitrogen-cycle, *Fems Microbiology Letters*, 7(2), 65-72.

- Constantz, J., W. N. Herkelrath, and F. Murphy (1988), Air encapsulation during Infiltration, *Soil Science Society of America Journal*, 52(1), 10-16.
- Corpe, W. A. (1980), Microbial surface components involved in adsorption of microorganisms onto surfaces, in *Adsorption of microorganisms to surfaces*, edited by G. Bitton and K. C. Marshall, pp. 105-144, John Wiley & Sons, New York.
- Cowan, M. M., T. M. Warren, and M. Fletcher (1991), Mixed species colonization of solid surfaces in laboratory biofilms, *Biofouling*, 3, 23-34.
- Cragg, B. A., R. J. Parkes, J. C. Fry, A. J. Weightman, P. A. Rochelle, and J. R. Maxwell (1996), Bacterial populations and processes in sediments containing gas hydrates (ODP Leg 146: Cascadia Margin), *Earth and Planetary Science Letters*, 139(3-4), 497-507.
- Cuisinier, O., and L. Laloui (2004), Fabric evolution during hydromechanical loading of a compacted silt, *International Journal for Numerical and Analytical Methods in Geomechanics*, 28(6), 483-499.
- Cunin, R., N. Glansdorff, A. Pierard, and V. Stalon (1986), Biosynthesis and metabolism of arginine in bacteria, *Microbiological Reviews*, 50(3), 314-352.
- Cunningham, A. B., W. G. Characklis, F. Abedeen, and D. Crawford (1991), Influence of biofilm accumulation on porous media hydrodynamics, *Environmental Science & Technology*, 25(7), 1305-1311.
- Cunningham, K. I., D. E. Northup, R. M. Pollastro, W. G. Wright, and E. J. Larock (1995), Bacteria, fungi and biokarst in Lechuguilla Cave, Carlsbad Caverns National Park, New Mexico, *Environmental Geology*, 25(1), 2-8.
- Cusack, F., S. Singh, C. McCarthy, J. Grieco, M. Derocco, D. Nguyen, H. Lappinscott, and J. W. Costerton (1992), Enhanced oil recovery - three-dimensional sandpack simulation of ultramicrobacteria resuscitation in reservoir formation, *Journal of General Microbiology*, 138, 647-655.

- D'Hondt, S., B. B. Jorgensen, D. J. Miller, A. Batzke, R. Blake, B. A. Cragg, H. Cypionka, G. R. Dickens, T. Ferdelman, K. U. Hinrichs, N. G. Holm, R. Mitterer, A. Spivack, G. Z. Wang, B. Bekins, B. Engelen, K. Ford, G. Gettemy, S. D. Rutherford, H. Sass, C. G. Skilbeck, I. W. Aiello, G. Guerin, C. H. House, F. Inagaki, P. Meister, T. Naehr, S. Niitsuma, R. J. Parkes, A. Schippers, D. C. Smith, A. Teske, J. Wiegel, C. N. Padilla, and J. L. S. Acosta (2004), Distributions of microbial activities in deep subseafloor sediments, *Science*, 306(5705), 2216-2221.
- Daniel, T. C., and J. Bouma (1974), Column studies of soil clogging in a slowly permeable soil as a function of effluent quality, *Journal of Environmental Quality*, 3(4), 321-326.
- Daniels, L., G. Fulton, R. W. Spencer, and W. H. Ormejohnson (1980), Origin of hydrogen in methane produced by *Methanobacterium thermoautotrophicum*, *Journal of Bacteriology*, 141(2), 694-698.
- Davidson, E. A., P. A. Matson, P. M. Vitousek, R. Riley, K. Dunkin, G. Garciamendez, and J. M. Maass (1993), Processes regulating soil emissions of NO and N₂O in a seasonally dry tropical forest, *Ecology*, 74(1), 130-139.
- de Vries, J. (1972), Soil Filtration of Wastewater Effluent and Mechanism of Pore Clogging, *Journal Water Pollution Control Federation*, 44(4), 565-573.
- DeJong, J. T., M. B. Fritzges, and K. Nusslein (2006), Microbially induced cementation to control sand response to undrained shear, *Journal of Geotechnical and Geoenvironmental Engineering*, 132(11), 1381-1392.
- Delage, P., and G. Lefebvre (1984), Study of the structure of a sensitive Champlain clay and of its evolution during consolidation, *Canadian Geotechnical Journal*, 21(1), 21-35.
- Delage, P., M. Audiguier, Y. J. Cui, and M. D. Howat (1996), Microstructure of a compacted silt, *Canadian Geotechnical Journal*, 33(1), 150-158.

- Dennis, M. L., and J. P. Turner (1998), Hydraulic conductivity of compacted soil treated with biofilm, *Journal of Geotechnical and Geoenvironmental Engineering*, 124(2), 120-127.
- Deutscher, R. L., and S. Fletcher (1990), Nucleation on active sites. 5.- The theory of nucleation rate dispersion, *Journal of Electroanalytical Chemistry*, 277(1-2), 1-18.
- Dewhurst, D., A. Aplin, J. Sarda, and Y. Yang (1998), Compaction-driven evolution of porosity and permeability in natural mudstones: An experimental study, *Journal of Geophysical Research - Solid Earth*, 103(B1), 651-661.
- Dewhurst, D. N., A. C. Aplin, and J. P. Sarda (1999), Influence of clay fraction on pore-scale properties and hydraulic conductivity of experimentally compacted mudstones, *Journal of Geophysical Research - Solid Earth*, 104(B12), 29261-29274.
- Diamond, S. (1971), Microstructure and pore structure of impact/compacted clays, *Clays and clay minerals*, 19(4), 239-&.
- Dinel, H., S. P. Mathur, A. Brown, and M. Levesque (1988), A field study of the effect of depth on methane production in peatland waters: Equipment and preliminary results, *Journal of Ecology*, 76(4), 1083-1091.
- Dodds, W. K., M. K. Banks, C. S. Clenan, C. W. Rice, D. Sotomayor, E. A. Strauss, and W. Yu (1996), Biological properties of soil and subsurface sediments under abandoned pasture and cropland, *Soil Biology & Biochemistry*, 28(7), 837-846.
- Dominguez, A., S. Bories, and M. Pratt (2000), Gas cluster growth by solute diffusion in porous media. Experiments and automaton simulation on pore network, *International Journal of Multiphase Flow*, 26, 1951-1979.
- Donlan, R. M., W. O. Pipes, and T. L. Yohe (1994), Biofilm formation on cast iron substrata in water distribution systems, *Water Research*, 28, 1497-1503.
- Donlan, R. M. (2002), Biofilms: Microbial life on surfaces, *Emerging Infectious Diseases*, 8(9), 881-890.

- Duddridge, J. E., C. A. Kent, and J. F. Laws (1982), Effect of surface shear stress on the attachment of *Pseudomonas fluorescens* to stainless steel under defined flow conditions, *Biotechnology and Bioengineering*, 24, 153-164.
- Edwards, G. (1990), *Biology the easy way*, 2nd ed., Barron's Educational Series Inc., New York.
- Ehrlich, H. L. (1996), *Geomicrobiology*, 3rd ed., xix, 719 p. pp., M. Dekker, New York.
- Estiu, G., and K. M. Merz (2006), Catalyzed decomposition of urea. Molecular dynamics simulations of the binding of urea to urease, *Biochemistry*, 45(14), 4429-4443.
- Fayer, M. J., and D. Hillel (1986), Air Encapsulation .1. Measurement in a Field Soil, *Soil Science Society of America Journal*, 50(3), 568-572.
- Fera, P., S. M. A., W. G. Characklis, and D. Prieur (1989), Seasonal variations in bacterial colonization of stainless steel, aluminum, and polycarbonate surfaces in a seawater flow system, *Biofouling*, 1, 251-261.
- Ferris, F. G., R. G. Wiese, and W. S. Fyfe (1994), Precipitation of carbonate minerals by microorganisms - Implications for silicate weathering and the global carbon dioxide budget, *Geomicrobiology Journal*, 12(1), 1-13.
- Fierer, N., J. P. Schimel, and P. A. Holden (2003), Variations in microbial community composition through two soil depth profiles, *Soil Biology & Biochemistry*, 35(1), 167-176.
- Finkelstein, Y., and A. Tamir (1985), Formation of gas bubbles in supersaturated solutions of gases in water, *AIChE Journal*, 31(9), 1409-1419.
- Firestone, M. K., R. B. Firestone, and J. M. Tiedje (1980), Nitrous oxide from soil denitrification: Factors controlling its biological production, *Science*, 208(4445), 749-751.
- Fletcher, M. (1988), Attachment of *Pseudomonas fluorescens* to glass and influence of electrolytes on bacterium-substratum separation distance, *Journal of Bacteriology*, 170, 2027-2030.

- Fletcher, M., J. M. Lessman, and G. I. Loeb (1991), Bacterial surface adhesives and biofilm matrix polymers of marine and freshwater bacteria, *Biofouling*, 4, 129-140.
- Folk, R. L. (1993), SEM imaging of bacteria and nanobacteria in carbonate sediments and rocks, *Journal of Sedimentary Petrology*, 63(5), 990-999.
- Fontes, D. E., A. L. Mills, G. M. Hornberger, and J. S. Herman (1991), Physical and chemical factors influencing transport of microorganisms through porous media, *Applied and Environmental Microbiology*, 57(9), 2473-2481.
- Ford, R. M., and R. W. Harvey (2007), Role of chemotaxis in the transport of bacteria through saturated porous media, *Advances in Water Resources*, 30(6-7), 1608-1617.
- Forsythe, S. J., J. M. Dolby, A. D. B. Webster, and J. A. Cole (1988), Nitrate-reducing and nitrite-reducing bacteria in the achlorhydric stomach, *Journal of Medical Microbiology*, 25(4), 253-259.
- Fourie, A. B., B. A. Hofmann, R. J. Mikula, E. R. F. Lord, and P. K. Robertson (2001), Partially saturated tailings sand below the phreatic surface, *Geotechnique*, 51(7), 577-585.
- Frankenberger, W. T., F. R. Troeh, and L. C. Dumenil (1979), Bacterial effects on hydraulic conductivity of soils, *Soil Science Society of America Journal*, 43(2), 333-338.
- Fredrickson, J. K., D. L. Balkwill, J. M. Zachara, S. M. W. Li, F. J. Brockman, and M. A. Simmons (1991), Physiological diversity and distributions of heterotrophic bacteria in deep cretaceous sediments of the Atlantic Coastal Plain, *Applied and Environmental Microbiology*, 57(2), 402-411.
- Fredrickson, J. K., J. P. McKinley, B. N. Bjornstad, P. E. Long, D. B. Ringelberg, D. C. White, L. R. Krumholz, J. M. Suflita, F. S. Colwell, R. M. Lehman, T. J. Phelps, and T. C. Onstott (1997), Pore-size constraints on the activity and survival of

- subsurface bacteria in a late Cretaceous shale-sandstone sequence, northwestern New Mexico, *Geomicrobiology Journal*, 14(3), 183-202.
- Gallagher, P. M., and J. K. Mitchell (2002), Influence of colloidal silica grout on liquefaction potential and cyclic undrained behavior of loose sand, *Soil Dynamics and Earthquake Engineering*, 22(9-12), 1017-1026.
- Gannon, J., Y. H. Tan, P. Baveye, and M. Alexander (1991a), Effect of sodium chloride on transport of bacteria in a saturated aquifer material, *Applied and Environmental Microbiology*, 57(9), 2497-2501.
- Gannon, J. T., V. B. Manilal, and M. Alexander (1991b), Relationship between cell surface properties and transport of bacteria through soil, *Applied and Environmental Microbiology*, 57(1), 190-193.
- Garcia-Bengochea, I., C. W. Lovell, and A. G. Altschaeffl (1979), Pore distribution and permeability of silty clays, *Journal of the Geotechnical Engineering Division - ASCE*, 105(7), 839-856.
- Garcia-Viloca, M., J. Gao, M. Karplus, and D. G. Truhlar (2004), How enzymes work: Analysis by modern rate theory and computer simulations, *Science*, 303(5655), 186-195.
- Gerth, W. A., and E. A. Hemmingsen (1980), Heterogeneous nucleation of bubbles at solid-surfaces in gas-supersaturated aqueous solutions, *Journal of Colloid and Interface Science*, 74(1), 80-89.
- Gollapudi, U. K., C. L. Knutson, S. S. Bang, and M. R. Islam (1995), A new method for controlling leaching through permeable channels, *Chemosphere*, 30(4), 695-705.
- Greenfield, L. J. (1963), Metabolism and concentration of calcium and magnesium and precipitation of calcium carbonate by a marine bacterium, *Annals of the New York Academy of Sciences*, 109(1), 23-&.
- Griffiths, F. J., and R. C. Joshi (1989), Change in pore-size distribution due to consolidation of clays, *Geotechnique*, 39(1), 159-167.

- Griffiths, F. J., and R. C. Joshi (1990), Clay fabric response to consolidation, *Applied Clay Science*, 5, 37-66.
- Gupta, R. P., and D. Swartzendruber (1962), Flow-associated reduction in the hydraulic conductivity of quartz sand, *Soil Science Society Proceedings*, 6-10.
- Gupta, R. P., and D. Swartzendruber (1964), Entrapped air content and hydraulic conductivity of quartz sand during prolonged liquid flow, *Soil Science Society Proceedings*, 9-12.
- Harvey, R. W., L. H. George, R. L. Smith, and D. R. LeBlanc (1989), Transport of microspheres and indigenous bacteria through a sandy aquifer - Results of natural gradient and forced gradient tracer experiments, *Environmental Science & Technology*, 23(1), 51-56.
- Hattori, T. (1973), *Microbial life in the soil: An introduction*, vi, 427 p. pp., M. Dekker, New York,.
- Hausinger, R. P. (1993), *Biochemistry of Nickel*, Plenum Press, New York.
- Heling, D. (1970), Micro-fabrics of shales and their rearrangement by compaction, *Sedimentology*, 15(3-4), 247-&.
- Hemmingsen, E. A. (1975), Cavitation in gas-supersaturated solutions, *Journal of Applied Physics*, 46(1), 213-218.
- Hemmingsen, E. A. (1977), Spontaneous formation of bubbles in gas-supersaturated water, *Nature*, 267(5607), 141-142.
- Heywood, B. R., S. Hill, K. Pitt, P. Tibble, and S. Williams (2000), Biogenic inspiration for the controlled nucleation and growth of inorganic materials, *Mat. Res. Soc. Symp.*, 620, M4.5.1-M4.5.12.
- Hicher, P. Y., H. Wahyudi, and D. Tessier (2000), Microstructural analysis of inherent and induced anisotropy in clay, *Mechanics of Cohesive - Frictional Materials*, 5(5), 341-371.

- Horsrud, P., E. F. Sonstebo, and R. Boe (1998), Mechanical and petrophysical properties of north sea shales, *International Journal of Rock Mechanics and Mining Sciences*, 35(8), 1009-1020.
- Howard-Jones, M. H., V. D. Ballard, A. E. Allen, M. E. Frischer, and P. G. Verity (2002), Distribution of bacterial biomass and activity in the marginal ice zone of the central Barents Sea during summer, *Journal of Marine Systems*, 38(1-2), 77-91.
- Ishihara, K. (1970), Approximate forms of wave equations for water-saturated porous materials and related dynamic modulus, *Soils and Foundations*, 10(4), 10-38.
- Ishihara, K., Y. Huang, and H. Tsuchiya (1998), Liquefaction resistance of nearly saturated sand as correlated with longitudinal velocity, in *Poromechanics - A tribute to Maurice A. Biot*, edited by J. F. Thimus, et al., pp. 583-586, Balkema, Rotterdam.
- Ismail, M. A., H. A. Joer, M. F. Randolph, and A. Meritt (2002), Cementation of porous materials using calcite, *Geotechnique*, 52(5), 313-324.
- Jabri, E., M. B. Carr, R. P. Hausinger, and P. A. Karplus (1995), The crystal structure of urease from *Klebsiella aerogenes*, *Science*, 268(5213), 998-1004.
- Johns, D., H. Williams, K. Farrish, and S. Wagner (2004), Denitrification and soil characteristics of wetlands created on two mine soils in east Texas, USA, *Wetlands*, 24(1), 57-67.
- Juang, C. H., and R. D. Holtz (1986), Fabric, pore-size distribution, and permeability of sandy soils, *Journal of Geotechnical Engineering - ASCE*, 112(9), 855-868.
- Kalish, P. J., J. A. Stewart, E. O. Bennett, and W. F. Rogers (1964), The effect of bacteria on sandstone permeability, *Journal of Petroleum Technology*, 16(7), 805-814.
- Katz, A., A. Alimova, M. Xu, E. Rudolph, M. K. Shah, H. E. Savage, R. B. Rosen, S. A. McCormick, and R. R. Alfano (2003), Bacteria size determination by elastic light scattering, *IEEE Journal of Selected Topics in Quantum Electronics*, 9(2), 277-287.

- Kieft, T. L., E. M. Murphy, D. L. Haldeman, P. S. Amy, B. N. Bjornstad, E. V. McDonald, D. B. Ringelberg, D. C. White, J. Stair, R. P. Griffiths, T. C. Gsell, W. E. Holben, and D. R. Boone (1998), Microbial transport, survival, and succession in a sequence of buried sediments, *Microbial Ecology*, 36(3), 336-348.
- Kile, D. E., D. D. Eberl, A. R. Hoch, and M. M. Reddy (2000), An assessment of calcite crystal growth mechanisms based on crystal size distributions, *Geochimica Et Cosmochimica Acta*, 64(17), 2937-2950.
- Kim, D. S., and H. S. Fogler (2000), Biomass evolution in porous media and its effects on permeability under starvation conditions, *Biotechnology and Bioengineering*, 69(1), 47-56.
- Kjelleberg, S., B. A. Humphrey, and K. C. Marshall (1983), Initial phases of starvation and activity of bacteria at surfaces, *Applied and Environmental Microbiology*, 46(5), 978-984.
- Kokusho, T. (2000), Correlation of pore-pressure B-value with P-wave velocity and poisson's ratio for imperfectly saturated sand or gravel, *Soils and Foundations*, 40(4), 95-102.
- Korber, D. R., J. R. Lawrence, B. Sutton, and D. E. Caldwell (1989), Effect of laminar flow velocity on the kinetics of surface recolonization by Mot⁺ and Mot⁻ *Pseudomonas fluorescens*, *Microbial Ecology*, 18, 1-19.
- Kozisek, Z., P. Demo, and K. Sato (2000), Nucleation on active sites: evolution of size distribution, *Journal of Crystal Growth*, 209(1), 198-202.
- Krampitz, G., and W. Witt (1979), Biochemical aspects of biomineralization, *Topics of Current Chemistry*, 78, 57-144.
- Kristiansen, R. (1981), Sand filter trenches for purification of septic tank effluent: I. The clogging mechanism and soil physical environment, *Journal of Environmental Quality*, 10(3), 353-357.

- La-Mer, V. K. (1952), Nucleation in phase transitions, *Industrial and Engineering Chemistry*, 44(6), 1270-1277.
- Lapierre, C., S. Leroueil, and J. Locat (1990), Mercury intrusion and permeability of Louiseville clay, *Canadian Geotechnical Journal*, 27(6), 761-773.
- Lappin-Scott, H. M., F. Cusack, and J. W. Costerton (1988), Nutrient resuscitation and growth of starved cells in sandstone cores: A novel approach to enhanced oil recovery, *Applied and Environmental Microbiology*, 54(6), 1373-1382.
- Lee, A., J. Fox, and S. Hazell (1993), Pathogenicity of *Helicobacter pylori* - A perspective, *Infection and Immunity*, 61(5), 1601-1610.
- Li, X., and Y. C. Yortsos (1994), Bubble growth and stability in an effective porous medium, *Physics of Fluids*, 6(5), 1663-1676.
- Lockamy, V. L., J. M. Huang, H. Shields, S. K. Ballas, S. B. King, and D. B. Kim-Shapiro (2003), Urease enhances the formation of iron nitrosyl hemoglobin in the presence of hydroxyurea, *Biochimica Et Biophysica Acta-General Subjects*, 1622(2), 109-116.
- Loeb, G. I., and R. A. Neihof (1975), Marine conditioning biofilms, *Advances in Chemistry*, 145, 319-335.
- Logan, B. E., S. E. Oh, I. S. Kim, and S. Van Ginkel (2002), Biological hydrogen production measured in batch anaerobic respirometers, *Environmental Science & Technology*, 36(11), 2530-2535.
- Lohnes, R. A., E. R. Tuncer, and T. Demirel (1976), Pore structure of selected hawaiian soils, *Transportation Research Records*, 612, 76-79.
- Lowenstam, H. A., and L. Margulis (1980), Evolutionary prerequisites for early phanerozoic calcareous skeletons, *Biosystems*, 12(1-2), 27-41.
- Lowenstam, H. A. (1981), Minerals formed by organisms, *Science*, 211(4487), 1126-1131.

- Lowenstam, H. A., and S. Weiner (1983), Mineralization by organisms and the evolution of biomineralization, in *Biomineralization and biological metal accumulation*, edited by P. Westbroek and E. W. de Jong, pp. 191-203.
- Lubetkin, S. D. (2003), Why is it much easier to nucleate gas bubbles than theory predicts?, *Langmuir*, 19(7), 2575-2587.
- MacLeod, F. A., H. M. Lappin-Scott, and J. W. COSTERTON (1988), Plugging of a model rock system by using starved bacteria, *Applied and Environmental Microbiology*, 54(6), 1365-1372.
- Madigan, M. T., J. M. Martinko, J. Parker, and T. D. Brock (2003), *Brock biology of microorganisms*, 10th ed., xxv, 1019, [1056] p. pp., Prentice Hall/Pearson Education, Upper Saddle River, NJ.
- Marchesi, J. R., A. J. Weightman, B. A. Cragg, R. J. Parkes, and J. C. Fry (2001), Methanogen and bacterial diversity and distribution in deep gas hydrate sediments from the Cascadia Margin as revealed by 16S rRNA molecular analysis, *FEMS Microbiology Ecology*, 34(3), 221-228.
- Martens, C. S., and R. A. Berner (1974), Methane production in interstitial waters of sulfate-depleted marine sediments, *Science*, 185(4157), 1167-1169.
- McCalla, T. M. (1950), Studies on the effect of microorganisms on rate of percolation of water through soils, *Soil Science Society of America Proceedings*, 15, 182-186.
- Mccoy, W. F., J. D. Bryers, J. Robbins, and J. W. Costerton (1981), Observations of fouling biofilm formation, *Canadian Journal of Microbiology*, 27(9), 910-917.
- McDowell, G. R., and M. D. Bolton (1998), On the micromechanics of crushable aggregates, *Geotechnique*, 48(5), 667-679.
- Mitchell, J. K. (1993), *Fundamentals of soil behavior*, 2nd ed., xiii, 437 p. pp., Wiley, New York.

- Mitchell, J. K., and J. C. Santamarina (2005), Biological Considerations in Geotechnical Engineering, *ASCE Journal of Geotechnical and Geoenvironmental Engineering*, 131(10), 1222-1233.
- Mitchell, R., and Z. Nevo (1964), Effect of Bacterial Polysaccharide Accumulation on Infiltration of Water through Sand, *Applied Microbiology*, 12(3), 219-&.
- Miyata, M., W. S. Ryu, and H. C. Berg (2002), Force and velocity of Mycoplasma mobile gliding, *Journal of Bacteriology*, 184(7), 1827-1831.
- Moat, A. G., and J. W. Foster (1995), *Microbial Physiology*, Third Edition ed., Wiley-Liss, Inc., New York.
- Mobley, H. L. T., and R. P. Hausinger (1989), Microbial ureases - Significance, regulation, and molecular characterization, *Microbiological Reviews*, 53(1), 85-108.
- Mohan, S. B., M. Schmid, M. Jetten, and J. Cole (2004), Detection and widespread distribution of the *nrfA* gene encoding nitrite reduction to ammonia, a short circuit in the biological nitrogen cycle that competes with denitrification, *Fems Microbiology Ecology*, 49(3), 433-443.
- Monger, H. C., L. A. Daugherty, W. C. Lindemann, and C. M. Liddell (1991), Microbial precipitation of pedogenic calcite, *Geology*, 19(10), 997-1000.
- Moura, I., and J. J. G. Moura (2001), Structural aspects of denitrifying enzymes, *Current Opinion in Chemical Biology*, 5(2), 168-175.
- Mueller, R. F. (1996), Bacterial transport and colonization in low nutrient environments, *Water Research*, 30(11), 2681-2690.
- Nakamura, M., H. Kanbe, and J. I. Matsumoto (1993), Fundamental studies on hydrogen production in the acid-forming phase and its bacteria in anaerobic treatment processes - The effects of solids retention time, *Water Science and Technology*, 28(7), 81-88.

- Negre, M., P. Leone, J. Trichet, C. Defarge, V. Boero, and M. Gennari (2004), Characterization of model soil colloids by cryo-scanning electron microscopy, *Geoderma*, 121(1-2), 1-16.
- Nemati, M., E. A. Greene, and G. Voordouw (2005), Permeability profile modification using bacterially formed calcium carbonate: comparison with enzymic option, *Process Biochemistry*, 40(2), 925-933.
- Nevo, Z., and R. Mitchell (1967), Factors affecting biological clogging of sand associated with ground water recharge, *Water Research*, 1(3), 231-&.
- Newberry, C. J., G. Webster, B. A. Cragg, R. J. Parkes, A. J. Weightman, and J. C. Fry (2004), Diversity of prokaryotes and methanogenesis in deep subsurface sediments from the Nankai Trough, Ocean Drilling Program Leg 190, *Environmental Microbiology*, 6(3), 274-287.
- Oberdorfer, J. A., and F. L. Peterson (1985), Wastewater injection: Geochemical and biogeochemical clogging processes, *Ground Water*, 23(6), 753-761.
- Ofek, I., and R. J. Doyle (1994), *Bacterial adhesion to cells and tissues*, Chapman & Hall, New York.
- Okubo, T., and J. Matsumoto (1983), Biological clogging of sand and changes of organic constituents during artificial recharge, *Water Research*, 17(7), 813-821.
- Olson, M. S., R. M. Ford, J. A. Smith, and E. J. Fernandez (2004), Quantification of bacterial chemotaxis in porous media using magnetic resonance imaging, *Environmental Science & Technology*, 38(14), 3864-3870.
- Parkes, R. J., B. A. Cragg, S. J. Bale, J. M. Getliff, K. Goodman, P. A. Rochelle, J. C. Fry, A. J. Weightman, and S. M. Harvey (1994), Deep bacterial biosphere in Pacific Ocean sediments, *Nature*, 371(6496), 410-413.
- Parkes, R. J., B. A. Cragg, and P. Wellsbury (2000), Recent studies on bacterial populations and processes in subseafloor sediments: A review, *Hydrogeology Journal*, 8(1), 11-28.

- Parraga, J., M. A. Rivadeneyra, R. Delgado, J. Iniguez, M. Soriano, and G. Delgado (1998), Study of biomineral formation by bacteria from soil solution equilibria, *Reactive & Functional Polymers*, 36(3), 265-271.
- Paulsen, J. E. (1995), Microbial water diversion technique - Designed for near well treatment in low temperature sandstone reservoirs in the North Sea, paper presented at 5th International Conference on Microbial Enhanced Oil Recovery and Related Biotechnology for Solving Environmental Problems, Plano, TX.
- Pease, D. C., and L. R. Blinks (1947), Cavitation from solid surfaces in the absence of gas nuclei, *Journal of Physical and Colloid Chemistry*, 51(2), 556-567.
- Penumadu, D., and J. Dean (2000), Compressibility effect in evaluating the pore-size distribution of kaolin clay using mercury intrusion porosimetry, *Canadian Geotechnical Journal*, 37(2), 393-405.
- Pettit, N. M., A. R. J. Smith, R. B. Freedman, and R. G. Burns (1976), Soil urease: activity, stability and kinetic properties, *Soil Biology & Biochemistry*, 8(6), 479-484.
- Phelps, T. J., S. M. Pfiffner, K. A. Sargent, and D. C. White (1994), Factors influencing the abundance and metabolic capacities of microorganisms in eastern coastal-plain sediments, *Microbial Ecology*, 28(3), 351-364.
- Polacco, J. C., and M. A. Holland (1993), Roles of urease in plant cells, *International Review of Cytology - A Survey of Cell Biology*, vol 145, 145, 65-103.
- Raiders, R. A., M. J. McInerney, D. E. Revus, H. M. Torbati, R. M. Knapp, and G. E. Jenneman (1986), Selectivity and depth of microbial plugging in Berea sandstone cores, *Journal of Industrial Microbiology*, 1(3), 195-203.
- Rebata-Landa, V., and J. C. Santamarina (2006), Mechanical limits to microbial activity in deep sediments, *Geochem. Geophys. Gesisyst.*, 7(Q11006, doi:10.1029/2006GC001355).

- Reynolds, C. M., D. C. Wolf, and J. A. Armbruster (1985), Factors related to urea hydrolysis in soils, *Soil Science Society of America Journal*, 49(1), 104-108.
- Rice, R. C. (1974), Soil clogging during infiltration of secondary effluent, *Journal Water Pollution Control Federation*, 46(4), 708-716.
- Richardson, D. J., B. C. Berks, D. A. Russell, S. Spiro, and C. J. Taylor (2001), Functional, biochemical and genetic diversity of prokaryotic nitrate reductases, *Cellular and Molecular Life Sciences*, 58(2), 165-178.
- Rijnaarts, H. H., W. Norde, E. J. Bouwer, J. Lyklema, and J. Zehnder (1993), Bacterial adhesion under static and dynamic conditions, *Appl. Environ. Microbiol.*, 59, 3255-3265.
- Rivadeneira, M. A., R. Delgado, A. Delmoral, M. R. Ferrer, and A. Ramoscormenzana (1994), Precipitation of calcium carbonate by *Vibrio spp.* from an inland saltern, *FEMS Microbiology Ecology*, 13(3), 197-204.
- Ronen, D., B. Berkowitz, and M. Magaritz (1989), The development and influence of gas bubbles in phreatic aquifers under natural flow conditions, *Transport in Porous Media*, 4(3), 295-306.
- Rosenberg, M., E. A. Bayer, J. Delarea, and E. Rosenberg (1982), Role of thin fimbriae in adherence and growth of *Acinetobacter calcoaceticus* Rag-1 on hexadecane, *Applied and Environmental Microbiology*, 44(4), 929-937.
- Rosenberg, M., and S. Kjelleberg (1986), Hydrophobic interactions: Role in bacterial adhesion, *Advances in Microbial Ecology*, 9, 353-393.
- Ross, N., R. Villemur, L. Deschenes, and R. Samson (2001), Clogging of a limestone fracture by stimulating groundwater microbes, *Water Research*, 35(8), 2029-2037.
- Sadava, D., H. C. Heller, G. H. Orians, W. K. Purves, and D. Hillis (2006), *Life: The Science of Biology*, 8th Edition ed., W H Freeman & Co (Sd).
- Sanchez-Moral, S., V. Soler, J. C. Canaveras, E. Sanz-Rubio, R. Van Grieken, and K. Gysels (1999), Inorganic deterioration affecting the Altamira Cave, N Spain:

- quantitative approach to wall-corrosion (solutional etching) processes induced by visitors, *Science of the Total Environment*, 244, 67-84.
- Santamarina, J. C., and D. Fratta (1998), *Introduction to discrete signals and inverse problems in civil engineering*, xiii, 327 p. pp., ASCE Press, Reston, Va.
- Santamarina, J. C., K. A. Klein, and M. A. Fam (2001), *Soils and waves : [particulate materials behavior, characterization and process monitoring]*, xix, 488 p. pp., J. Wiley & Sons, Chichester, England ; New York.
- Santamarina, J. C., K. A. Klein, Y. H. Wang, and E. Prencke (2002), Specific surface: determination and relevance, *Canadian Geotechnical Journal*, 39(1), 233-241.
- Sarkar, A. K., G. Georgiou, and M. M. Sharma (1994), Transport of bacteria in porous media. 1.- An experimental investigation, *Biotechnology and Bioengineering*, 44(4), 489-497.
- Scholl, M. A., A. L. Mills, J. S. Herman, and G. M. Hornberger (1990), The influence of mineralogy and solution chemistry on the attachment of bacteria to representative aquifer materials, *Journal of Contaminant Hydrology*, 6, 321-336.
- Schultze-Lam, S., D. Fortin, B. S. Davis, and T. J. Beveridge (1996), Mineralization of bacterial surfaces, *Chemical Geology*, 132(1-4), 171-181.
- Shaw, J. C., B. Bramhill, N. C. Wardlaw, and J. W. Costerton (1985), Bacterial fouling in a model core system, *Applied and Environmental Microbiology*, 49(3), 693-701.
- Sherif, M. A., I. Ishibashi, and C. Tsuchiya (1977), Saturation effects on initial soil liquefaction, *Journal of the Geotechnical Engineering Division-ASCE*, 103(8), 914-917.
- Sherwood, J. L., J. C. Sung, R. M. Ford, E. J. Fernandez, J. E. Maneval, and J. A. Smith (2003), Analysis of bacterial random motility in a porous medium using magnetic resonance imaging and immunomagnetic labeling, *Environmental Science & Technology*, 37(4), 781-785.

- Sills, G. C., S. J. Wheeler, S. D. Thomas, and T. N. Gardner (1991), Behavior of offshore soils containing gas bubbles, *Geotechnique*, 41(2), 227-241.
- Sills, G. C., and R. Gonzalez (2001), Consolidation of naturally gassy soft soil, *Geotechnique*, 51(7), 629-639.
- Simkiss, K., and K. M. Wilbur (1989), *Biom mineralization : cell biology and mineral deposition*, xiv, 337 p. pp., Academic Press, San Diego.
- Simms, P. H., and E. K. Yanful (2001), Measurement and estimation of pore shrinkage and pore distribution in a clayey till during soil-water characteristic curve tests, *Canadian Geotechnical Journal*, 38(4), 741-754.
- Simms, P. H., and E. K. Yanful (2004), A discussion of the application of mercury intrusion porosimetry for the investigation of soils, including an evaluation of its use to estimate volume change in compacted clayey soils, *Geotechnique*, 54(6), 421-426.
- Simon, J. (2002), Enzymology and bioenergetics of respiratory nitrite ammonification, *Fems Microbiology Reviews*, 26(3), 285-309.
- Sinclair, J. L., and W. C. Ghiorse (1989), Distribution of aerobic bacteria, protozoa, algae, and fungi in deep subsurface sediments, *Geomicrobiology Journal*, 7(1-2), 15-31.
- Sinclair, J. L., S. J. Randtke, J. E. Denne, L. R. Hathaway, and W. C. Ghiorse (1990), Survey of microbial populations in buried valley aquifer sediments from Northeastern Kansas, *Ground Water*, 28(3), 369-377.
- Skempton, A. W. (1954), The pore-pressure coefficients A and B, *Geotechnique*, 4, 143-147.
- Soares, M. I. M., S. Belkin, and A. Abielovich (1988), Biological groundwater denitrification: Laboratory studies, *Water Science and Technology*, 20(3), 189-195.

- Sparks, A. D. W. (1963), Theoretical considerations of stress equations for partly saturated soils, paper presented at Third African Conference on Soil Mechanics and Foundation Engineering, Salisbury, Rhodesia.
- Sridharan, A., and A. G. Altschaeffl (1971), Pore size distribution studies, *Journal of the Soil Mechanics and Foundations Division - Proceedings of the ASCE*, SM5, 771-787.
- Stenstrom, T. A. (1989), Bacterial hydrophobicity: An overall parameter for the measurement of adhesion potential to soil particles, *Applied and Environmental Microbiology*, 55(1), 142-147.
- Stocks-Fischer, S., J. K. Galinat, and S. S. Bang (1999), Microbiological precipitation of CaCO_3 , *Soil Biology & Biochemistry*, 31(11), 1563-1571.
- Sun, Y., K. T. Wan, K. P. Roberts, J. C. Bischof, and B. J. Nelson (2003), Mechanical property characterization of mouse zona pellucida, *IEEE Transactions on Nanobioscience*, 2(4), 279-286.
- Swartzendruber, D., and R. P. Gupta (1964), Possible role of methane in affecting the hydraulic conductivity of fine quartz sand, *Soil Science Society of America Journal*, 98(2), 73-77.
- Tamura, S., K. Tokimatsu, A. Abe, and M. Sato (2002), Effects of air bubbles on B-value and P-wave velocity of a partly saturated sand, *Soils and Foundations*, 42(1), 121-129.
- Tanaka, H., D. R. Shiwakoti, N. Omukai, F. Rito, J. Locat, and M. Tanaka (2003), Pore size distribution of clayey soils measured by mercury intrusion porosimetry and its relation to hydraulic conductivity, *Soils and Foundations*, 43(6), 63-73.
- Taylor, S. W., and P. R. Jaffe (1990), Biofilm growth and the related changes in the physical properties of a porous medium . 1. Experimental investigation, *Water Resources Research*, 26(9), 2153-2159.

- Teng, H. H., and P. M. Dove (1997), Surface site-specific interactions of aspartate with calcite during dissolution: Implications for biomineralization, *American Mineralogist*, 82(9-10), 878-887.
- Thomas, R. E., W. A. Schwartz, and T. W. Bendixen (1966), Soil chemical changes and infiltration rate reduction under sewage spreading, *Soil Science Society of America Proceedings*, 30(5), 641-&.
- Thwaites, J. J., and U. C. Surana (1991), Mechanical properties of *Bacillus subtilis* cell walls - Effects of removing residual culture medium, *Journal of Bacteriology*, 173(1), 197-203.
- Thwaites, J. J., U. C. Surana, and A. M. Jones (1991), Mechanical properties of *Bacillus subtilis* cell walls - Effects of ions and lysozyme, *Journal of Bacteriology*, 173(1), 204-210.
- Tiedje, J. M., A. J. Sextone, D. D. Myrold, and J. A. Robinson (1982), Denitrification: ecological niches, competition and survival, *Antoine van Leeuwenhoek*, 48, 569-583.
- Tim, U. S., S. Mostaghimi, and T. A. Dillaha (1988), Modeling the movement and persistence of bacteria and viruses in porous media, *AZO paper No. 88-2627*.
- Treves, D. S., B. Xia, J. Zhou, and J. M. Tiedje (2003), A two-species test of the hypothesis that spatial isolation influences microbial diversity in soil, *Microbial Ecology*, 45(1), 20-28.
- Tsukamoto, Y., K. Ishihara, H. Nakazawa, K. Kamada, and Y. N. Huang (2002), Resistance of partly saturated sand to liquefaction with reference to longitudinal and shear wave velocities, *Soils and Foundations*, 42(6), 93-104.
- Updegraff, D. M. (1982), Plugging and penetration of reservoir rock by microorganisms, paper presented at International Conference in Microbial Enhancement of Oil Recovery, U.S. Department of Energy, Bartlesville, OK; Washington, DC.

- Valdes, J. R., and J. C. Santamarina (2005), Particle-entrained fluid flow in porous media: Clogging and flushing, *SPE, (Accepted for publication)*.
- van Beek, C. G. E. M., and D. van der Kooij (1982), Sulfate reducing bacteria in groundwater from clogging and non-clogging shallow wells in the Netherlands river region, *Ground Water*, 20(3), 298-302.
- van Beek, C. G. E. M. (1984), Restoring well yield in the Netherlands, *Journal American Water Works Association*, 76(10), 66-72.
- Vandevivere, P., and P. Baveye (1992a), Relationship between transport of bacteria and their clogging efficiency in sand columns, *Applied and Environmental Microbiology*, 58(8), 2523-2530.
- Vandevivere, P., and P. Baveye (1992b), Effect of bacterial extracellular polymers on the saturated hydraulic conductivity of sand columns, *Applied and Environmental Microbiology*, 58(5), 1690-1698.
- Vandevivere, P., and P. Baveye (1992c), Saturated hydraulic conductivity reduction caused by aerobic bacteria in sand columns, *Soil Science Society of America Journal*, 56(1), 1-13.
- Vasseur, G., I. Djeranmaigre, D. Grunberger, G. Rousset, D. Tessier, and B. Velde (1995), Evolution of structural and physical parameters of clays during experimental compaction, *Marine and Petroleum Geology*, 12(8), 941-954.
- Vogels, G. D., and C. V. D. Drift (1976), Degradation of purines and pyrimidines by microorganisms, *Bacteriology Reviews*, 40, 403-468.
- Ward, C. A., A. Balakris, and F. C. Hooper (1970), On thermodynamics of nucleation in weak gas-liquid solutions, *Journal of Basic Engineering - Transactions of the ASME*, 92, 695-704.
- Ward, S. G., and R. L. Whitmore (1950), Studies of the viscosity and sedimentation of suspensions. Part 1- The viscosity of suspension of spherical particles, *British Journal of Applied Physics*, 1(11), 286-290.

- Warren, L. A., P. A. Maurice, N. Parmar, and F. G. Ferris (2001), Microbially mediated calcium carbonate precipitation: Implications for interpreting calcite precipitation and for solid-phase capture of inorganic contaminants, *Geomicrobiology Journal*, 18(1), 93-115.
- Wellsbury, P., R. A. Herbert, and R. J. Parkes (1996), Bacterial activity and production in near-surface estuarine and freshwater sediments, *FEMS Microbiology Ecology*, 19(3), 203-214.
- Wellsbury, P., I. Mather, and R. J. Parkes (2002), Geomicrobiology of deep, low organic carbon sediments in the Woodlark Basin, Pacific Ocean, *FEMS Microbiology Ecology*, 42(1), 59-70.
- Wheeler, S. J. (1988), A conceptual model for soils containing large gas bubbles, *Geotechnique*, 38(3), 389-397.
- Whiffin, V. S., L. A. van Paassen, L. A. van Paassen, and M. P. Harkes (2007), Microbial carbonate precipitation as a soil improvement technique, *Geomicrobiology Journal*, 24, 1-7.
- Wilhelm, E., R. Battino, and R. J. Wilcock (1977), Low-pressure solubility of gases in liquid water, *Chemical Reviews*, 77(2), 219-262.
- Wilt, P. M. (1986), Nucleation rates and bubble stability in water carbon dioxide solutions, *Journal of Colloid and Interface Science*, 112(2), 530-538.
- Wood, W. W., and R. L. Bassett (1975), Water quality changes related to development of anaerobic conditions during artificial recharge, *Water Resources Research*, 11(4), 553-558.
- Xu, J. G., D. A. Heeraman, and Y. Wang (1993), Fertilizer and temperature effects on urea hydrolysis in undisturbed soil, *Biology and Fertility of Soils*, 16(1), 63-65.
- Yang, J. (2002), Liquefaction resistance of sand in relation to P-wave velocity, *Geotechnique*, 52(4), 295-298.

- Yang, J., S. Savidis, and M. Roemer (2004), Evaluating liquefaction strength of partially saturated sand, *Journal of Geotechnical and Geoenvironmental Engineering*, 130(9), 975-979.
- Yang, Y. L., and A. C. Aplin (1998), Influence of lithology and compaction on the pore size distribution and modelled permeability of some mudstones from the Norwegian margin, *Marine and Petroleum Geology*, 15(2), 163-175.
- Yao, X., M. Jericho, D. Pink, and T. Beveridge (1999), Thickness and elasticity of gram-negative murein sacculi measured by atomic force microscopy, *Journal of Bacteriology*, 181(22), 6865-6875.
- Yates, M. V., and S. R. Yates (1987), Modeling microbial fate in the subsurface environment, *Critical Reviews in Environmental Control*, 17(4), 307-344.
- Yegian, M. K., E. Eseller-Bayat, A. Alshawabkeh, and A. S. (2007), Induced partial saturation for liquefaction mitigation: Experimental investigation, *Journal of Geotechnical and Geoenvironmental Engineering*, 133(4), 372-380.
- Yoshimi, Y., K. Tanaka, and K. Tokimatsu (1989), Liquefaction resistance of a partially saturated sand, *Soils and Foundations*, 29(3), 157-162.
- Zantua, M. I., L. C. Dumenil, and J. M. Bremner (1977), Relationships between soil urease activity and other soil properties, *Soil Science Society of America Journal*, 41(2), 350-352.
- Zavarzin, G. A. (2002), Microbial geochemical calcium cycle, *Microbiology*, 71(1), 1-17.
- Zhang, C. L., A. V. Palumbo, T. J. Phelps, J. J. Beauchamp, F. J. Brockman, C. J. Murray, B. S. Parsons, and D. J. P. Swift (1998), Grain size and depth constraints on microbial variability in coastal plain subsurface sediments, *Geomicrobiology Journal*, 15(3), 171-185.
- Zhang, X. Y., and K. N. Houk (2005), Why enzymes are proficient catalysts: Beyond the Pauling paradigm, *Accounts of Chemical Research*, 38(5), 379-385.

- Zheng, D., G. A. Taylor, and G. Gyananath (1994), Influence of laminar flow velocity and nutrient concentration on attachment of marine bacterioplankton, *Biofouling*, 8, 107-120.
- Zhou, J. Z., B. C. Xia, D. S. Treves, L. Y. Wu, T. L. Marsh, R. V. O'Neill, A. V. Palumbo, and J. M. Tiedje (2002), Spatial and resource factors influencing high microbial diversity in soil, *Applied and Environmental Microbiology*, 68(1), 326-334.
- Zhou, J. Z., B. C. Xia, H. Huang, A. V. Palumbo, and J. M. Tiedje (2004), Microbial diversity and heterogeneity in sandy subsurface soils, *Applied and Environmental Microbiology*, 70(3), 1723-1734.
- Zottola, E. A. (1991), Characterization of the attachment matrix of *Pseudomonas fragi* attached to non-porous surfaces, *Biofouling*, 5, 37-55.
- Zweifel, U. L., and A. Hagstrom (1995), Total counts of marine-bacteria include a large fraction of non-nucleoid-containing bacteria (ghosts), *Applied and Environmental Microbiology*, 61(6), 2180-2185.

VITA

VERONICA REBATA-LANDA

Verónica was born in Lima, Perú on August 4th, 1979. She received a B.S. in Science and Engineering with specialization in Civil Engineering from Pontificia Universidad Católica del Perú on July, 2001 before coming to Georgia Tech to pursue a masters and a doctorate in Civil and Environmental Engineering with the Geosystems group on July, 2003. She received her M.S. in August 2005 and her Ph.D. in August 2007.